BIF-005-112-68

VOLUME II

TECHNICAL PROPOSAL

5 JULY 1968

BETA SYSTEM

MODEL HG-469B

hycon

700 ROYAL OAKS DRIVE
MONROVIA, CALIFORNIA

(387)

CONTENTS

CONTENTS (Continued)

Section 1

BETA SYSTEM REQUIREMENTS

1.1 INTRODUCTION

The Hycon Company is pleased to submit this proposal to manufacture and deliver four engineering models, four preproduction units, and twelve production units of the Beta System, Model HG-469B, including those retained for testing. The general theory of image motion detection systems is described in Section 2 and the specific Hycon system is detailed in Section 3. The Hycon Beta System is the outgrowth of an extensive in-house research program which resulted in the HG-453 production model single axis sensor, shown in Figure 1-1. Section 4 is devoted to maintainability, safety, and reliability.

1.2 PERFORMANCE

Principle performance characteristics of the Beta System, as detailed in Specification EC-701A, Rev. 6, form the basis for the Hycon Beta System, Model HG-469B, Figure 1-2.

1.2.1 Functional Characteristics. The HG-469B will sense image velocity at the center of the format of the scene image and resolve it into two vector components along perpendicular axes X and Y. The HG-469B will provide the following output signals:

a. Image Velocity

b. Lock-on Signal

c. Operational Readiness Monitoring

d. Diagnostic Monitoring

e. Subthreshold image plane irradiance indication

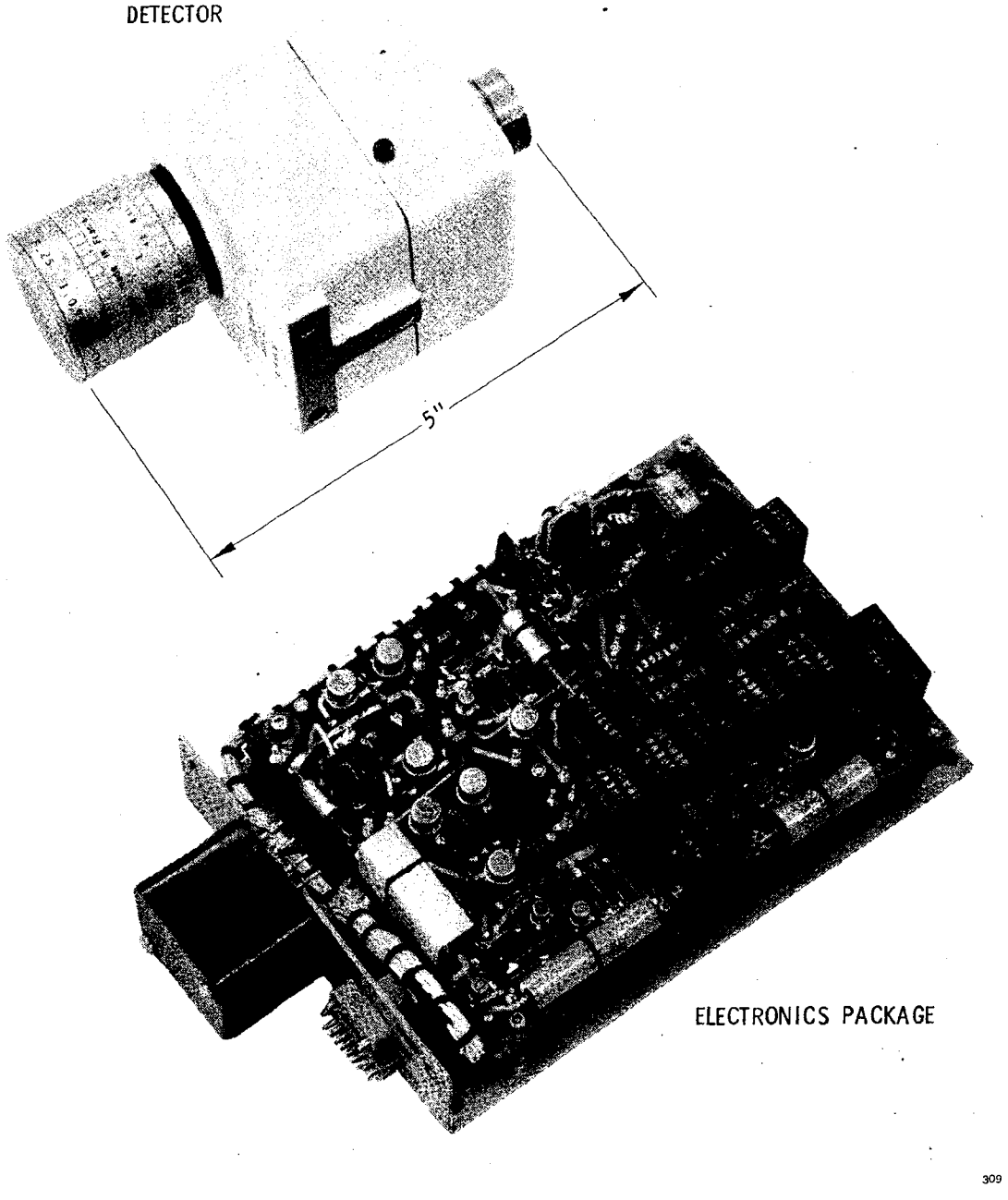

Figure 1-1. HG-453 Production Model Sensor

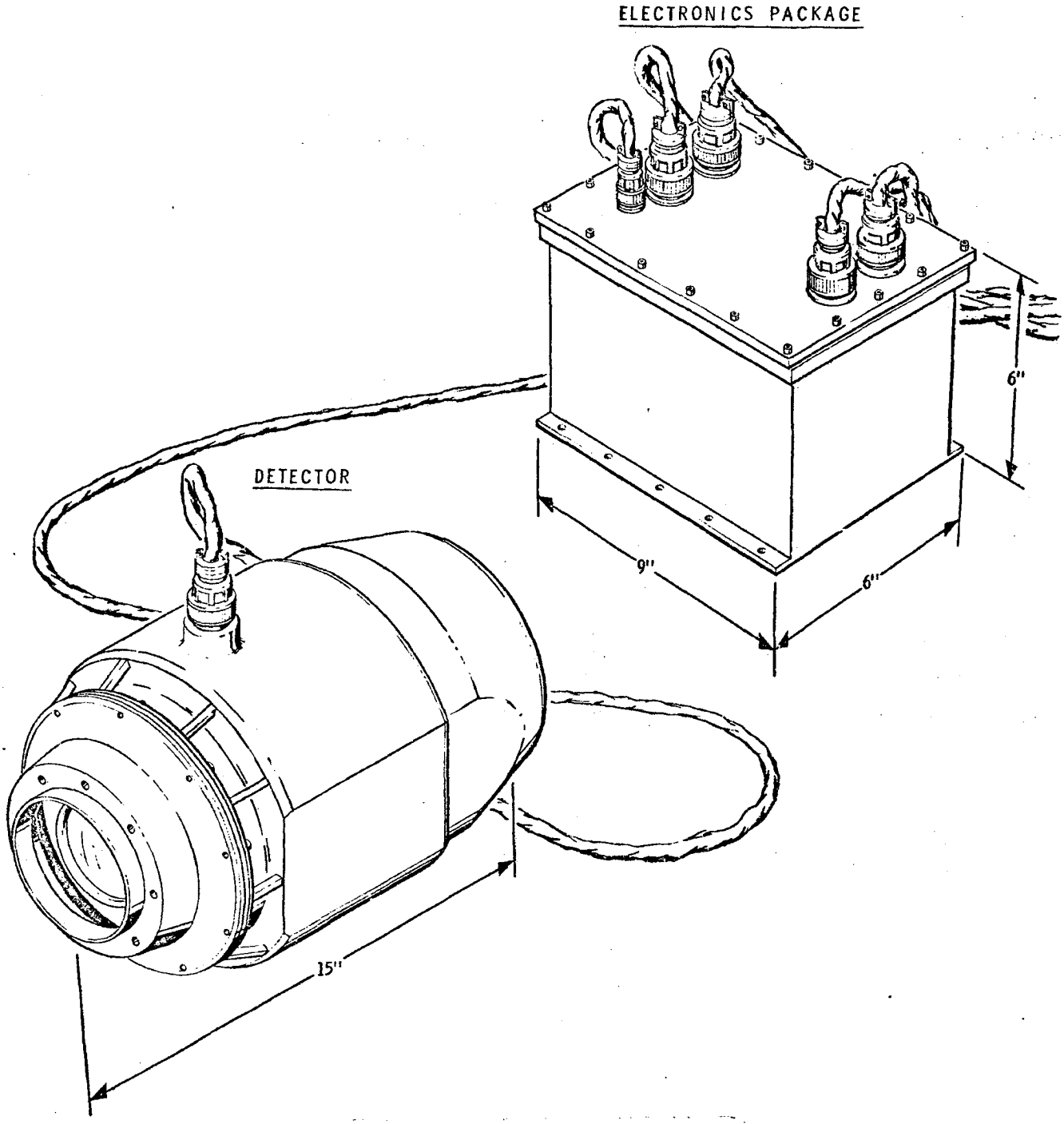

Figure 1-2.
Beta System, Model HG-469B

1.2.2 Primary Performance Characteristics

1.2.2.1 Image Velocity Output Signals. The output image velocity signals of the Beta System will be proportioned to the components of the image velocity vector resolved along the reference, perpendicular axes. The reference axes will be indexed coincident to the Beta System base.

The image velocity signal for each of the two axes will be of analog form with a maximum of +5 VDC. A separate sense or sign signal shall be provided for each axis. The nominal gradient will be 16.67 volts/inch/second.

a. Dynamic Range. The Beta System will provide single-valued voltages representative of true image velocities from 0 to 0.3 inch/second (600 micro rad/sec) in the primary image plane. Image rotational velocity in the image plane will not be sensed.

b. Linearity. The relationship between true image velocity and indicated image velocity will be of the form V-True = K x V-Ind for true image velocity between 0.0225 inch/sec (45 micro rad/sec) and 0.3 inch/sec (600 micro rad/sec) where:

V-True = true image velocity and

V-Ind = indicated image velocity

The three sigma limits of K including noise are 0.738 and 1.55. Signal-to-noise ratio for the image velocity range stated will be greater than two.

c. Saturation. The Beta System will not saturate for true image velocities of less than 0.3 inch/sec (600 micro rad/sec). When saturated, the Beta System will provide a signal indicating this condition for each axis. The minimum for this condition will be a polarity signal corresponding to the velocity

polarity for velocities up to 0.5 inch/sec. The Beta System will be capable of recovering within 0.5 seconds of receiving an input within its dynamic range from saturation periods up to two seconds.

d. Frequency Response. The dynamic response of the Beta System over the frequency range from 0 to 60 rad/sec will resemble that of a device with a single lag located between 6 rad/sec and 60 rad/sec. The desired location of the lag is at 7 rad/sec. In addition a notch filter will be located at 188.4 rad/sec.

e. Null Accuracy. When the true image velocity is equal to or less than 0.0225 inch/sec (45 micro rad/sec), the indicated velocity, as provided by the Beta System will be in error by no more than 0.010 inch/sec (20 micro rad/sec).

1.2.2.2 Lock-on Signal. The Beta System will provide a signal for each axis indicating the image lock-on status. The output will be 3.5 to 5.0 vdc when the image is in the locked-on condition and 0.5 $\pm$.5 vdc when not locked or saturated.

1.2.2.3 Operational Readiness Signal. The Beta System will provide an output signal to denote operational readiness.

a. The signal magnitude will be a 3.5 to 5.0 vdc when it is operationally ready.

b. The signal magnitude shall be 0.5 to $\pm$0.5 vdc when it is not operationally ready.

1.2.2.4 Diagnostic Monitoring Signals. Necessary diagnostic monitoring signals will be provided for telemetry monitoring as required. The test points will provide continuous output signals within the range of 0 to 5 vdc.

1.2.2.5 Subthreshold Irradiance Signal. The Beta will provide an output signal to indicate when the average input irradiance in the primary image plane is insufficient for proper Beta performance.

a. The signal magnitude will be 3.5 to 5.0 vdc when sufficient light exists.

b. The signal magnitude will be 0.5 $\pm$0.5 vdc when insufficient light exists.

1.3 ACCEPTANCE AND QUALIFICATION TESTING

1.3.1 An extensive design evaluation and test program will be performed according to applicable portions of the Integrated Test Plan which has been prepared in accordance with MSM-T-101-1. Hycon's Integrated Test Plan is presented in the Mangement Volume (Volume I), Appendix A2.

Section 2

THEORY AND BACKGROUND

2.1 INTRODUCTION

This section describes the basis of operation of typical image velocity sensors in terms which lead to a general understanding of methods. This allows comparison of known methods and enlightens the search for improved types. The operation of such systems is best treated by mathematical theory which makes use of basic statistical principles and the Fourier Transform relationships between power spectra and correlation functions. This section presents the elements of the theory in the form of results, the detailed origin of which may be found in cited reports and references, in a sequence which leads to the needed generalized understanding of image velocity measurement techniques.

2.2 BASIC REQUIREMENTS

The Beta System is required to provide image velocity information which may be used, either in open-loop or closed-loop systems, to minimize resultant image plane relative motion, that is, to achieve image motion compensation (IMC). In many cases, the image plane shear during the exposure interval is small to begin with, so that high percentage accuracy in Beta System operation is not a primary aim. However, very little drift or null error can be tolerated.

In addition to null stability and small null error, speed of response is very important in permitting adequate corrections for image velocity changes resulting from platform or vehicle attitude perturbations or altitude change with flight. Since platform motion may be relatively great prior to exposure, the Beta System must not be subject to saturation from large image velocities, or must recover

very rapidly from such saturation. Adequate velocity range, with good linearity, is necessary in closed-loop operation for stable, rapid covergence to null velocity. Saturation or inadequate gain (scale) uniformity will generally lead to instability in the form of blocking (nonlinear) oscillations or sustained hunting. The use of the image velocity sensor in a servo loop imposes additional requirements on its transfer phase and gain, and, further demands at least nominally linear operation.

The fundamental notion is that image velocity can be corrected if it can be measured. In reality, different parts of the image may have different velocities because of altitude variations within the field of view, or because of slant range distribution resulting from large obliquity angles. Where image velocity is such a velocity distribution, the image velocity sensor can be expected to provide a weighted average image velocity. Determination of the optimum field of view for the Beta system involves consideration of terrain and altitude statistics.

Because of the one-time character of most photographic missions, reliability outranks detailed performance as a requirement. In seeking reliability, one not only tries to stay with well-known, highly developed techniques, but also seeks simplicity in operating principle and make-up. Fortunately, great improvements have been made in reliability of electronic circuits, largely through development of very rugged, compact semiconductor devices. With such components, necessary circuit functions can be implemented with very small size, weight, and power limitations.

2.3 TERRAIN LIGHT PATTERNS

The basic information input to the sensor is the pattern of terrain light

and shade within the instantaneous field of view. Brightness or luminance (L) of the terrain may be expressed in footlamberts or equivalent units. We will assume the pattern is spatially random, average luminance is L_o, and fluctuations of brightness about the average is normally distributed with variance σ_L^2. The quantity σ_L^2 represents the amount of useful information in the terrain pattern, and may be referred to as terrain power. Figure 2-1 presents a one-dimensional terrain luminance distribution.

It will be important in our considerations to know, or to assume, the manner in which this terrain power is distributed as a function of spatial wave numbers. The terrain-power spectrum P_T is the (two-dimensional) function of (two) spatial wave numbers which represents the density (over $+\infty$ to $-\infty$ in each of the wave number variables), excluding a small region at the origin (due to L_o), is the total terrain power σ_L^2. A one-dimensional power spectrum is sketched in figure 2-2.

We are not in a position to characterize P_T very well; even if one had a typical terrain power spectrum, it is certain that it would be found atypical for many terrain scenes. This is a philosophical problem rather than statistical ignorance. The performance of a Beta system depends, in some cases critically, upon the amount of terrain power falling within prescribed regions of the terrain power spectrum, and performance estimates are therefore sensitive to the functional form assumed. If photographs of typical terrain specimens were available for analysis, a few samples of terrain spectra could be computed; however, neither such samples nor hypotheses can bridge the gap between the a'posteriori results of experiments and the a'priori estimation of subsequent trials.

For purposes of discussion, assume that the terrain power spectrum has the

~~SECRET/D~~

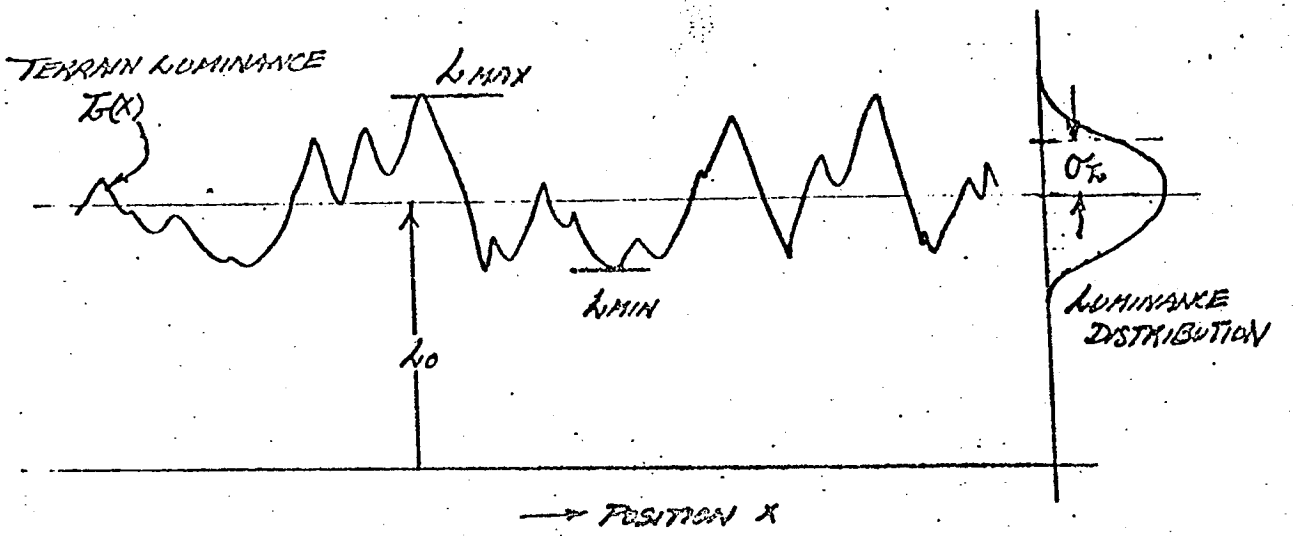

Figure 2-1. Hypothetical Luminance Pattern for a One-dimensional Terrain. (Terrain Power = σ_L^2).

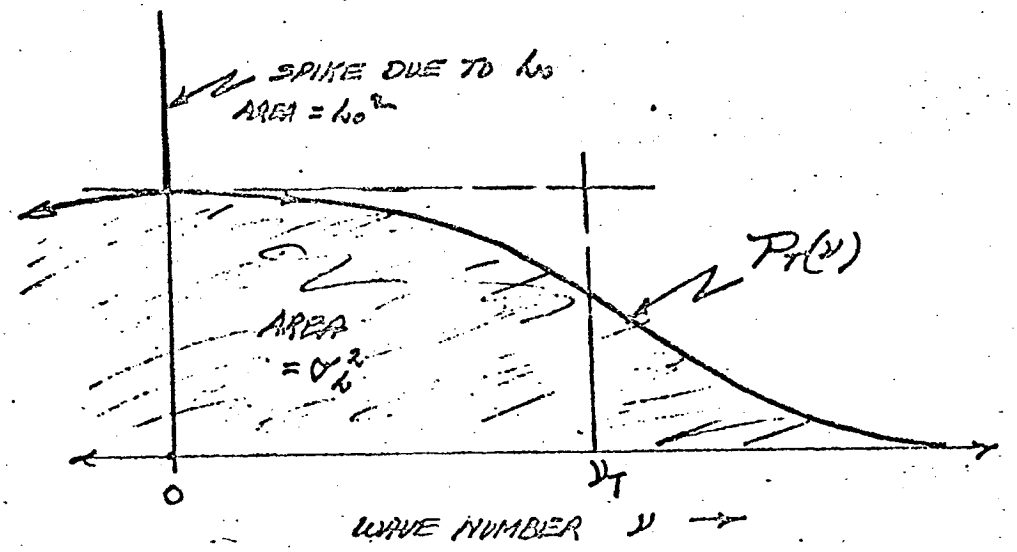

Figure 2-2. One-dimensional Terrain Power Spectrum.

~~SECRET/D~~

form

$$P_T = P_o\left(\frac{\nu_T^2}{\nu_T^2+\nu^2+\mu^2}\right)^n + L_o^2\,\delta\left(\nu^2+\mu^2\right) \qquad (2.1)$$

where $n > 1$ in order that the total power be finite. The delta function represents the average component. When the integrations are performed, we obtain

$$P_o = \frac{\sigma_L^2(n-1)}{\pi\nu_T^2} \qquad (2.2)$$

It is usual to characterize the variations in luminance of well defined targets, such as bar charts used for resolution testing, by the contrast ratio, defined as the ratio of L max to L min (L max being typical of a bright element and L min the dark element). With random patterns having normal or near-normal distributions of brightness, this characterization must be reinterpreted in a very subjective manner. To make contact between σ_L, representing the normal distribution of luminance in the terrain, and the contrast ratio, we may choose for L max that value which is exceeded only rarely, and a similar value on the lower end for L min. If we take these bounds at $\pm 2\sigma_L$, "rarely" is 2.3% of the time. For this condition:

$$\text{Contrast Ratio} \approx \frac{L_o+2\sigma_L}{L_o-2\sigma_L} \approx 1+\frac{4\sigma_L}{L_o} \quad \text{FOR} \quad \frac{\sigma_L}{L_o} \ll 1. \qquad (2.3)$$

For example, a contrast ratio of 1.2:1 would correspond to $\sigma_L = L_o/20$

2.4 GENERATION OF THE PHOTOSIGNAL

The Beta system receives the image of the terrain as formed by an optical system. Each element of the terrain of luminance L in footlamberts is imaged as a corresponding element of illuminance I in footcandles, where

$$I = \frac{1}{4f^2} \times (\text{transmission factors}) \qquad (2.4)$$

f being the f-number (relative aperture) of the optical system. The transmission factors represent loss due to atmospheric scattering and optical reflectance, and due to transmission losses.

The field of view of the Beta system is defined by an aperture, which may have any shape and may be shaded or apodized to improve performance. All of the image light transmitted by the aperture is collected and/or falls upon a photosensor of sensitivity S (amperes per watt). The resulting photocurrent or signal is thus proportional to the integral of the product of image illuminance and aperture transmission, integration being taken over the entire aperture. As the image moves with respect to the aperture, the weighting function, represented by the aperture transmittance, scans across the image, and the resulting photosignal fluctuates accordingly. The properties of this fluctuating signal depend in a concisely definable manner upon the power spectra of the terrain and upon the aperture.

The integral of the product of a weighting function and a second function in which the weighting function shifts along the axis of variables while the second function remains fixed in position is well known in many phases of mathematics, where the operation is called convolution or folding. Furthermore, in transform theory, convolution is shown to be equivalent to the product of the transforms of the two functions. These relations become particularly direct and useful to us in the domain of Fourier transforms. As a consequence of these known principles, it can be shown that the power spectrum of the photosignal is proportional to the product of the power spectra of the aperture and of the terrain, with suitable scaling for velocity (in going from wave number to frequency), as shown in figure 2-3.

In estimating performance of an image velocity system, the error in velocity

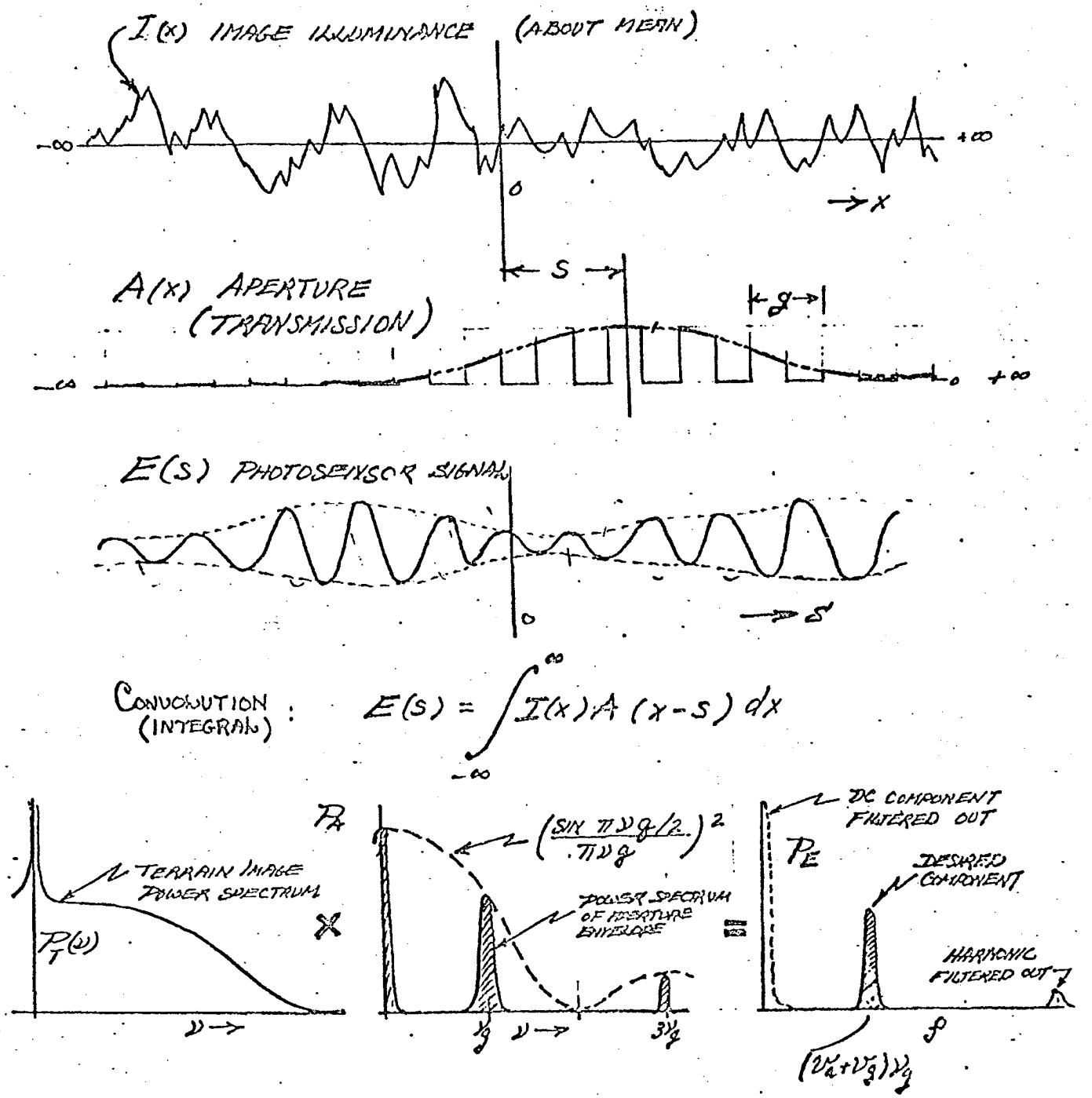

Figure 2-3. Generation of Photosignal E(s). (Passing terrain image illumination through aperture A(x). The corresponding multiplication of power spectra to obtain P_E is illustrated at the bottom of the figure.)

measurement is derived from the power spectrum of the photosignal. For this reason we are concerned with power spectra rather than amplitude spectra. The convolution theorem of Fourier transforms is not only an important tool, but is sufficient for our analysis.

Photosensors differ, from the point of view of our analysis, primarily in sensitivity and noise properties. Photomultiplier tubes have relatively low sensitivities, but the high gains achieved by electron multiplication permit operation of subsequent stages at low impedance. This virtually eliminates the source of thermal noise but shot noise remains, increased somewhat by dynode action. Photodiodes show higher sensitivities, but include thermal noise and shot noise in consideration. As light level decreases, the choice of photosensor may shift from photodiode to photomultiplier because of thermal noise advantage.

2.5 APERTURES AND SPECTRAL PROPERTIES

2.5.1 Spectral Properties

Since the spectrum of the aperture combines with that of the terrain (image) to determine performance, we now consider the properties of several types of apertures. The distinctions between various diverse categories of image velocity instruments can be best understood in terms of the spectral properties of the apertures and their interaction with the image velocity and spectrum.

Each static aperture may be represented by a transmission which is a function of two spatial dimensions, x in the forward direction and y in the transverse direction. Let ν and μ be the corresponding conjugate wave numbers. Then the amplitude spectrum of the aperture is a function of both ν and μ, given by the Fourier Transform

$$\tilde{A}(\nu,\mu) = \int_{-\infty}^{+\infty}\int_{-\infty}^{+\infty} A(x,y)\, e^{2\pi i(x\nu + y\mu)}\, dx\,dy. \qquad (2.5)$$

in which $A(x,y)$ is the aperture transmission and $\tilde{A}(\nu,\mu)$ is the aperture amplitude spectrum. The aperture power spectrum is equal to the square of the absolute value of the amplitude spectrum:

$$P_A(\nu,\mu) = |\tilde{A}(\nu,\mu)|^2 \qquad (2.6)$$

As an example, consider a rectangular aperture of forward length W and transverse width W. The power spectrum of such a uniform rectangular aperture has the form

$$P_A(\nu,\mu) = \left(\frac{\sin \pi W \nu}{\pi \nu}\right)^2 \left(\frac{\sin \pi W \mu}{\pi \mu}\right)^2 . \qquad (2.7)$$

which is illustrated in figure 2-4. Since the photosignal resulting from the use of this aperture is a convolution of the aperture with the image, we know by the convolution theorem of Fourier transforms that the amplitude spectrum of the photosignal is equal to the product of the amplitude spectra of the aperture and the image (or terrain, scaled for the optical demagnification).

But we don't know the amplitude spectrum of the image; we know (even in principle) only the power spectrum. And we don't want the amplitude spectrum of the photosignal; we want only the power spectrum.

Let us consider the formation of the photosignal in more detail. The signal $E(t)$ is given by the integral

$$E(t) = \int_{-\infty}^{+\infty}\int_{-\infty}^{+\infty} A(x - v_a t, y)\, I(x,y)\, dx\, dy . \qquad (2.8)$$

This integral may be described as the integral of the product of two quantities. Going now to Fourier transforms, we may make an entirely equivalent statement: the transform $\tilde{E}(f)$ is equal to the values lying on the f axis of the convolution

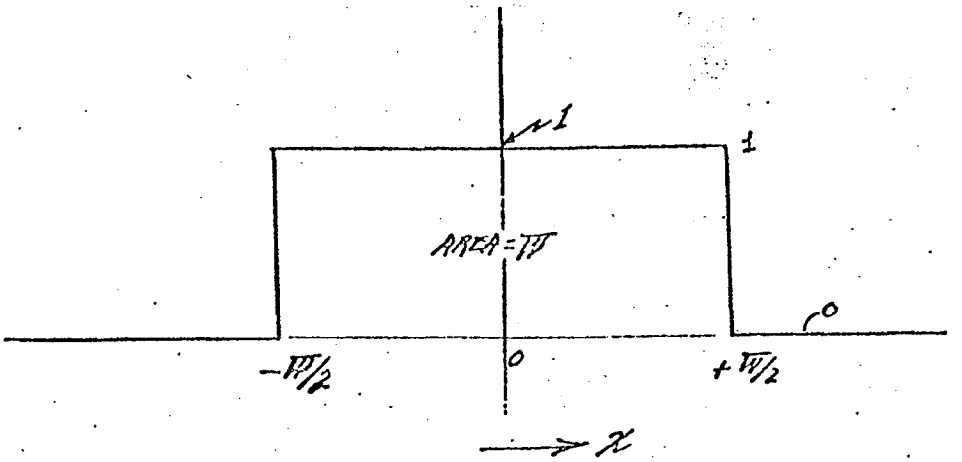

1) A ONE-DIMENSIONAL "RECTANGULAR" APERTURE

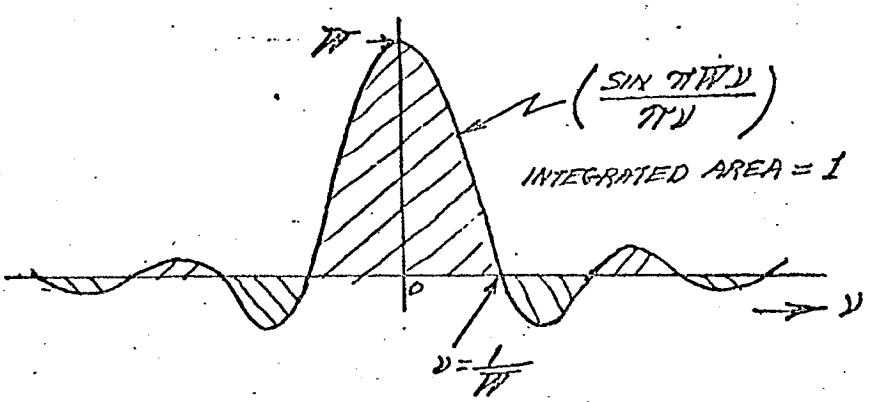

2) FOURIER TRANSFORM OR AMPLITUDE SPECTRUM OF APERTURE

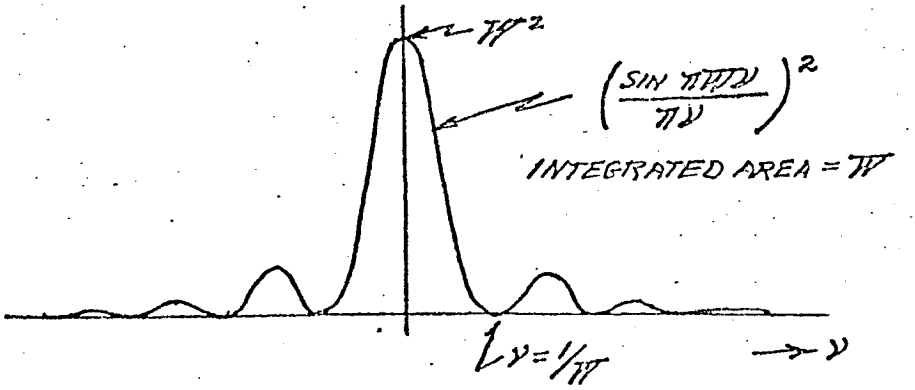

3) |FOURIER TRANSFORM|² OR POWER SPECTRUM OF APERTURE

Figure 2-4. One-dimensional Aperture Amplitude and Power Spectra.

of $\tilde{A}(\nu,\mu;f)$ and $\tilde{T}(\nu,\mu;f)$:

$$E(f) = \tilde{A}(\nu,\mu;f) * \tilde{I}(\nu,\mu;f)\Big|_{\nu,\mu=0} . \qquad (2.9)$$

where the asterisk is a conventional symbol for convolution. Because time enters into equation (2.8) as well as the spatial variables x and y, we must operate in a three-dimensional transform space involving f, ν, and μ. The convolution is over this entire space. But the manipulations are made simple by the fact that I(x,y) is not a function of time and, therefore, its transform $\tilde{I}(\nu,\mu;f)$ exists only in the f=0 plane. Further, since the aperture moves linearly with velocity V_a, the transform $\tilde{A}(\nu,\mu;f)$ exists only on a plane $f=V_a\,\nu$. These restrictions result in the full convolution process reducing to a simple projection of $\tilde{I}(\nu,\mu)$ onto the f axis by reflection in the plane $f=V_a\nu$ with weighting $\tilde{A}(\nu,\mu)$. Figure 2-5 illustrates this process of derivation.

The fact remains that, in projecting $\tilde{I}(\nu,\mu)$ by means of $\tilde{A}(\nu,\mu)$ onto the f axis to form $\tilde{E}(f)$, many different elements of $\tilde{I}(\nu,\mu)$ contribute to each element of $\tilde{E}(f)$. When we square $\tilde{E}(f)$ to create P_E we get cross products in addition to sums of squares. But it is usual to assume that the components of power spectra are not mutually correlated, and on this basis we may expect the cross terms to vanish in the average. Therefore, the square of the projected sums of products is equal to the sum of the projected product of squares, or

$$P_E(f) = P_A(\nu,\mu;f) * P_T(\nu,\mu;f) . \qquad (2.10)$$

Hence, we need concern ourselves only with the power spectra and with their multiplication and reflection in the plane of slope V_a, as determined by the motion.

For a simple fixed aperture showing no periodic structure, the aperture transform lies about the origin on the locus plane $f = V_a\nu_g$. The photosignal then

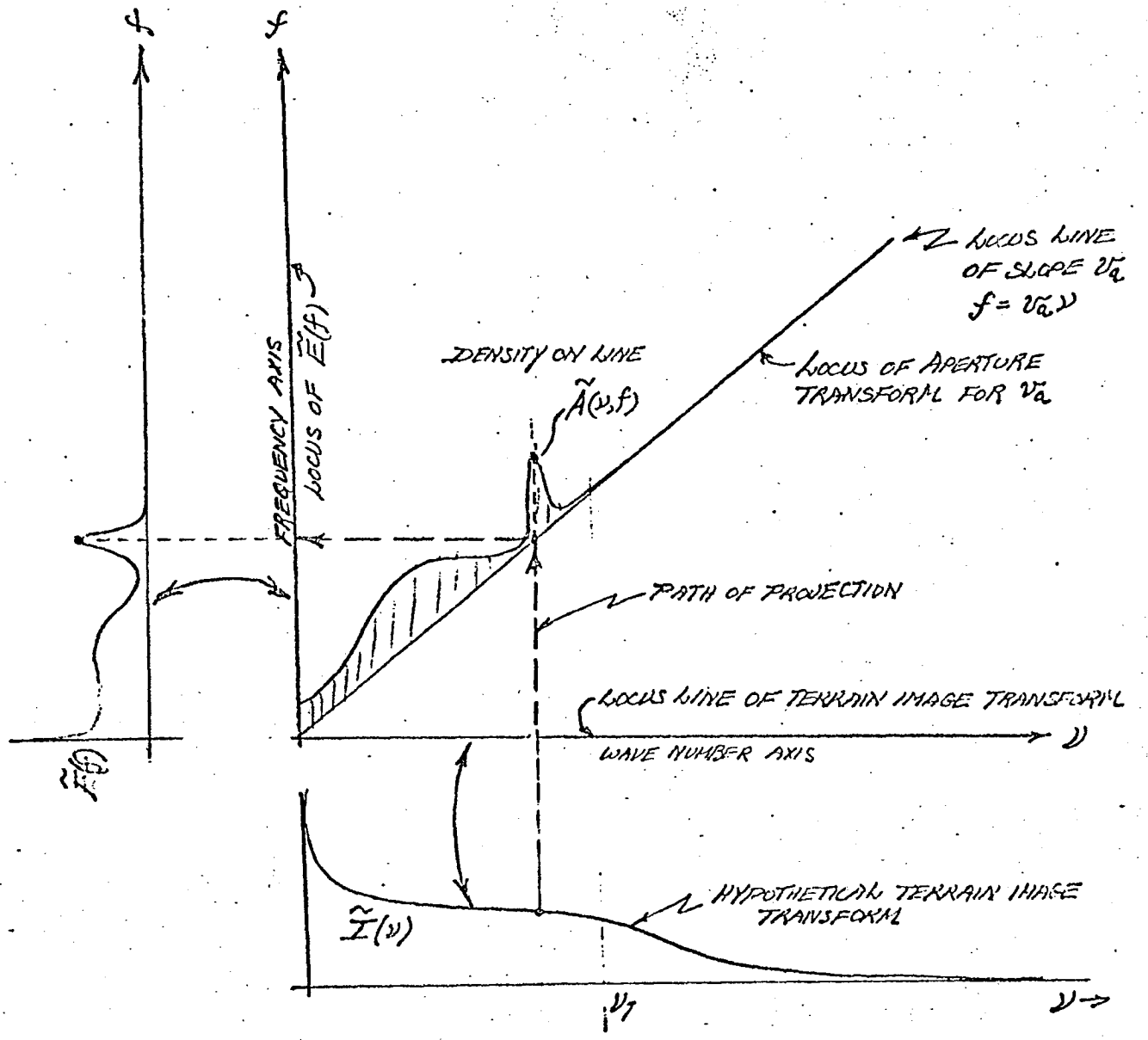

Figure 2-5. One-dimensional Case. (Projection of $\tilde{I}(\nu)$ into $\tilde{E}(f)$ by means of aperture transform $\tilde{A}(\nu, f)$, the locus of which is determined by the aperture velocity V_a (relative to the image). Because $I(\nu)$ exists only along ν axis, and $\tilde{A}(\nu, f)$ exists only along $f = V_a \nu$, convolution becomes a simple projection. In more complex situations, this simplification does not hold.)

has a power spectrum which is concentrated about f=0 and has width proportional to V_a.

Now consider an aperture which consists of a square-wave grid of density within the normal outline of the aperture. The aperture transform consists of replications of the transform of the outline spaced along the locus plane $f=V_a\nu$ at intervals equal to ν_g, the grid wave number. The amplitude of the successive images are equal to the amplitudes of the harmonics of the wave structure within the aperture. If a sinusoidal grid is used there will be three patches of density on the locus plane: one at the origin, of amplitude 1/2 representing the average transmission; and one at $(\pm\nu_g, 0)$, of amplitude 1/4 corresponding to the two cisoidal components.

As velocity V_a changes, the locus plane tilts accordingly (with tilt components V_{ax} and V_{ay}) and the narrow band projections move up and down the frequency axis.

If the aperture is not extended, as in the fixed-grid case, but is highly localized as is a pinhole or slit, the aperture transform becomes very broad, and its projection yields an $\tilde{E}(f)$ which is correspondingly broadband.

To this point, we have mentioned only fixed apertures in which velocity V_a appears only because of the motion of the aperture across the image. Such apertures are evidently worthless under null-velocity conditions and they could not be used for servo image stabilization. The treatment becomes more interesting when we allow the aperture to become dynamic. Suppose that the grid moves continuously across the aperture outline at a high velocity V_g. The transform of this aperture exist on planes of slope V_a centered along a line of slope V_g. The projections of the transform density $\tilde{A}(\nu, f)$ upon the f=0 plane are the same as for V_g=0, the fixed grid case, but the frequencies of the harmonics are moved out harmonic multiples of $V_g\nu_g$ beyond their former positions. Now the spectrum

$\tilde{E}$ (f) does not collapse to zero frequency as V_a goes to zero. As the locus planes $f = V_a \nu$ tilt with velocity, the narrowband peaks of $\tilde{E}$ (f) move about a new origin $f = V_g \nu_g$ (for the sinusoidal grid). Hence the failure of operation at null velocity and the ambiguity in sign is entirely avoided by moving the grid within the aperture. This is the basis of the phase-rate-measurement.

2.5.2 Aperture Modulation

Optimum design of a spatial filter IVS requires careful consideration of aperture shape and shading in relation to grid spatial frequency. The choice of grid spatial frequency is relatively easy to make, being based on observation of measured spectra of typical scenes. Not so obvious, however, is the choice of "best" aperture shape and apodization (shading).

Previous studies have established that a circular aperture is best because it results in minimum noise due to transverse image velocity components. This section derives the optimum relationship between grid spatial frequency and aperture diameter by means of Fourier Transform methods, and establishes the attenuation factor for D.C. aperture modulation in terms of grid wave number, aperture diameter, and the degree of Gaussian edge diffusion.

"Aperture modulation" is a cogent consideration because it can be the limiting factor in the ability of an IVS to function properly under conditions of high scattered light (haze) and/or low scene contrast. Aperture modulation manifests itself in the following forms:

a) "scalloping" or periodic low frequency noise superimposed on the output voltage of the IVS

b) apparent "drop-outs"

c) in the extreme case, complete inability to discern scene motion in the presence of overwhelming "haze" light.

Fortunately, aperture modulation can be reduced a million-fold by employing a moderate degree of aperture edge gradient diffusion.

In the Hycon Beta System, aperture shading can be effected either at the input field lens or in proximity to each channel's photomultiplier tube. The use of a single common shading mask at the field lens has the advantage of simultaneously compensating both the X and Y channels, while protecting the field lens from dirt and scratches. Individual X and Y aperture masks, in the form of a small hole punched in a thin metal plate and situated between the disc and each photomultiplier tube, would be an alternate solution.

2.5.3 Aperture Response to Mean Illumination

The response of the IVS to background or mean illumination can be understood and computed in terms of the aperture amplitude spectrum and the terrain amplitude spectrum. Figure 2-6 illustrates the manner in which the terrain amplitude spectrum may be projected, by reflection in the aperture amplitude spectrum, upon the temporal frequency axis to yield the amplitude spectrum of the photodetector signal. While the amplitude spectra of the terrain and the output signal are complex, for purposes of discussion and illustration we show only the moduli in Figure 2-6.

The IVS may be considered to consist of a grid, moving at velocity V_g (with respect to a stationary terrain), upon which is superimposed a (circular) aperture moving at a much slower velocity V_a. The grid transmission is a periodic squarewave of spatial frequency ν_g. The radius of the circular aperture is a.

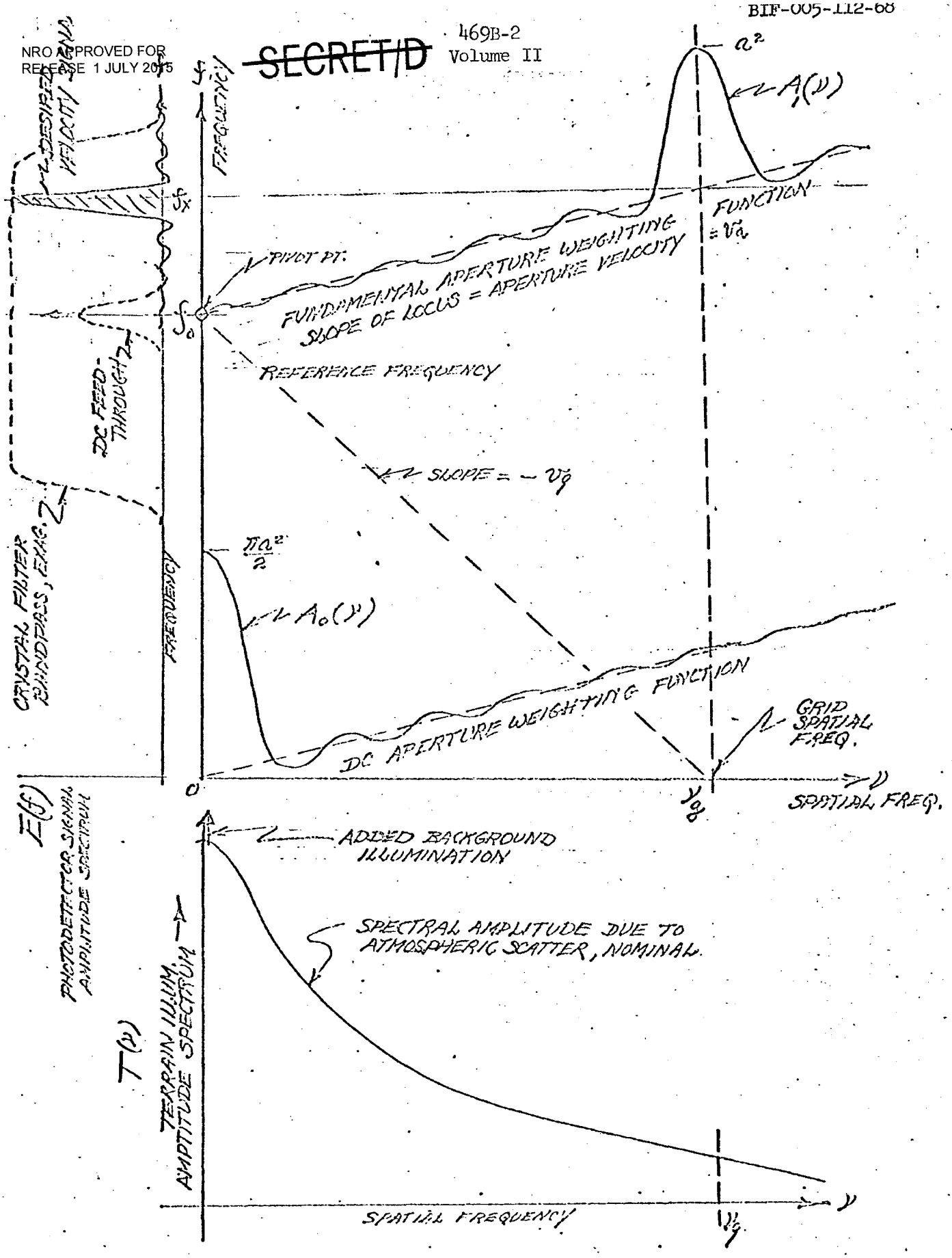

Figure 2-6. Illustrating the Derivation of Output Spectrum By Projecting the Terrain Illumination Spectrum Onto Frequency Axis by Means of the Aperture Spectrum.

The amplitude spectrum of the combined aperture-grid is found by convolving the spectra of the moving aperture with that of the rapidly moving grid. When this is done, it is found that the density of the combined aperture-grid amplitude spectra lie wholly along lines of slope V_a which intersect the frequency axis at multiples of $V_g \nu_g = f_o$, where f_o is the "carrier frequency" of the IVS system. Because the rectangular grid has only zeroth plus odd harmonies, there is one such line of slope through the origin, other through $\pm f_o$, $\pm 3f_o$, $\pm 5f_o$, etc. However, a filter is used to eliminate signal components outside a narrow region about $\pm f_o$. This region is shown, grossly exaggerated, in Figure 2-6 as "crystal filter bandpass". The slope is also very greatly exaggerated in the figure.

We have said that the aperture amplitude spectrum exists only on the lines of slope V_a. Along these lines, the amplitude spectral density is distributed in the exact form of the amplitude spectrum of the circular aperture alone (without the grid) with the origins shifted by multiples of ν_g. Thus a weight function of peak magnitude $\pi a^2/2$ occurs about the origin due to the D.C. component of grid transmission, another falls at $\pm \nu_g$ (on the line of slope V_a through $f = \pm f_o$) due to the fundamental component of the grid, its amplitude being $\pi a^2/\pi$. These features are shown in Figure 2-6 labeled $A_o(\nu)$ and $A_1(\nu)$.

The output signal spectrum E(f) is obtained by taking the value of the terrain amplitude spectrum $T(\nu)$, multiplying it by $A_1(\nu)$ [for the fundamental case], and replotting the resulting product as E(f) where $f = \nu(V_g + V_a)$. $A_1(\nu)$ is highly localized to the region close to ν_g; hence, we expect most of the signal to consist of components near $f_x = \nu_g(V_g + V_a)$. But the terrain amplitude spectrum invariably rises rapidly near the origin of ν, and it may

have a large singular peak at the origin due to mean illumination, especially if such background illumination is added. Therefore, it is possible for the product of the large D.C. amplitude of $T(\nu \approx o)$ and the residual ripples of $A_1(\nu \approx o)$ to have a resultant magnitude comparable to $A_1(\nu_g)T(\nu_g) = E(\nu_g)$ if special care is not taken to keep the ripples of $A_1(\nu \approx o)$ very small.

When D.C.-feedthrough occurs, it appears as a photodetector output component at the carrier frequency f_o which beats with the desired component at f_x. When the "feedthrough" is small, the effective frequency of the output wave is sinusoidally modulated at the difference frequency; for larger feedthrough, the modulation becomes quite non-linear. The effects can be computed readily by analyzing the rotation of the vector resultant of the superposition of a fixed and a rotating vector.

The amount of feedthrough depends upon the magnitudes of $A_1(\nu)$ and $T(\nu)$. Since $T(\nu)$ is invariably much larger at $\nu = o$ than elsewhere, we may concern ourselves almost wholly with $A_1(\nu \approx o)$, minimizing this value as far as necessary by weighting the transmission pattern of the aperture (not the grid).

2.5.4 Aperture Amplitude Spectrum of Circular Aperture

The amplitude spectrum of a circular aperture of radius 'a' is

$$A(\nu) = \pi a^2 \frac{2J_1(2\pi a \nu)}{(2\pi a \nu)} \qquad (2.11)$$

where J_1 is the first-order Bessel function. In the IVS, a = 3.56 cm and ν_g - 3.67 cm^{-1} . The argument of the Bessel function $2\pi a \nu_g = 82$ when ν_g is substituted for ν, corresponding to the condition for D.C. (remember that

$$A_1(\nu) = \frac{\pi a^2}{\pi} \frac{2J_1[2\pi a|\nu-\nu_g|]}{2\pi a|\nu-\nu_g|} \qquad (2.12)$$

because of the shift or origin to ν_g).

The amplitude of the waves of $J_1(z)$ for large z is given approximately by

$$\text{Ampl.}\left[J_1(z)\right] \approx \frac{1}{\sqrt{\pi z/2}} \qquad (2.13)$$

When $z = 82$, $J_1(82) \approx 0.81$ in amplitude; hence

$$\frac{2J_1(82)}{82} \approx 0.002$$

and we conclude that the aperture "response to D.C." for an undiffused circular aperture is 0.2%. This means that if $T(\nu \approx o)$ were 500 times as large as $T(\nu \approx \nu_g)$, which it might well be under some circumstances, the "feedthrough" would equal the desired signal, leading to very serious errors in the velocity output.

2.5.5 Aperture Diffusion

To reduce the response of the aperture to the large contributions from $T(\nu \approx o)$, we seek a multiplier in the spectral space (ν) which is unity near $\nu = \nu_g$ and falls off rapidly away from $\nu = \nu_g$, especially reaching small values as ν approaches zero. The "convolution theorem" of Fourier Transforms tells us that multiplication by such a weighting function (attenuator) in ν-space is equivalent to convolution of the circular aperture by a "diffusing function" in the physical x-space. Further, the diffusing function and the weighting function are Fourier Transform mates.

For example, if we use a diffusing function

$$L(\gamma) = \frac{1}{2\pi\beta^2} e^{-\frac{\gamma^2}{2\beta^2}}$$

where γ is the radius and β is the width (parametric) of the circularly symmetric diffusing function, the weighting function in ν-space is

$$F(\rho) = e^{-2\pi^2\beta^2\rho^2} \tag{2.14}$$

where ρ is the radius vector in ν-space. $F(\rho)$ is a function which is unity at the origin and falls of exponentially with ρ^2.

Suppose that we wish to attenuate the "feedthrough" by a factor "d"; then

$$1/d = e^{-2\pi^2\beta^2\nu_c^2}$$

and

$$\beta = \frac{1}{\pi\nu_c}\sqrt{\frac{\ln d}{2}} \tag{2.15}$$

If d = 1000, ln d = 6.908, and $\beta = 0.16$. Since a = 3.56, $\beta/a = 1/22$. A slide taken through the center of the diffusing function would drop to half-amplitude in a (radial) distance

$$\gamma_{\frac{1}{2}} = \beta\sqrt{2\ln 2} = 1.18\beta \tag{2.16}$$

After diffusion, the circular aperture transmission will fall off at the edges at a (midpoint) slope of slightly less than $\sqrt{1/2\pi\ \beta^2}$.

Note that the "attenuation" d increases very much more repaidly than β; thus slightly increased diffusion provides marked decrease in the response to background illumination.

2.6 EXTRACTING VELOCITY INFORMATION

We have seen that the shape and make-up of the aperture largely determines the spectrum of the photosignal. Extended apertures yield narrowband photosignals at a carrier frequency dependent upon the grid wave frequency $V_g \nu_g$. Without grid wave number ν_g, the carrier frequency goes to zero leaving a low-pass signal with bandwidth dependent on the aperture bandwidth and the velocity. Very small apertures yield wideband photosignals by virtue of wideband aperture spectra. These two types of signal, wide and narrowband, have very different noise susceptibilities, as illustrated in Figure 2-7 because of the received light energies (small for small apertures) and circuit bandwidths (large bandwidths admit proportionately large noise contributions) and different methods must be used to extract the desired velocity information from the photosignal.

When the information contained in the photosignal is broadband, such as that produced by a flying-spot (aperture), one must resort to correlative techniques: successive cycles of the signal are compared to determine the shifts produced by the forward velocity V_a. Since no integration (to speak of) occurs in generating the signal, it must be processed in the time domain. The aperture may be enlarged to approximate a typical correlation element in the interest of higher signal without loss of information. Such a correlation element is the Fourier transform of the terrain power spectrum; to a good degree of approximation, the terrain may be considered to be made

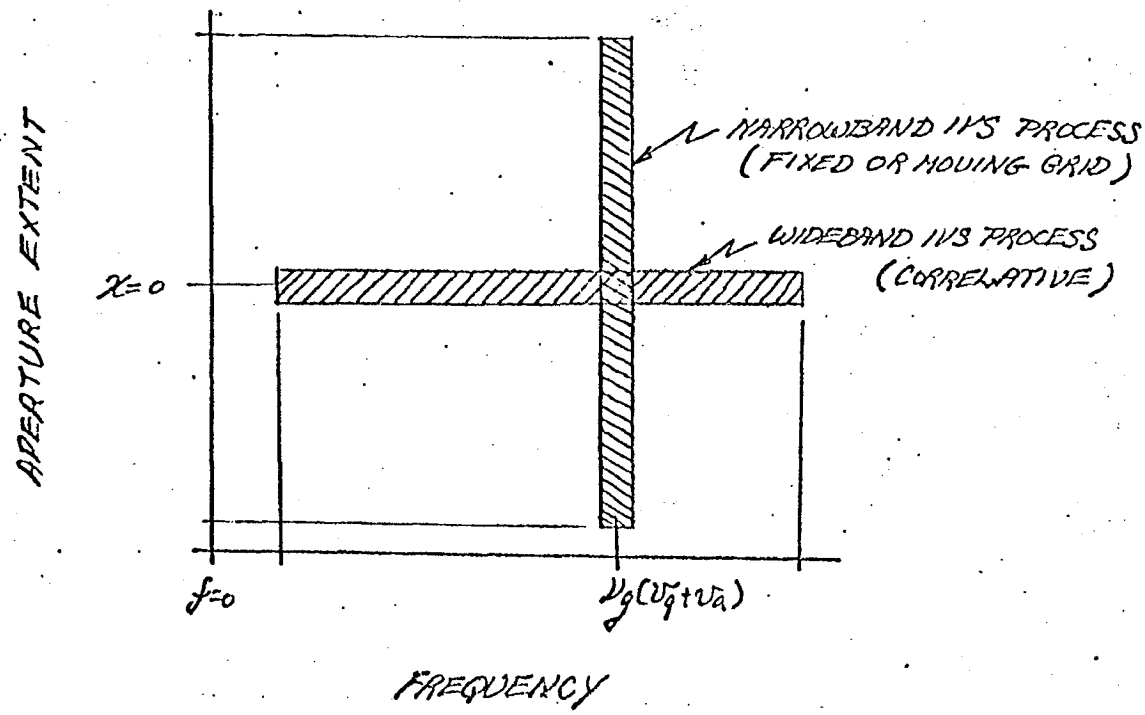

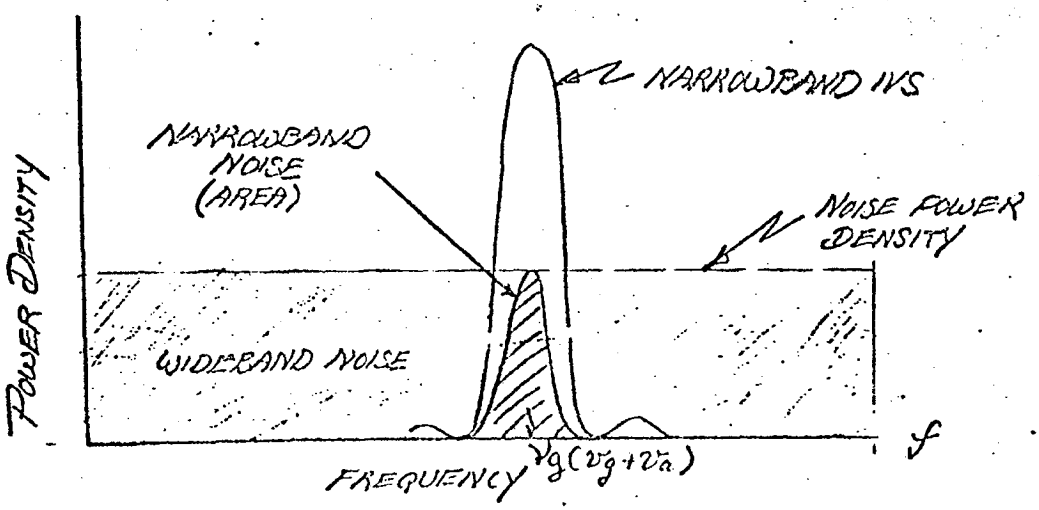

Figure 2-7. Bandwidth Difference and Noise Susceptibility of Correlative and Frequency Measuring Beta Systems.

up of small tiles, the luminance of each tile being independent of every other, the area of each tile being equal to the mean area covered by the (two-dimensional) terrain autocorrelation function. The number of such tiles within the field of view represents the number N of independent samples available to the correlative process of velocity estimation.

Extended apertures, such as grids, perform an integration over the field of view. When the grid is periodic, the resulting signal represents the harmonic component of the terrain at wave number ν_g, and the spectrum of the signal is a narrow peak at $f = \nu_g(V_a + V_g)$ of width determined by the spectrum of the aperture outline or envelope. Narrowband signals must be processed in the frequency domain. The velocity information is now contained in the frequency of the signal and the location of the spectral peak.

Two ways are used to estimate the frequency of such a narrowband signal: counting the number of zero-crossings per unit time or correlating the signal with a local oscillator of known frequency (the latter being the phase-lock method). A convenient hybrid of these methods correlates not the full wave shape, but locks the local oscillator to the square wave signal which results from strong limiting of the original photosignal. Such limiting is essential in achieving wide dynamic range. A further advantage of this hybrid method is that the local oscillator may be square wave also. The phase-lock then occurs not between the sinewaves (of slowly varying phase and amplitude) but between similar square waves. Simple switching and logic circuits can therefore be used in lieu of linear multipliers and integrators, advantages well known in telemetry.

Although we reserve the term correlative method for image velocity sensing techniques which cross-correlative successive time-sequence photo-signals to estimate velocity, all techniques must involve correlation in some form. The various techniques are generally identified by specific titles. However, filtering, integrating grid transmission times terrain luminance, matching local oscillator waveform to photosignal, etc. are all forms of the basic mathematical operation of correlation.

2.7 ERROR

2.7.1 Sources

To devise several ways of doing the same job is often possible. This is evidently true in the case of image velocity systems. The differences in performance generally are of two types: probable error, and dynamic response. Usually speed of response can be traded for probable error, since both are factors in the basic instrumental limitation, the rate of information input (or the noise bandwidth of the process under observation).

The performance of physical systems in real life is strongly conditioned by noise, and the sources of noise which are operative in a given situation determine the resultant error.

Since terrain constitutes a random pattern in motion, it generates a noise which we will call pseudo velocity. Our term arose in the following way in the analysis of grid-aperture systems. When terrain is viewed by the photo sensor

through a sinusoidal grid, the photocurrent is proportional to the amplitude of the sinusoidal component of wave number ν_g in the terrain within the field of view. If this component were coherent in successive fields of view (i.e., if the wave merely was a continuation of the original one, without change in amplitude or phase), then the photocurrent would oscillate sinusoidally at a frequency $V_a \nu_g$. This frequency can be interpreted as indicating a velocity V_a. If the ν_g component is not coherent (as in a random pattern), the photocurrent wave form will shift in relative phase (as well as amplitude) as the forward velocity introduces new elements into the field of view, and the apparent frequency will fluctuate with these phase variations; the velocity estimate will be V_a plus the pseudo velocity due to the random pattern.

The pseudo velocity is completely dependent on the aperture power spectrum. The purpose of the aperture (envelope) is to define the field, but its detailed design is motivated by the desire to minimize the pseudo velocity error. We have referred to this noise as terrain noise since it represents the noise in the velocity signal due to the random terrain pattern.

Terrain noise includes both amplitude and phase fluctuations of the photosignal due to terrain randomness. In strongly limited signal processing, we are concerned only with phase fluctuations, or in most cases, only with zero crossings. However, amplitude fluctuation is important, since the question of signal drop out is often raised. Given an operating threshold (Emin) for reliable operation, say Emin in the zero crossing and/or phaselock modes of operation, the probability of dropout is given by the area of the Rayleigh distribution

$$\rho(R) = \frac{R}{\sigma_E^2} e^{-R^2/2\sigma_E^2} \qquad R \geq 0 \qquad (2.17)$$

lying below R = Emin the area is

$$\text{(Prob. of drop out)} = 1\text{-}e^{-(\text{Emin})^2 / 2\sigma_E^2}$$

where σ_E^2 is the total photosignal power. The probability distribution for the duration of drop out is a more complex statistical problem involving the form of the signal power spectrum P_E. Since Emin can be made very small in modern electronic circuits, a more critical consideration is probably whether the signal becomes lost in the noise, even though the signal still exceeds the threshold.

A second source of noise is the shot effect due to discrete arrival of electrons and photons. For simple photosensors, such as photodiodes, the shot noise current is given by

$$B_S = 2\epsilon B_W i_o (\text{amperes})^2 \qquad (2.18)$$

where ϵ is the electronic charge, B_W is the noise bandwidth of the signal channel, and i_o is the mean photocurrent. Current due to background illuminance plus-dark current constitutes i_o. When electron multiplication takes place, the shot noise is enhanced by the factor s/(s-1), where s is the dynode multiplication factor.

Another noise contribution is due to thermal effects in the input impedance, other circuit components being negligible contributors because of lower impedance levels. The thermal or Johnson noise is given by

$$B_T = \frac{4KTB_W}{R} (\text{amperes})^2 \qquad (2.19)$$

where k is Boltzmann's Constant, T the absolute temperature, and R the effective impedance of the input circuit. Thermal noise is to be considered for semiconductor photosensors, but is not a factor in photomultipliers.

Semiconductor noise is a contributing factor in cases involving low frequencies since this type of noise is inversely proportional to frequency. Carrier systems avoid this noise contribution by virtue of their operation at frequencies well above the region of semiconductor noise. Circuit noise becomes less significant in successive stages due to the increase in signal levels. In well designed circuits using modern components, it is believed that circuit noise makes a negligible contribution to the overall noise problem.

The aperture may contribute signal disturbances of both random and systematic character. For example, random variations in grid spacing line width, or density will show up in the aperture power spectrum as decreased power (light loss) in the desired frequency component; these kinds of (draftmanship) errors do not cause peak spreading or distortion, and their effect is, therefore, not really significant. However, systematic errors in grid period, such as those due to grid-disc eccentricity, will cause frequency modulation at disc frequency. Such low-frequency FM can be minimized by (1) careful location of reference sensors to compensate for residual eccentricity, and (2) eliminating the surviving output variations by filtering, which, at high disc speeds, lies well above the required output bandwidth.

The effects of all random noise sources can be obtained by superposing their corresponding power spectra:

 ~~SECRET/D~~

1) Terrain noise has the total power and spectral distribution resulting from the convolution of the aperture power spectrum with the terrain power spectrum, as described in subsection 2.5.

2) Shot and thermal noise contributions have the power densities given in equations 2.12 and 2.13 not including the Bw factor.

The total noise power from these sources is that given in the cited equations. The spectral distribution is that of the signal channel, which is determined by the bandpass characteristics of the circuits employed. For example, in a double cascade of bandpass filters, with each simple resonant circuit of quality factor Q at frequency f_1, the bandwidth is

$$B_W = \frac{\pi f_1}{2Q} \tag{2.20}$$

and the power spectrum is of the form

$$\left[\frac{f_1^2}{f_1^2 + 4Q^2(f - f_1)^2} \right]^2 \tag{2.21}$$

3) Semiconductor noise and circuit noise, where significant, have 1/f and circuit bandpass behavior, respectively. In general, these will not be significant in preferred types of image velocity sensors.

The effects of noise are described by different formulas for different types of sensors.

2.7.2 Correlative Systems. Such systems are unusually susceptible to noise because (1) signal power is quite low due to the necessary use of small apertures, and (2) noise bandwidth is large to accomodate the required signal information. Velocity error distribution for correlative systems can be assumed to be normal with variance σ^2_{VC} . A block diagram for a typical correlative system is illustrated in figure 2-8. The velocity tracking signal is derived from the difference of the early and late correlators. The correlation value produced by each of the correlators has an error associated with it which is dependent upon the degree of existing correlation ρ and the number N of independent

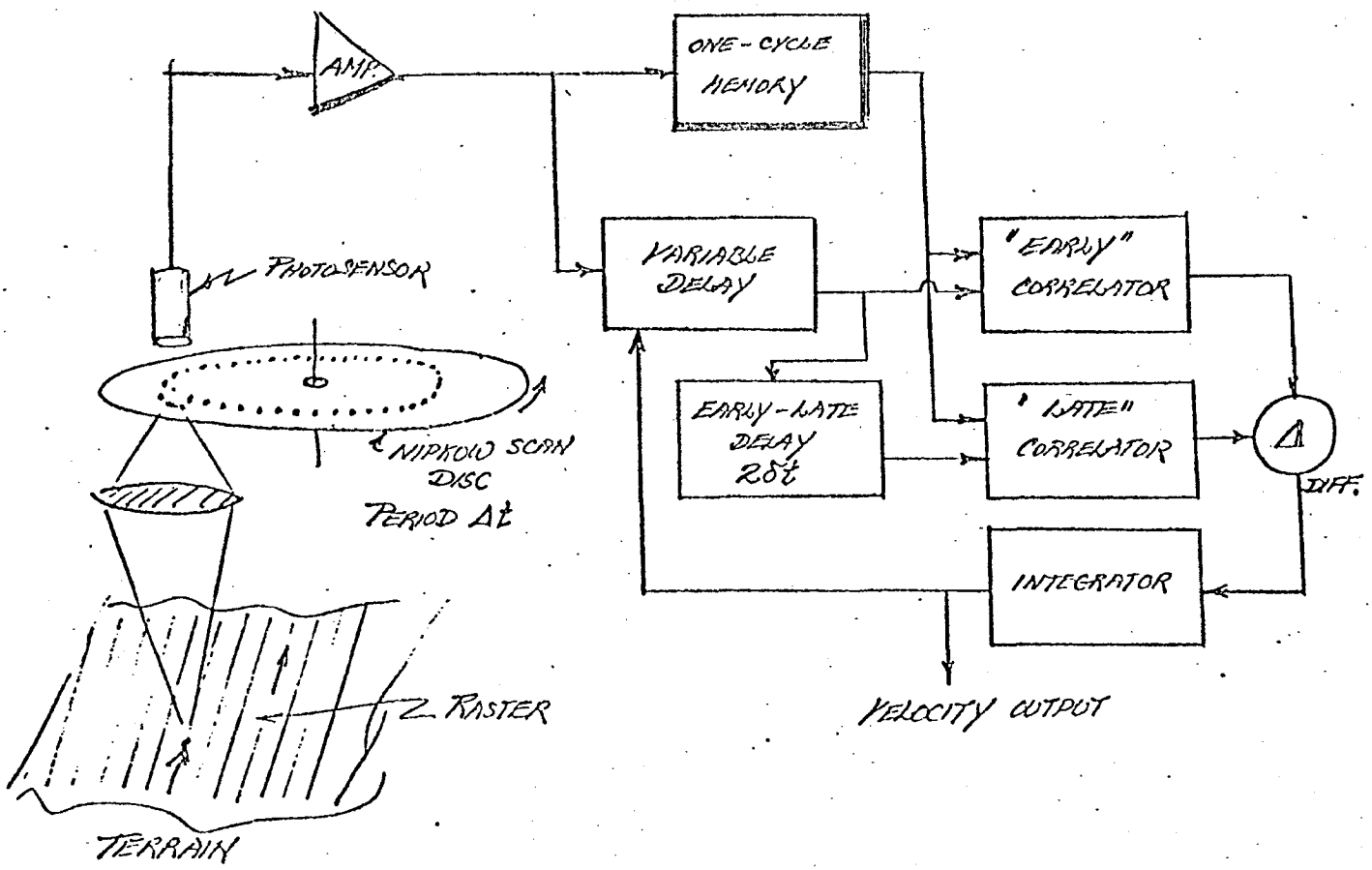

Figure 2-8. Correlative System Block Diagram.

tiles of terrain which enter into the place of continuous functions is a justifiable approximation which permits us to make use of tabulated values (from the work of F. N. David[1] and of Karl Holzinger[2]) of the correlation error.

The number N is equal to the scanned area divided by the correlation area of the terrain (the mean area of the Fourier transform of the terrain power spectrum), assuming that the correlations are performed once per scan interval (Δt). Existing correlation ρ can be deduced in terms of the power spectra of the photosignal due to terrain (essentially the scaled terrain power spectrum), the power spectrum of the noise, and the early-late time shift $\pm \delta t$, a small part of Δt (generally $\delta t < \Delta t/N$). However, in the noise power spectrum we must include Terrain noise due to failure to trace over the same tiles in consecutive scans. The basic assumption of the correlative method is that the signals being correlated are, hopefully, identical except for the displacement due to the motion in the forward direction. However, some noise is introduced by the shift of field of view, even though the scan occurs in a raster of lines parallel to the forward direction. If some lateral velocity exists, the scans will not see exactly the same sequence of tiles, and the correlation then drops off. Thus, an adequate treatment of the errors of a correlative system must take into account that the translational and vibrational effects on the retrace distribution.

Let us assume that the lateral displacement of traces for the interval Δt is characterized by a distribution $P_{\Delta t}(Y)$. Then we may expect that the

---

[1] David, F.N., "Tables of the Ordinates and Probability Integral of the Distribution of the Correlation Coefficient in Small Samples", Cambridge, England: The University Press, 1938.

[2] Holzinger, K., "Tables of the Probable Error of the Coefficient of Correlation as Found by the Product Moment Method", No. XII, Cambridge University Press, 1925.

average correlation of the sequence of terrain tiles will be

$$\bar{\rho}_T = \int_{-\infty}^{+\infty} P(y)\rho(o,y)\,dy. \qquad (2.22)$$

where $\rho(X,Y)$ is the terrain correlation function. The total photosignal power is then

$$P_E \bar{\rho}_T^2 + P_E(1-\bar{\rho}_T^2) + P_N. \qquad (2.23)$$

where P_E is the power of the terrain signal and P_N is the noise due to thermal and shot effects. Renormalizing, we obtain the signal to noise ratio

$$\text{Sig/noise} = \frac{P_E \bar{\rho}_T^2}{P_E(1-\bar{\rho}_T^2) + P_N} = \frac{\rho_*^2}{1-\rho_*^2}. \qquad (2.24)$$

which may be used to compute the resulting, reduced peak value of signal correlation (ρ_*). The shape of the correlation function is obtained by taking the Fourier transform of the combined power spectra (or the sum of the individual transforms). In order to obtain the required steering signals, it is necessary to operate off the peak a short distance on either side, ($\pm \Delta X$ in displacement) and to take the difference of the resulting correlations. The slope of this difference at null is $2(d\rho/dx)\big|_{\Delta X}$. The situation is illustrated in figure 2-9.

The uncertainty in the null position is $\sqrt{2}$ times the uncertainty in $\rho(\Delta X)$ divided by the slope at null. The uncertainty in the null position

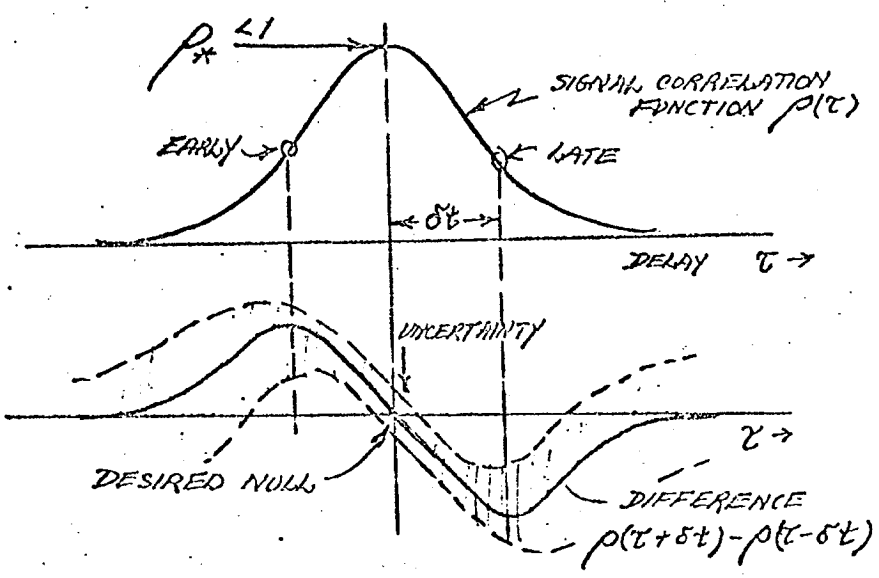

Figure 2-9. Derivation of Steering Signals from Early-Late Correlations.

(Uncertainty in null position)

is also equal to $\Delta t \sigma_V$, where σ_V is the velocity error of the correlative type sensor. Hence, if we can find the uncertainty in $\rho(\Delta X)$, we have a complete method for finding the velocity error.

The uncertainty in evaluating a correlation coefficient is dependent upon the actual value of ρ for the sampled population, and upon the number of independent samples N. The complete distribution function is given by F. N. David as

$$P(\gamma) = \frac{(1-\rho^2)^{\frac{N-1}{2}}(1-\gamma^2)^{\frac{n-4}{2}}}{\pi(n-3)!} \frac{d^{n-2}}{d(\gamma\rho)^{n-2}}\left(\frac{\arccos(-\rho\gamma)}{\sqrt{1-\rho^2\gamma^2}}\right) \quad (2.25)$$

where γ is the uncertain value derived by computation on the limited sample. Fortunately, this equation has been converted to tabular values and graphs for typical values, figure 2-10 shows probabilities for small N. For large N and small ρ, the uncertainty in the computed correlation is well represented by:

$$\sigma_\rho = (1-\rho^2)/\sqrt{N} \quad (2.26)$$

Knowing $\rho(X)$ from the Fourier transform of the total power spectrum scaled to peak value ρ_*, we may evaluate it for $X = \Delta X$, also determine the slope $(d\rho/dx)|_{\Delta X}$. The velocity error is then completely computable as outlined above.

The numerical values of error depend upon the particular make-up of the particular Beta system.

2.7.3 Zero Crossing. Frequency measuring types of image velocity sensors have been used for many years with only moderate success. The error evaluation

~~SECRET/D~~

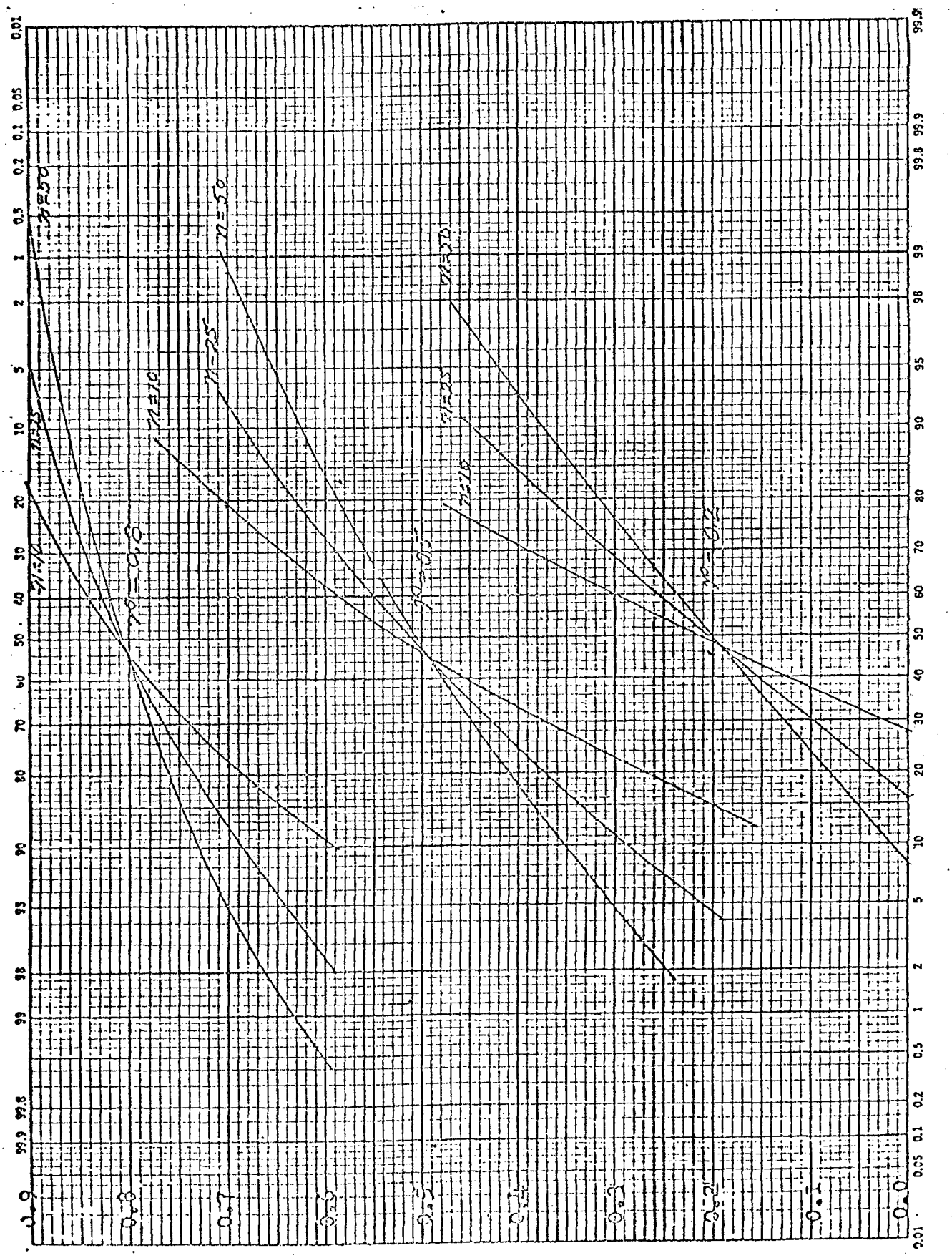

Figure 2-10. Probability Integral of Correlation Coefficient Distribution.

involves an examination of the errors involved in counting the zero-crossings of the signal waveform during a specified interval. The longer the counting interval (or filter time constant), the smaller the variance of the counts determined. The expected number of zero-crossings is

$$\bar{N}_o = \left\{ \int_{-\infty}^{+\infty} f^2 w(\delta) d\delta \Big/ \int_{-\infty}^{+\infty} w(\delta) d\delta \right\}^{1/2} \qquad (2.27)$$

in which $w(\delta)$ is the power spectral density of the signal, or $P_E(\delta)$ in our case. The variance of N_o is difficult to obtain analytically. See discussion by J. S. Bendat.[3]

In the absence of complete statistical results for the effect of counting time (or averaging time) upon the variance of the velocity, we resort to an approximation as follows.

Consider a narrowband Gaussian noise, the photosignal resulting from a fixed grid. The waveform will be characterized by an autocorrelation function which consists of a cosine wave of frequency within an envelope which is the correlation function for the outline of the aperture. See figure 2-11. This correlation will be high (near unity) for delays close to $\tau_1 = 1/\sqrt{a}\, v_g$, slightly less at $2\tau_1$, etc. If a zero-crossing (negative going, perhaps) exists at $t = 0$ we may expect one near τ_1; at τ_1 the curve will lie $\sigma\sqrt{1 - R^2(\tau_1)}\, Z$ above the zero axis, σ being the root mean square wave amplitude (square root power), $R(\tau_1)$ the correlation at τ_1, and Z a normally distributed random variable of zero mean and unit variance.

---

[3] Bendat, J.S., "Principles and Applications of Random Noise Theory", J. Wiley & Sons, 1958.

~~SECRET/D~~

The error in zero-crossing interval is obtained by dividing the amplitude error by minus the wave slope. The slope is approximately $2\sqrt{2}\ \pi\sigma/\tau_1$, and the interval becomes

$$\frac{-\tau\sqrt{1-R^2(\tau_1)}}{2\pi\sqrt{2}}\ z$$

as illustrated in figure 2-12.

Now let us determine τ_1 by observing the time taken for a known number (N_T) of zero-crossings to occur in one direction. The time variance of this observation will be

$$\frac{N_T\,\tau_1^2\left[1-R^2(\tau_1)\right]}{8\pi^2}$$

and the fractional root mean square time error is

$$\frac{\sigma_T}{T}=\frac{1}{(N_T\tau_1)}\times\frac{(N_T\tau_1)\sqrt{1-R^2(\tau_1)}}{\sqrt{N_T}\ 2\sqrt{2}\ \pi}=\frac{1}{2\pi}\sqrt{\frac{1-R^2(\tau_1)}{2N_T}}\qquad(2.28)$$

The fractional velocity error is the same quantity.

In carrying through this approximation for velocity error due to zero counting we have not counted zeros per given time, but time per given zeros. The troubles which arise in statistical theory due to the discreteness of zero-crossings do not occur in physical systems used in the Beta system. This is because such systems operate, generally, in terms of time rather than count, and our treatment is consistent with this distinction.

The results expressed in (2.28) are expected to be low by the factor $\sqrt{\pi/4}$.

~~SECRET/D~~

~~SECRET/D~~

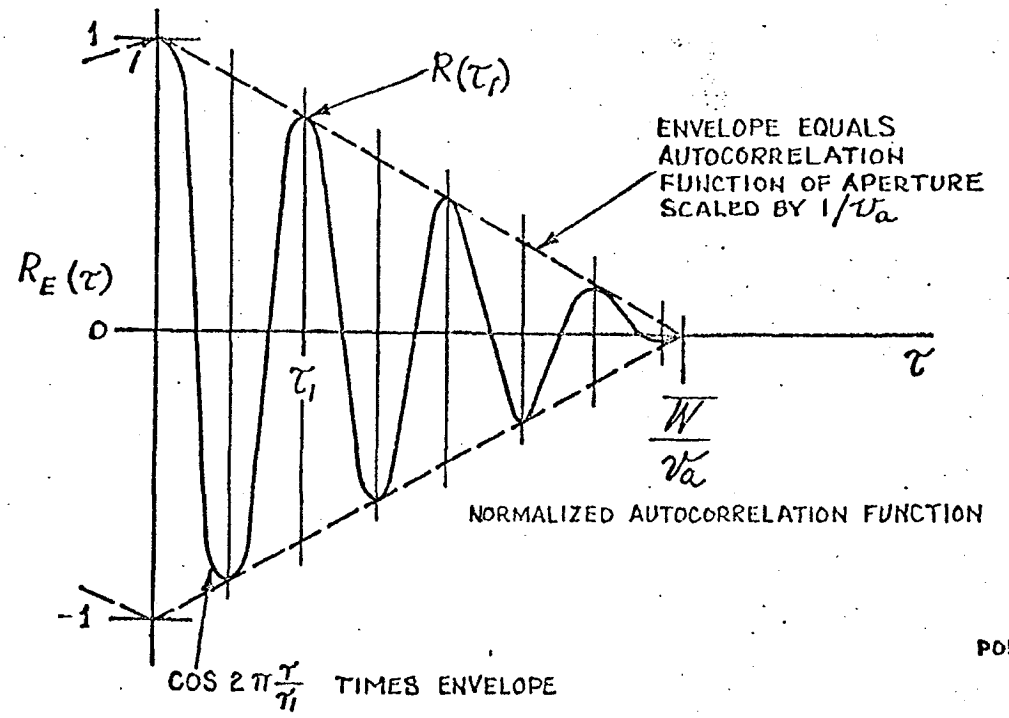

Figure 2-11. Autocorrelation Function of Photosensor Output Signal $E(t)$ for Rectangular Aperture width W and velocity V_a . $\tau_1 = 1/[\nu_g(V_a V_g)]$.)

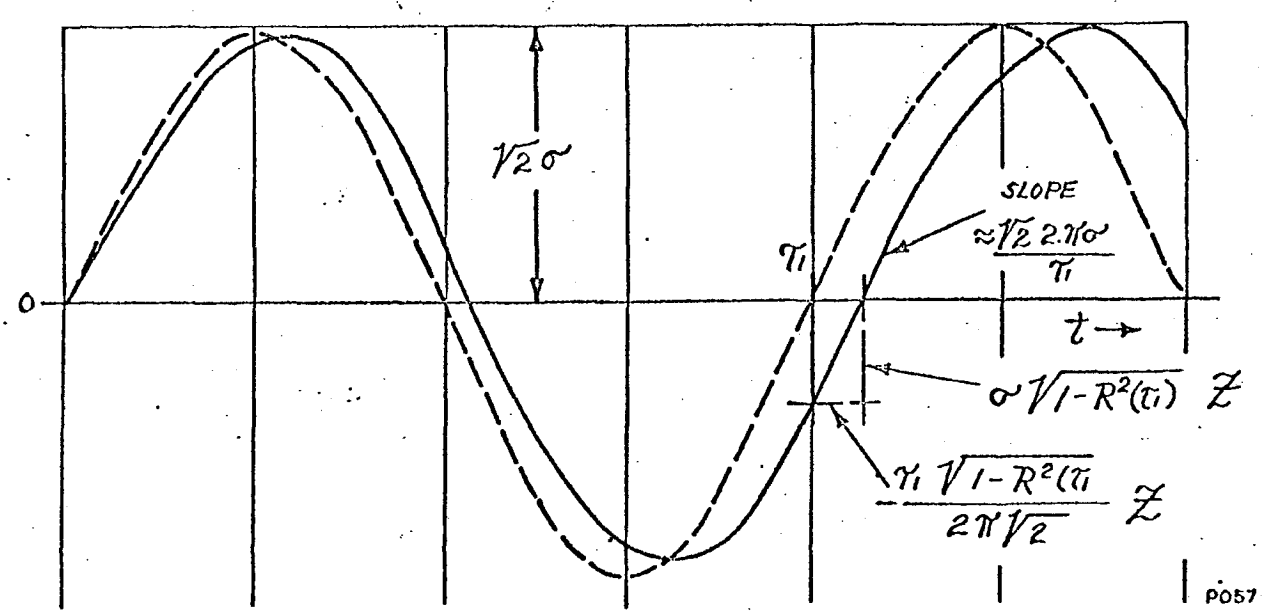

Figure 2-12. Random-Time Error Derivation of Zero Crossings. (For bandwidth limited noise in terms of normalized autocorrelation function of photosensor signal. Z is a normally distributed noise with zero mean and unit variance, having uniform power spectral distribution for $-\frac{1}{2t_1} \leq f \leq +\frac{1}{2t_1}$, otherwise zero.)

~~SECRET/D~~

The reason is that we have ignored the fluctuation of the amplitude of the photosignal wave, setting it equal to $\sqrt{2\sigma}$. A more rigorous treatment, which includes the amplitude, has yielded the larger result.

The error in the frequencing measuring case is thus shown to be dependent upon $R(\tau_1)$ and N_T . R itself is the autocorrelation function relating to the aperture envelope. The term $\tau_1 = 1/V_a v_g$ may be quite large when V_a is small. In addition, for a given interval of averaging, N_T will decrease as V_a does. The result, which depends in detail upon the shape of $R(\tau)$ is essentially that the fractional velocity error is inversely proportional to V_a Such a reasonable outcome conceals the fact that the timing process utilizes multivibrator waveforms, in conventional devices, which require long time constant filtering to avoid noisy velocity outputs.

2.7.4 Phase Lock. A phase-lock loop makes use of a null-correlator or phase error detector and a local oscillator which can be phase modulated in proportion to the phase error derived from the detector. Many ways of implementing the phase-lock principle exist, but most telemetry and instrumentation applications of phase-lock use strongly limited waveforms which look like square waves of non-uniform period. The local oscillator then takes the form of a voltage-variable astable multivibrator which generates a square wave of frequency proportional to the phase error voltage. This is the usual FM phase-lock method.

A second method uses the same type of phase comparison, but uses a phase-shifted, fixed-frequency, reference oscillator in lieu of the variable frequency oscillator. The fixed frequency wave is then shifted forward or back in phase at a rate sufficient to keep step with the wave being tracked. The voltage applied to the phase shifter is the integral of the phase error voltage, which remains

proportional to phase rate and, therefore, to velocity. The advantage of the phase-shifting technique is that relative velocities can be determined; that is, the reference frequency, which is phase shifted, need not be constant. This allows compensation for unwanted signal variations, such as the elimination of tape wow in the magnetic tape recording of telemetry records.

The error in a phase-lock loop depends upon the averaging time employed in the phase comparator and upon the significance of various spectral components of the signal. Our interest will be primarily in a phase-lock method in which the signal bandwidth is very much less than the bandwidth of the phase-lock loop, so the filtering is explicitly associated with the output filters and not with the loop. We are then concerned only with the fluctuations which survive the output filter.

The output of the phase tracking system is the rate of shift necessary to keep up with the input waveform. The variance in this phase rate may be computed from the zero-crossing interval τ_1 and the probability for phase fluctuations, $\Delta\phi$, given by

$$P(\Delta\phi) = \frac{1-\rho^2(\tau_1)}{2\pi}(1-\beta^2)^{-3/2}\left\{\beta\sin^{-1}\beta + \frac{\pi\beta}{2} + \sqrt{1-\beta^2}\right\} \qquad (2.29)$$

where $\beta = \rho(\tau_1)\cos\Delta\phi$ and $\rho(\tau_1)$ is the signal correlation function. On the assumption of Gaussian form for $\rho(\Delta\phi)$ where $\rho(\tau_1)$ is nearly unity, we obtain a phase variance

$$\sigma^2_{\Delta\phi} = \frac{2\left[1-\rho^2(\tau_1)\right]}{\pi\rho^2(\tau_1)} \qquad (2.30)$$

and a consequent velocity variance

$$\sigma_V^2 = \frac{1}{(2\pi \nu_g \tau_1)^2} \times \frac{2\left[1-\rho^2(\tau_1)\right]}{\pi \rho^2(\tau_1)} \qquad (2.31)$$

This variance represents the total noise power in the output prior to filtering. The noise is uniformly distributed over a total bandwidth of $f_1 = (V_a + V_g)\ \nu_g$. An output filter of low-pass bandwidth Bwo will then show an output velocity variance B_{wo}/f_1 times that of equation (2.31).

2.7.5 Analysis

Figure 2-13 illustrates the factors and relationships involved in transforming the terrain brightness B into the photocurrent I. The terrain brightness B (x,y) when imaged through a lens of f-number N, optical efficiency E, and collective transmission factors $\bar{V}$, produces an image illumination $EVB(x,y)/4N^2$ foot candles. If the effective aperture, including the spatial effects of grid transmission, is A(x,y), the integrated photocurrent is:

$$I = \frac{EVS}{4N^2} \iint_{\text{aperture}} B\ (x,y)\ A\ (x,y)\ dxdy \quad \text{amperes} \qquad (2.32)$$

where we have used the same coordinates for the terrain and its image, mapping one upon the other using an unspecified magnification. The magnification is significant only in relating the grid period to a corresponding period in the terrain pattern.

As the optical system of Figure 2-13 is translated with respect to the terrain, the photocurrent fluctuates about its mean, i_o. For a 50% opaque grid, the D.C. photocurrent is

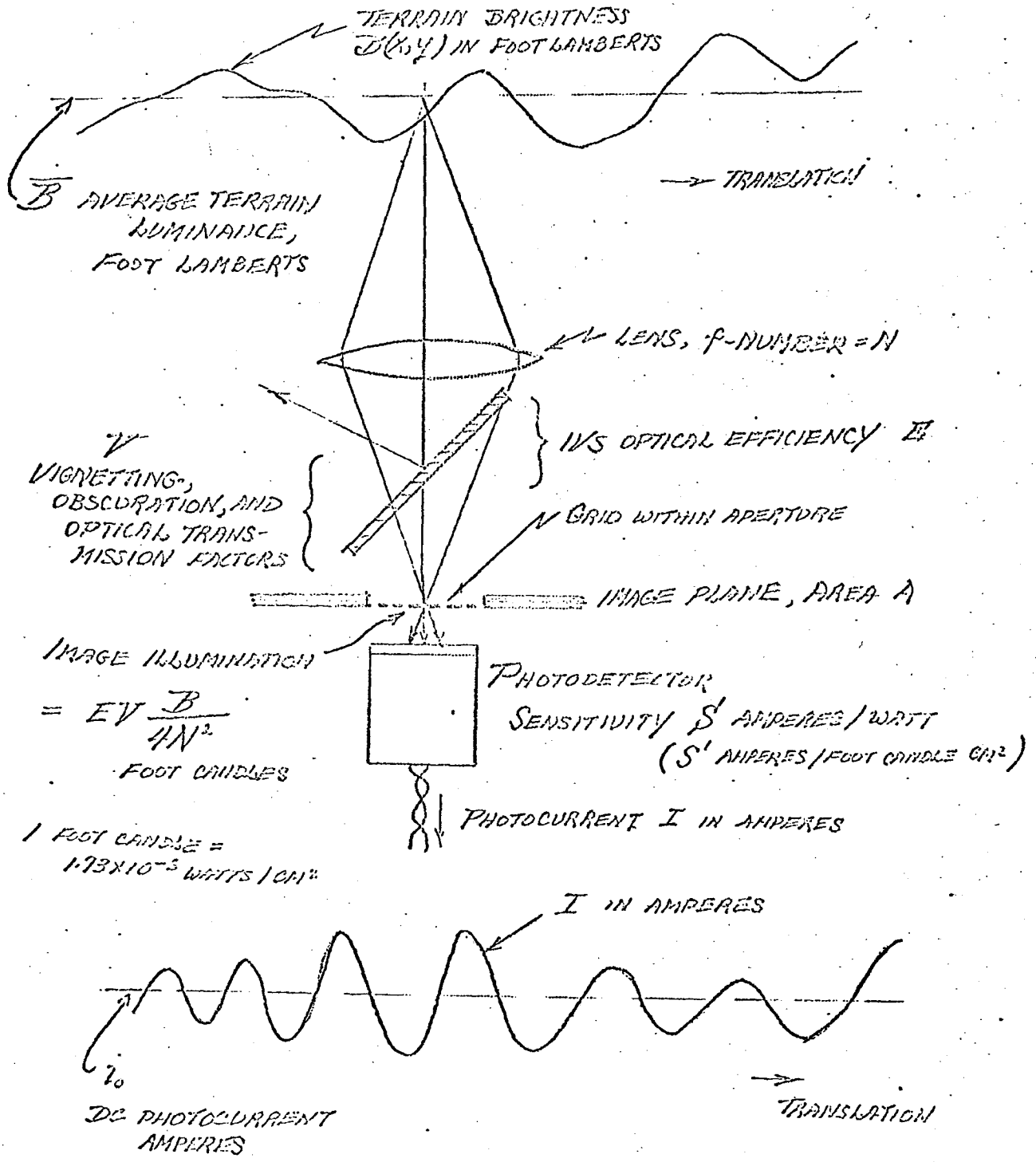

Figure 2-13. Illustrating the dependence of photocurrent I upon terrain brightness B and optical parameters.

$$i_o = \frac{EVS'A\bar{B}}{8N^2} \quad \text{amperes} \qquad (2.33)$$

where A is the entire area of the aperture. Note that the average image illumination does not involve magnification.

The fluctuation of the photocurrent will have a mean square value P_T.

$$P_T = \left(\frac{EVS'}{4N^2}\right)^2 \int\int_{-\infty}^{+\infty} P_A(\nu,\mu) P_B(\nu,\mu) d\nu d\mu \qquad (2.34)$$

where $P_A(\nu, \mu)$ is the power spectrum of the aperture and $P_B(\nu, \mu)$ is the power spectrum of the terrain luminance.

This simple relation between P_T, P_A, and P_B holds even for the moving grid-moving aperture situation provided P_A is the power spectrum of the dynamic aperture, $|\tilde{A}|^2(\nu,\mu,f$, projected on the (ν, μ) plane.

2.7.6 Velocity Error

The effect of light level enters through the noise power, P_N, which is the sum of the photocurrent mean square fluctuation due to thermal and shot effects:

$$P_N = \left\{2e i_o + \frac{4KT}{R}\right\} B_W \qquad (2.35)$$

where B_W is the noise bandwidth of the signal channel.

The variance (mean square error) of the velocity determination by the Beta System is

$$\sigma_{\dot{V}_a}^2 = \left(\frac{1}{2\pi \nu_g \tau_1}\right)^2 \frac{4(1-\rho)}{\pi} \qquad (2.36)$$

where ν_g is the grid wave number, τ_1 is the period of the carrier frequency and ρ is the photocurrent normalized autocorrelation for lag τ_1.

The autocorrelation $\rho(\tau_1)$ is easily shown to be the weighted average of the autocorrelations for the terrain signal and the noise

$$\rho(\tau_1) = \frac{P_T \rho_T(\tau_1) + P_N \rho_N(\tau_1)}{P_T + P_N} \qquad (2.37)$$

The noise autocorrelation is simply that associated with the filters which limit the signal channel. The terrain correlation is obtained as the convolution of the correlation functions of the aperture and the terrain.

Because τ_1 is the period of the carrier signal produced by the grid motion, there is little evidence of grid motion in the formulae, since only the envelope of the correlation function of aperture is used.

2.7.7 Correlation Functions

The signal channel of the Beta System is limited in frequency by a cascade of two single-resonant filters, each of the form, relative to f_1, the carrier frequency

$$P_F(\zeta) = \frac{1}{1 + f^2/f_o^2} \quad \text{single filter spectra density,}$$

whence $$R_F(\tau) = \frac{\pi f_o}{2} e^{-2\pi f_o |\tau|} \quad \text{single filter autocorrelation}$$

The correlation for the dual (cascaded) filter is obtained by convolving two single-filter correlations:

$$R_{FF}(\tau) = \frac{\pi f_o}{2} e^{-2\pi f_o |\tau|} \left\{ 1 + 2\pi f_o |\tau| \right\} \qquad (2.38)$$

from which the normalized correlation is found to be, for small τ, approximately

$$\rho_N = \left(1 - 4\pi^2 f_0^2 \tau^2\right). \tag{2.39}$$

The autocorrelation for the aperture will depend, in envelope, only upon the shape and transmission weighting of the aperture without the grid. A circular aperture of radius R and uniform transmission has a correlation $C(\lambda)$

$$C(\lambda) = R^2 (2\Psi - \sin 2\Psi) \tag{2.40}$$

where $\lambda = 2R\cos\Psi$.

The variable λ is the displacement variable; it is related to τ by the aperture velocity V_a; i.e. $\lambda = V_a \tau$. For small values of τ_1, with which we are concerned,

$$C(\lambda \to 0) \approx \pi R^2 \left(1 - \frac{2\lambda}{\pi R}\right). \tag{2.41}$$

The desired signal correlation would then be as follows (assuming that the terrain spectrum is much broader than the aperture spectrum):

$$\rho_T = \left(1 - \frac{2V_a \tau}{\pi R}\right). \tag{2.42}$$

A better Beta System is obtained if the edges of the aperture are shaded or diffused. We may consider that the diffused aperture A_D is formed by convolving the original sharp edged aperture A by a diffusing function in the form of a

two-dimensional Gaussian probability function D (r).

$$D(r) = \frac{1}{2\pi\beta^2} e^{-\frac{r^2}{2\beta^2}}. \tag{2.43}$$

Here β characterizes the width of the diffuser. An approximate result, good where λ is small relative to β, is

$$C_D(\lambda) = \pi R^2 \left\{ 1 - \frac{\lambda^2}{4\beta R\sqrt{\pi}} \right\} \tag{2.44}$$

from which one obtains

$$\rho_r(r) = \left\{ 1 - \frac{V_a^2 r^2}{4\beta R\sqrt{\pi}} \right\}. \tag{2.45}$$

The advantage of the diffusion lies in the fact that $\rho(r)$ for the diffused aperture falls off quadratically while the undiffused correlation drops linearly with r.

Whenever $$\frac{2V_a r_1}{\pi R} > \frac{V_a^2 r_1^2}{4\beta R\sqrt{\pi}} \quad \text{or} \quad \frac{2}{\pi R} > \frac{V_a r_1}{4\beta R\sqrt{\pi}}. \tag{2.46}$$

The diffusion is advantageous when $8\beta > V_a r\sqrt{\pi}$, within the range of validity of the approximation C_D.

2.7.8 General Error Formula

Having all the parts derived in previous sections, it is a simple matter to put these parts together into one complete formula for the velocity variance $\sigma_{V_a}^2$.

$$\sigma_{V_a}^2 = \left(\frac{\pi f_x}{f_1}\right)\left(\frac{1}{2\pi\nu_3 r_1}\right)\left(\frac{4}{\pi}\right)\left(\frac{\frac{V_a^2 r_1^2 P_T}{4\beta R\sqrt{\pi}} + 4\pi^2 f_o^2 r_1^2 P_N}{P_T + P_N}\right) \tag{2.47}$$

$$= \frac{4 f_x}{f_1} \left(\frac{1}{2\pi \nu_g} \right)^2 \left(\frac{\frac{V_a^2 P_T}{4 \beta R \sqrt{\pi}} + 4\pi^2 f_o^2 P_N}{P_T + P_N} \right). \qquad (2.48)$$

When $V_a \rightarrow o$, the limiting velocity variance is

$$\sigma^2 (V_a \rightarrow o) = \frac{4 f_x f_o^2 P_N}{f_1 \nu_g^2 (P_T + P_N)}. \qquad (2.49)$$

In these formulae, f_x is the corner frequency of a single-pole output filter. The dimensions of ν_g are consistent with those desired for V_a.

It is significant that the variance contains no contribution from P_N when $V_a \rightarrow o$, but a large P_T (as a result of good luminance levels) decreases the variance due to P_N by the factor $(P_T + P_N)/P_N$.

2.8 COMPARISON OF METHODS

We come now to a comparison of three types of image velocity sensing systems: frequency measuring, delay correlative, and phase-rate measuring. The correlative method has small aperture and wide bandwidth. The others are large aperture narrowband systems.

While the wideband correlative method appears to make the most inclusive use of terrain power, it does so only at the expense of large noise acceptance. Were the signal power quite large, the noise penalty might be acceptable. But, in low-light situations the noise can easily swamp the needed signal and make velocity errors intolerably large. An aperture dimension will exist for which the improvement in light level just offsets the reduction in number of samples. This represents the minimum error achievable by the phase-rate system.

Such television-type tubes as the vidicon are capable of accumulating charges during exposure to light and releasing the charges when a scanning beam falls upon the individual areas. By virtue of this capability for integration, it would seem possible to achieve signal levels associated with maximum area apertures while using the full bandwidth of the terrain. But the noise bandwidth is still very much larger than that of possible narrowband systems by at least a factor of 1000.

The frequency measuring method employs a full yield aperture, thus acquiring almost the maximum signal levels achievable. However, since the frequency of the photosignal is $f = V_a \bar{\nu}_g$, the frequency is too low to afford the necessary accuracy together with adequate dynamic response. And, as we have noted earlier, the fixed-grid output fails entirely at zero velocity and below.

The phase-rate sensor retains the advantages of the frequency method:

a) high signal level

b) low noise bandwidth

but removes the problems of velocity ambiguity by usual carrier operation, which provides:

c) essentially unlimited range of velocity

d) high response speed.

These advantages are obtained without penalty in cost, complexity, size or weight.

~~SECRET/D~~

469B-2
Volume II

Section 3

DESIGN APPROACH

3.1 GENERAL DESCRIPTION

The Hycon Beta System, Model HG-469B, is a continuous analog device, capable of tracking random image motion having frequency components up to several hundred cycles per second with peak velocities of several inches per second. Because of the device's unique acquisition capability, no external input signals indicating initial motion direction are necessary, and there is no possibility of ambiguous polarity of output voltage versus input image motion direction.

The HG-469B is designed to sense and measure image velocity at the center of the format of the image provided and resolve it into two vector components along perpendicular axes. The HG-469B operates on the heterodyne principle and utilizes phase-rate measurement to determine image velocity. Its output is in the form of two unipolar analog voltages, one representing x and the other y. The magnitude of each voltage is proportional to its respective image velocity component, and the polarity of each voltage (separately supplied) is indicative of the direction of its corresponding image component. The full scale design range is ± 0.3 inch/sec (referred to the input image plane) for each orthogonal component, and the corresponding full scale output voltages are $+5.0$ volts for each component. Frequency response is that of a single lag located at 1 Hz plus a notch filter at 30 Hz.

The system consists of two major components, a detector assembly and an electronics package assembly.

~~SECRET/D~~

3.2 DETECTOR

The detector, shown schematically in figure 3-1 contains optical components for re-imaging a 2.8 inch diameter input format to 0.28 inch diameter. It also may contain a lamp array to provide a self-test capability.

3.2.1 Optical Subassembly. The 2.8 inch field will be formed by an f/7.0 system. The relayed images will lie in a plane parallel to the input object plane at a distance of 8.0 inches from it.

The two optical channels will be formed by an achromatic beam splitting surface.

The rays from the lens are divided by the first beam splitter into a vertical and a horizontal beam. The vertical beam is reflected by a series of 3 mirrors into a relay lens. The f/0.636 relay lens will cover a $10\frac{1}{2}^{o}$ field of view. The lens will be designed as a low resolution/high contrast lens. The horizontal beam from the first beam splitter is reflected at 90^{o} down to two penta-reflectors and out at right angles into a second relay lens. Both paths have exactly the same total length to a common focal plane. The lower image is inverted but not reverted and the upper image is rotated exactly 90^{o} with respect to the lower image.

3.2.2 Chopper Disc. This disc is a 4 inch diameter optical flat upon which has been deposited a precise pattern of alternate transparent and opaque sectors having equal angular dimensions. For the image scale condition existing after a reduction of 10:1 at the prime location, a disc having 1024 spatial cycles is optimum. Theory indicates that the grid clear dimension should correspond to the terrain correlation distance. Stated in other words, the statistical terrain particle diameter should be equal to the width of the grid clear zone. The mean grid clear zone width is approximately 0.005 inches, which when referenced to the earth at operational ranges represents terrain distances of 40 to 140 feet. The grid wave number, ν_g, is 92 cycles/inch.

~~SECRET/D~~

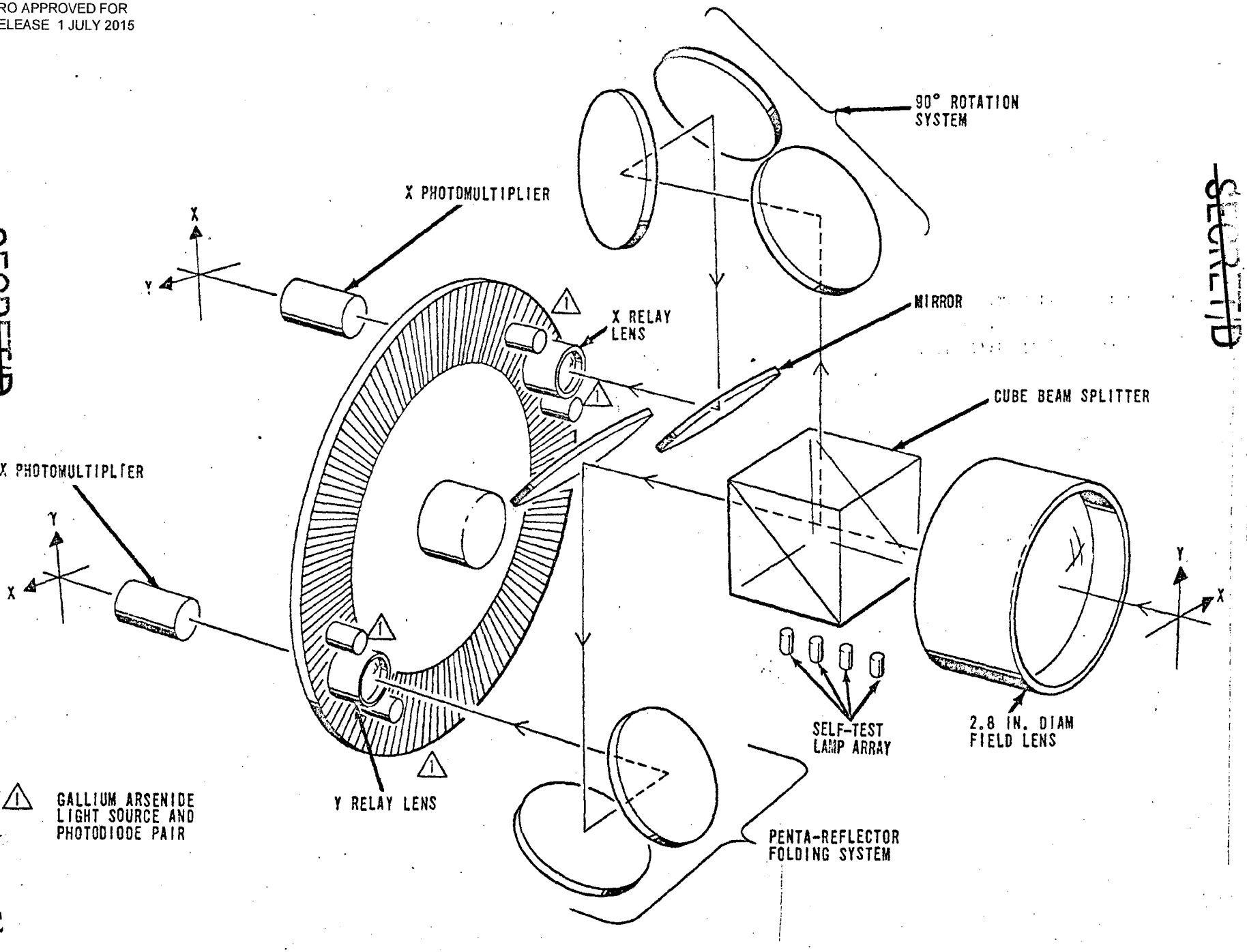

Figure 3-1. Detector Optical Schematic

SECRET/D

3.2.3 Aperture Shading. The physical dimensions of the image sensing aperture are established by an aperture mask located either between the lens and the front surface of the chopper disc or in front of the field lens. When located in either area the mask is deliberately spaced so that the mask shadow has unsharp edges. This edge gradient diffusion is referred to as "aperture shading".

In an image stabilizing system such as the HG-469B, there is usually a transverse image velocity component existing in each aperture in addition to the primary image velocity component. The optimum aperture shape is circular, since an aperture with circular symmetry will show no change in correlation with transverse velocity. Aperture "shading" or edge gradient diffusion minimizes the effects of finite aperture diameter. Shading provides a reduced weighting for the power contributions of image elements which are in the process of just entering or leaving the image aperture thereby minimizing perturbations due to spectral reflections and isolated "hot spots".

3.2.4 Detector Electronics. Output light from each of the light collecting systems is supplied to the x and y photomultipliers. The output signal from each of the photomultipliers is fed to its respective preamplifier. The output signal of these image preamplifiers is a carrier frequency of 30,720 Hz which is phase modulated by the ensemble of image elements. Detection of the rate of change of image carrier phase relative to a reference phase constitutes the principle of image velocity determination.

Means for generating separate x and y reference signals is provided by a pair of stationary reference light sources located on each side of the x and y image apertures. The light from these four reference sources is chopped by the rotating disc and the resulting A.C. light signal from each pair is received by its respective photodetector. The electrical output signals from each pair of detectors are summed and fed to their respective reference preamplifiers.

Automatic gain control is provided to the photomultipliers by varying the high voltage. The signal sensed for this purpose is the D.C. current of the "x" photomultiplier.

In summary, the detector portion contains the optical, mechanical and electrical components for generating and preamplifying four basic signals, x image carrier, x reference carrier, y image carrier and y reference carrier. These signals are supplied to the electronics package through a single cable having a length of 10 feet.

3.3 ELECTRONICS PACKAGE

The electronics package contains circuitry for generating all of the required outputs in response to the four basic detector signals. The functional split between the detector and the electronics package inherently results in most of the thermal dissipation occurring in the electronics package. As shown in figure 3-2, the following functional circuits are contained in the electronics package:

a. Four limiters, one for each of the basic detector output signals.

b. Four filters.

c. Digital tachometer and disc servo amplifier.

d. X and Y phase comparators.

e. X and Y phase modulators with associated integrators, gate generators, and output filters.

f. X and Y signal correlators.

g. Low voltage power supply.

h. CFE A/D converter.

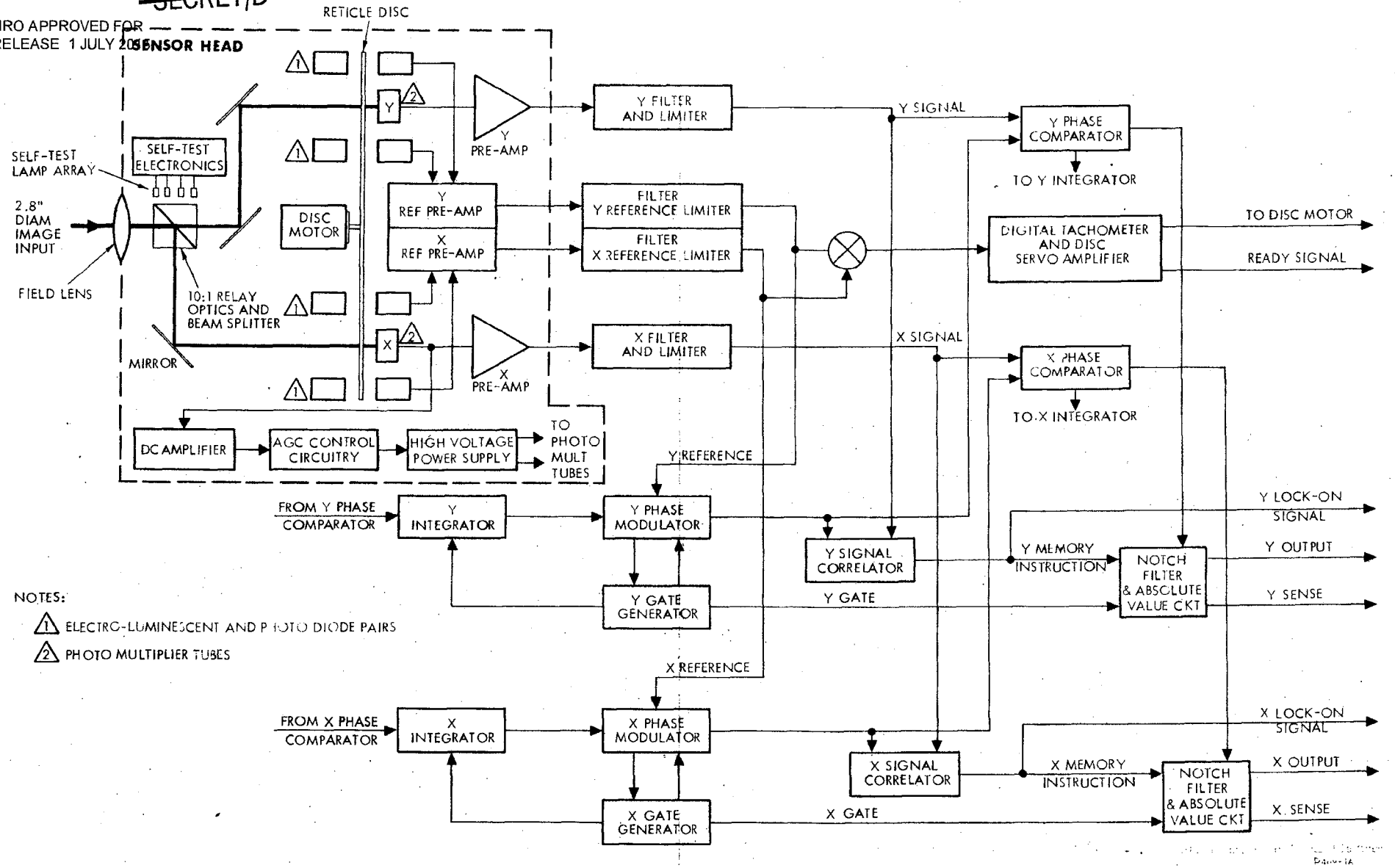

NOTES:

1. ELECTRO-LUMINESCENT AND PHOTO DIODE PAIRS
2. PHOTO MULTIPLIER TUBES

3.4 DESIGN DATA

This covers the broad design concept and detailed circuit design chosen to insure compliance with all aspects of the design specifications. Since the proposed Beta System is so similar to Hycon's HG-453 production sensor, frequent reference is made to experimental data obtained during the course of development and testing of the HG-453 device.

The point of departure is the generalized formulation[1] expressing proportional velocity error in terms of the basic system parameters.

This formula is:

$$\frac{\sigma V_a}{V_a} = \frac{1}{\pi \nu_g V_a}\sqrt{\frac{f_x}{f_1}}\sqrt{\frac{\sqrt{\pi}A_o M^2 V_a^2}{2\beta(8D-\sqrt{\pi}\beta)} + 4\pi^2 f_o^2 B_o}{A_o M^2 + B_o} \qquad (3.1)$$

For the Beta System, the various symbols are defined as follows:

V_a = the input image velocity in inches per second

σV_a = the r.m.s. error value of indicated velocity in inches per second

ν_g = the number of complete black and white grid cycles per inch which is 100

f_x = the lag "corner frequency" which is 1.0 Hz

f_1 = the carrier frequency which is 30,720 Hz, this is the product of the total number of black and white grid cycles (1024) and the rotational speed (30 rotations per second)

f_o = the half bandwidth of the carrier bandpass filter and is equal to $\frac{f_1}{2Q}$. For this system f_1 = 30,720 and Q - 1000, therefore f_o = 15.36 Hz

B_o = the mean square noise current due to shot and thermal effects

[1] This formulation is developed in a special report by Dr. Philip A. Shaffer Jr. (5 January 1967).

A_o = the mean square signal current at the carrier frequency

M = the modulation factor

D = the diameter of the circular image aperture, which is 0.28 inches

β = the dimension of edge diffusion of aperture, which is 0.014 inches

We rewrite the above formula for the case where $V_a = 0$, yielding the following simplified result which shows the r.m.s. null uncertainty:

$$\sigma V_a\,(V_a=0)=\frac{\sqrt{f_1 f_x}}{Q v_g}\sqrt{\frac{B_o}{A_o M^2+B_o}} \qquad (3.2)$$

From inspection of the above two formulas, it is apparent (and fortunate) that the optimum parameters in formula (3.1) resulting in the minimum value of $\frac{\sigma\ V_a}{V_a}$ also results in the minimum value of r.m.s. null uncertainty in formula (3.2).

With these fundamental relationships defined, the following paragraphs reasoning used in establishing the key design parameters.

3.4.1 Optical Scale, Disc Geometry, and Rotational Velocity. On the basis of experiments conducted by Hycon in the course of developing the HG-453 V/H sensor, it was found that spatial filters used in narrow band devices should be designed to look at terrain "cells" of 30 to 200 feet in diameter for terrain in general. This is in general agreement with the analysis of a large sample of terrain imagery.

When the image at the focal plane of the prime system is optically reduced by ten diameters in the process of being relayed to the Beta Sensor disc, the resulting image scale is then fully compatible with the 4-inch diameter 1024-cycle disc.

The nominal grid clear sector width in the sensing aperture is approximately .005 inches, which at a minimum operational slant range covers 40 feet of terrain and at a maximum operational slant range covers 140 feet of terrain.

The choice of disc r.p.m. involves both the f_x and f_1 terms in equations (3.1) and (3.2). Due to the effects of minor eccentricity in the mounting of the disc relative to the motor shaft, a small but measurable sinusoidal noise signal is generated having a frequency:

$$f_{ecc.} = \frac{RPM}{60} \qquad (3.3)$$

The disc should turn at a speed which will cause the disc eccentricity signal to fall at a frequency which is appreciably higher than the "corner frequency" of the single lag. Since in this system the single lag is placed at 6.3 radians/second or 1 Hz, a choice of 30 Hz/second is suitable. This is obtained by turning the disc at 1800 r.p.m. The resulting carrier frequency, f_1, is 30,720 Hz which is a very practical operating frequency for signal processing structures such as the filters and phase modulator multivibrators. Equation (3.1) shows that a small ratio of f_x to f_1 is desirable to minimize indicated velocity error, and in this case:

$$f_x/f_1 = \frac{1}{30,720} = 0.0000326$$

3.4.2 Disc Mounting Eccentricity Analysis. Figure 3-3 shows how the formula expressing Δf_c, the peak carrier frequency deviation, was derived. This formula is:

$$\Delta f_c = e/r\ f_c$$

where e is the eccentricity in inches, r is the disc radius, and f_c is the carrier frequency.

Since the method of signal processing employed responds only to the difference frequency between image and reference carriers, no eccentricity signal results when the image and reference apertures are at coincident locations relative to the disc. Thus the reference and image apertures are placed as close together

~~SECRET/D~~

SYMBOLOGY

θ - Angle subtended by one disc cycle (radians).
ω -Angular velocity of disc shaft (radians/second).
r -Disc radius (inches).
λ-Arc wavelength observed by point receiver, R_x (inches).
$\dot{S}$ -Disc velocity (inches/second) observed by point receiver.
T -Temporal period (seconds) observed by point receiver.

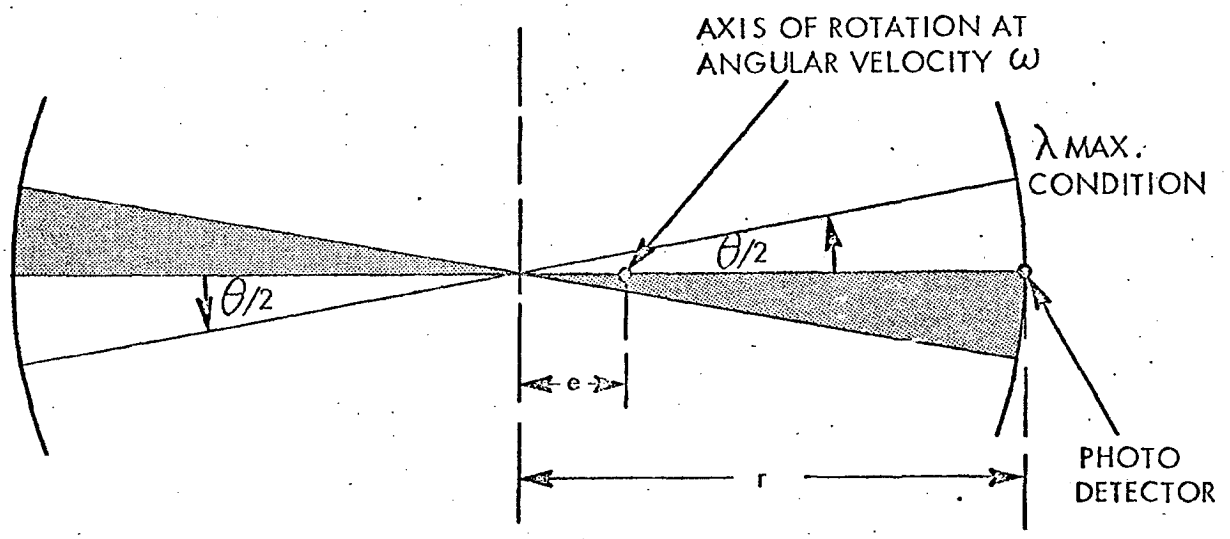

$$T = \frac{\lambda}{\dot{S}} = \frac{1}{f}.$$

$$\dot{S} = (r-e)\omega.$$

$\lambda_{max}=(r+e)\theta$ and $\lambda_{min}=(r-e)\theta$

$$T_{min} = \frac{\lambda_{min}}{(r-e)\omega} = \frac{(r-e)\theta}{(r-e)\omega} \rightarrow f_{max} = \frac{\omega}{\theta},$$

$$T_{max} = \frac{\lambda_{max}}{(r-e)\omega} = \frac{(r+e)\theta}{(r-e)\omega} \rightarrow f_{min} = \frac{(r-e)\omega}{(r+e)\theta} \quad \text{(position shown in sketch)}.$$

The peak-to-peak carrier frequency deviation is

$$2\Delta f_c = f_{max} - f_{min} = \frac{\omega}{\theta} - \frac{(r-e)\omega}{(r+e)\theta} \approx 2\frac{e}{r} f_c,$$

or Δf_c, the peak carrier deviation $= \frac{e}{r} f_c$.

Figure 3-3. Disc Eccentricity Analysis

as possible, at identical disc radii, to minimize differential frequency deviation. The peak differential frequency deviation produced by image and reference apertures separated by disc angle ϕ is:

$$f_{diff} = e/r\ f_c\ (1-\cos\phi)$$

An order of magnitude reduction in this peak differential frequency deviation is obtained by situating two reference generators symmetrically about the image aperture and summing their outputs.

Computing the magnitude of the 30 Hz eccentricity noise for the proposed system having the following properties:

e = eccentricity = 1×10^{-4} inches

r = radius = 1.75 inches

f_c = carrier frequency = 30,720 Hz

ϕ = angular separation of image and reference apertures centers = 8^o

$$\Delta f_{diff} = 0.1\ e/r\ f_c\ (1-\cos\phi)$$

$$= 0.1\ \frac{10^{-4}}{1.75}\ (3.07 \times 10)\ (.01) \qquad (3.6)$$

$$= 1.75 \times 10^{-3}\ \text{Hz}$$

The resulting root mean square velocity error due to eccentricity, V_{ae}, referred to the disc image scale is expressed by

$$\sigma V_{ae} = 0.707\ \Delta f_{diff}\ \ 1/\nu_g\ \frac{1}{1 + j\frac{(f_n)}{(f_x)}} \qquad (3.7)$$

Where f_n is the eccentricity frequency (30 Hz) and f_x is the corner frequency of the single lag filter (1 Hz).

Substituting, we have

$$\sigma V_{ae} = 0.707 \times 1.75 \times 10^{-3} \times 1 \times 10^{-2} \times \frac{1}{1 + j30}$$

$$= 4.1 \times 10^{-7}\ \text{inches/second}$$

Referred to the primary image plane, σV_{ae} is ten times as large, or 4.1×10^{-6} inches/second which is negligible compared to the total allowable null uncertainty of 0.01 inches/second.

3.4.3 Choice of Operating Bandwidth. It is evident from equation (3.2) that the null error of the HG-469B is highly dependent of the Q factor of the carrier bandpass filters. In equation (3.2), Q appears in the denominator, B_o is inversely proportional to Q, and the quantity $A_o M^2$ is large compared to B_o.

This results in σV_a being approximately proportional to $Q^{-3/2}$. The maximum value of Q, consistent with the requirements of signal bandwidth and carrier frequency stability, should therefore be employed.

The required signal bandwidth for a frequency modulated wave (see footnote 1) depends on both the frequency deviation, Δf_1, and the sinusoidal modulating frequency f_m. The ratio of Δf_1 to f_m is defined as the modulation index, β. The value of β determines the number of significant sideband pairs and this number can be calculated by the use of Bessel functions. Or more simply, a useful rule is that a frequency-modulated wave contains sideband components of importance on either side of the carrier wave over a frequency interval approximating the sum of the frequency deviation and the modulating frequency.

When the instantaneous frequency of a frequency-modulated wave is varied in a more complex manner than that corresponding to sinusoidal modulation, the frequency spectrum becomes very complicated. The sideband frequencies present include not only those that are obtained with each modulation frequency acting separately, but also various combination frequencies. However, although complex modulation greatly increases the number of frequency components present, it does not widen the frequency band occupied by the energy of the wave. To a first

approximation, this band is still approximately twice the sum of the maximum frequency deviation at the peak of the modulation cycle plus the highest modulating frequency involved.

To determine the maximum carrier frequency deviation for the HG-469B, the following formula is used:

$$\Delta f_1 \text{ max} - 0.1 \dot{S}_i \text{ max} \quad \nu g \qquad (3.8)$$

where the factor 0.1 accounts for the 10:1 optical reduction between the primary image plane and the disc plane, $\dot{S}_i$ max is the maximum image velocity in inches per second, and νg is the grid wave number in cycles per inch.

Substituting numerical values, we get:

$$\Delta f_1 \text{ max} = 0.1 \ (0.5) \ (100)$$

$$= 5 \text{ Hz}$$

The required signal bandwidth is:

$$BW_o = 2(5 + 1) = 12 \text{ Hz}$$

This bandwidth figure is very conservative because it assumes that the entire peak carrier deviation is due to a modulating frequency of 1 Hz.

An additional consideration involved in the choice of operating bandwidth is carrier frequency stability. In the HG-469B, carrier frequency is equal to the product of the total number of disc spatial cycles and the number of disc rotations per second. This causes the carrier frequency to vary directly as a function of disc speed, hence a description of the method used to servo control the disc speed and an error analysis will be given.

3.4.4 Disc Servo. Figure 3-4 is a functional block diagram of the disc servo. As shown in the upper left hand corner of figure 3-4, stationary reference illumination is provided on each side of the image aperture by a pair of gallium arsenide electroluminiscent diodes. Each diode radiates approximately twenty-five microwatts at a wavelength of 0.9 microns. The

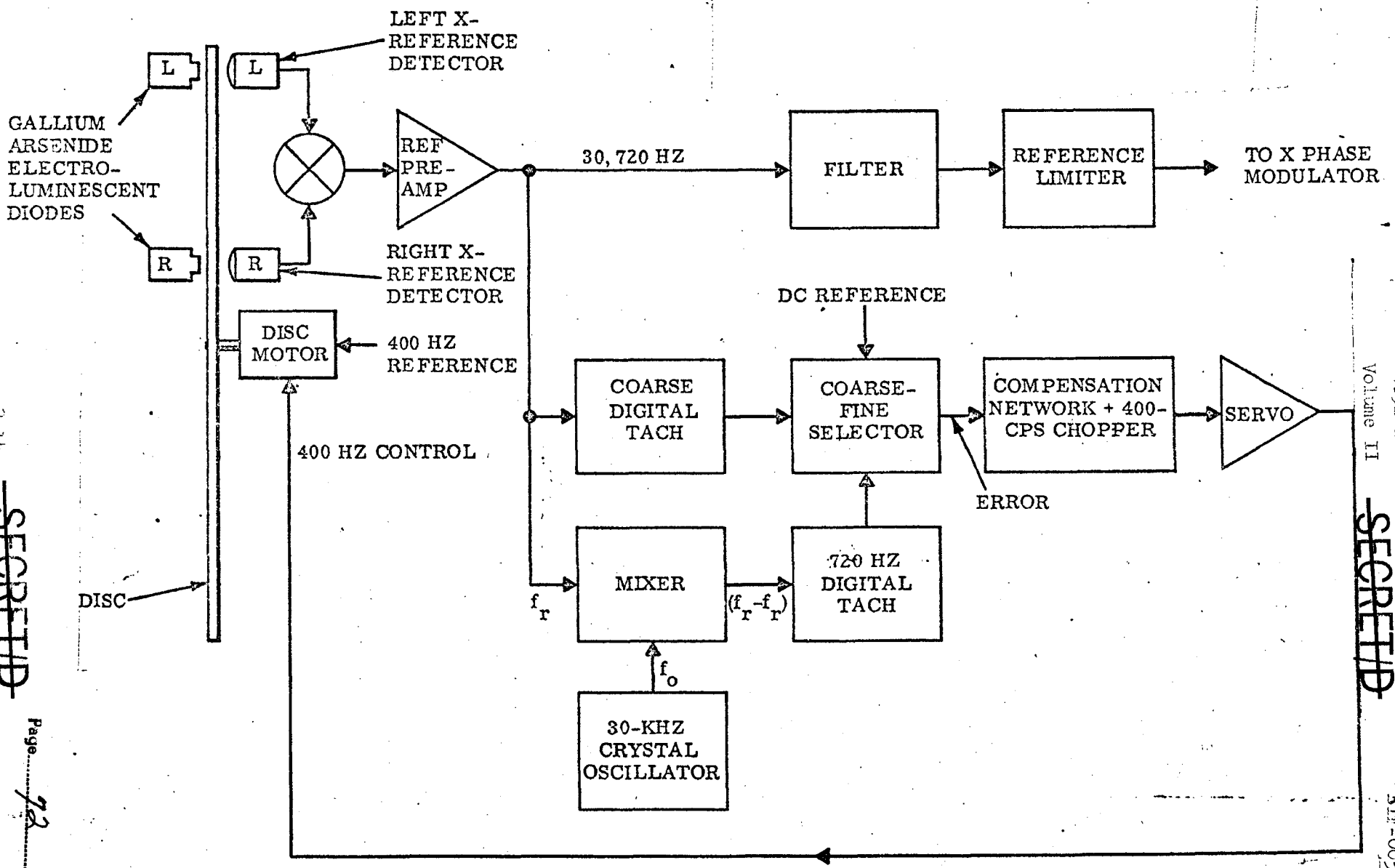

Figure 3-4. Functional Block Diagram, Disc Servo

SECRET/B

SECRET/B

chopped reference light emanating from the rear surface of the disc is collected by a pair of reference photodetectors. The resulting electrical outputs of these photodetectors are summed into the input of the x reference preamp. The output signal of the preamp has a frequency of 30,720 Hz when the disc shaft is turning at 30 rotations per second, the design center value. If the shaft speed is more or less than 1800 RPM, the carrier frequency is correspondingly higher or lower than 30,720 Hz.

In order to achieve a carrier frequency stability of 100 parts per million, or .01%, a coarse-fine type of error sensing is employed. A "coarse" digital tachometer (frequency-to-D.C. Converter) having a long-term stability of approximately 0.5% generates a D.C. voltage which is proportional to input frequency. This voltage is compared to a stable D.C. reference voltage corresponding to the desired reference frequency of 30,720 Hz. The difference between the tachometer output voltage and the D.C. reference voltage constitutes the coarse servo error signal which is fed into the servo compensation network. The output of the compensation network is chopped, amplified, and fed to the control phase of the disc servo motor which results in the reference frequency and servo shaft speed "pulling-in" to within 1% of design center value. The resulting frequency is then 30,720 Hz $\pm$1% which is fed into the mixer. A precise 30 Hz frequency ($\pm$.001%) generated by a crystal oscillator is supplied as a second input, f_o, to the mixer. As a result of the mixing or modulation process, frequencies corresponding to the sum and difference between f_r and f_o are generated. The sum frequency of approximately 60 KHz is discarded by a low pass filter connected in series with the mixer output leaving the difference frequency ($f_r - f_o$) of 720 Hz $\pm$300 Hz. This frequency is supplied as input to the fine digital tachometer. The fine digital tachometer produces an output D.C. voltage which is proportional to input frequency, and supplies this voltage as input to the

coarse-fine selector structure where it is compared to a precise D.C. reference voltage corresponding to 720 Hz. The difference between the fine tachometer voltage and the D.C. reference voltage constitutes the fine error signal. A logic circuit in the coarse-fine selector transfers the loop from the "coarse" to the "fine"mode at the instant the coarse error signal drops below 1%. In "fine" mode the disc speed and carrier frequency are locked to within .01% of design center value. This results in a reference carrier frequency of 30,720 ±3 Hz.

3.4.5 Bandpass Filters. The image channel signal to noise ratio is dependent upon the noise bandwidth. Accuracy is enhanced, especially at low light levels, by restricting channel bandwidth as far as possible. The choice of channel bandwidth involves consideration of both signal bandwidth and carrier frequency stability.

The total bandwidth is equal to twice the sum of the signal bandwidth and the carrier deviation due to disc servo stability or:

$$BW_o = 2(5 + 1 + 3) = 18 \text{ Hz}$$

The required bandpass filter Q in terms of operating bandwidth and carrier frequency is:

$$Q = \frac{fc}{BW_o} \qquad (3.9)$$

Substituting numerical values we get:

$$Q = \frac{30,720}{18} = 1770$$

It is important that identical phase responses be maintained in reference and image bandpass channels since any differential phase deviation rate between these signals is interpreted by the processing circuitry as a velocity. This consideration dictates the use of matched filters in both the image and reference channels.

3.4.6 Limiters. The use of hard limiting in the image and reference carrier channels (following the bandpass filters) enables the sensor to operate effectively over an extremely large range of terrain luminance. The limiters, or zero crossing detectors, are of the type which utilizes diode feedback around a high gain operational amplifier. This infinite clipping of the signal virtually eliminates phase distortion caused by amplitude fluctuations and noise. Other types of limiters such as the Schmitt trigger and multistage limiter clipping circuits can exhibit large errors in zero-crossing information. The Schmitt trigger introduces distortion due to its large on-off hysteresis characteristic. The circuit does not change state when the input signal passes through zero but at different levels for positive-going and negative-going signals.

Distortion in multistage limiters is caused by a shift in the average reference level after each successive stage of limiting. The shift in average level arises because the signal cannot be fully clipped in one operation. Large peaks (which may be of one polarity only) are clipped by the first stages of the limiter, thus altering the waveform to produce a different average level. The following limiter stage then clips the resultant signal about the new average level, which can completely change the character of the original signal.

The large voltage gain and dynamic range of the diode feedback limiters used in the HG-469B permit full clipping of reference and image carrier signals by a single stage of processing.

This results in precise determination of zero crossing information and maximum accuracy in subsequent processing circuitry.

3.4.7 Phase Comparator. In the HG-469B sensor, image angular velocity is obtained in terms of the rate of shift of phase of the reference wave needed

to keep in step with the terrain photosignal. Both signals are amplified, limited, and converted to sequences of pulses which are used to trigger the phase comparator and the phase modulator. The phase comparator is, in reality, a flip-flop which is set for each terrain signal pulse and is toggled for each reference pulse. The average output voltage of the flip-flop yields a phase error signal whose magnitude is proportional to the phase difference between reference and terrain zero crossings, and whose polarity is indicative of relative lead or lag.

This type of comparator is known as a sawtooth phase comparator[2]. The use of the sawtooth phase comparator as the error sensing element in the phase-lock loop of the HG-469B results in superior acquisition and tracking performance because its output is linear for phase differences of plus and minus 180 degrees. In the phase-lock loop, loop gain is the product of the gains of the phase comparator, integrator and phase modulator. The dependence of overall loop performance on loop gain is of prime importance. For a specified noise bandwidth, a phase-lock loop having a damping factor of 0.5 yields optimum acquisition performance. Acquisition is defined as locking the output phase of the reference phase modulator onto the phase of the terrain signal that is perturbed by noise. The range of damping factors from 0.5 to 0.85 yields near optimum performance, while decreasing the damping factor below 0.5 causes rapidly deteriorating performance.

The effects of a drop in loop gain are significant in two respects. First, a lower gain results in decreased noise bandwidth. Secondly, the loop damping factor and natural frequency are adversely affected by a low loop gain. The overall effect of a nonlinear phase comparator characteristic would be a decreased

[2]Bell System Technical Journal, March 1962

ability to acquire and track terrain signals over a wide range of light levels.

3.4.8 Phase Modulator. The output signal of the sawtooth phase comparator is fed into a loop compensation amplifier having proportional plus integral transfer characteristics. The output of the loop compensation amplifier supplies input to both the phase-lock loop integrator and the output filter amplifier. This input signal to the integrator constitutes the wide band analog of the rate of change in the phase difference between reference and image carriers. Output voltage from the integrator is used to control the phase modulator.

The phase modulator consists of a string of seven voltage-variable delay multivibrators. Phase is retarded (with respect to the reference) by increasing the delay interval of each member of the string. Ultimately, the string will have been extended or collapsed to its fullest extent. When one of these conditions is sensed, the whole string is reset a multiple number of waves to its midrange delay, ready to continue with the process. The voltage which drives the delay string is not the comparator output but the integral of it. Any phase error will cause the phase shift to grow until the phase error is nulled. The speed of the phase-lock loop is quite high, as allowed by the high operating frequency, hence, the loop is capable of following velocity fluctuation to the order of 1000 Hz, well beyond the required limits.

3.4.9 Signal Correlator. In any type of instrument designed for measuring image velocity, a built-in provision for monitoring terrain signal quality and tracking loop performance is highly desirable. A monitor signal can be effectively used in the sensor to maximize the accuracy of the sensor output voltage.

The HG-469B sensor employs a cross-correlator to monitor the degree of coherence between the image carrier signal and the phase modulated reference

signal existing at the output of the phase modulator chain. The output of this cross-correlator, or signal correlator, is at a predetermined maximum value when the following two conditions exist:

1. The received image carrier signal displays a signal-to-noise ratio equal to or greater than approximately 20 db.
2. The phase-tracking loop is tightly locked on with a phase error of less than 5 degrees.

In the event that either the image carrier signal-to-noise ratio decreases, or the tracking performance of the phase-lock loop drops, the resultant output voltage of the signal correlator is reduced. The signal correlator output voltage is supplied to an amplitude comparator. This amplitude comparator determines whether the correlation level is above or below a predetermined acceptable value. If the level is acceptable, the output filter amplifier is allowed to accept the velocity analog voltage from the phase-lock loop. If the correlation level is momentarily substandard for any reasons, the output filter amplifier is automatically thrown into memory for the duration of the unacceptable correlation condition.

In operation of any type of image velocity sensor occasional short periods of time will occur when the image signal-to-noise ratio falls below the threshold required for acceptable operation. By the use of signal correlator and memory feature of the output filter amplifier, the HG-469B sensor design maximizes the accuracy of image velocity output voltage.

~~SECRET/D~~

3.5 EQUIPMENT CHARACTERISTICS

3.5.1 Size. The Beta System consists of two major components: the detector and the electronics package. The detector shell approximates a barrel shape (See Figure 1-3) with a maximum diameter of 10 inches and a length, including adaptor, of 15.2 inches. The electronic package is a rectangular box, with optimum dimensions of 9 inches (length), 6 inches (width) and 7 inches (height). Several reductions in size may be made, with added design time, to accomplish a package of 9" x 6" x 6" as specified.

3.5.2 Weight. The following table lists major subassembly weights for the Beta System. For comparison purposes, the weights of the present configuration are listed as well as a revised configuration utilizing the single path herringbone concept involving simplified optics (see Appendix A2). The weights are realistic estimates using basic aluminum structures for low cost fabrication. Further refinements utilizing beryllium and/or magnesium structures for reduced weights with increased fabrication costs are in process.

TABLE 3-1.

Detector	Present Configuration	Herringbone
Optics	12.00	4.00
Structure/Support	7.00	6.25
Electronics	1.00	1.50
SUBTOTAL	20.00	11.75
Electronic Package		
Electronics	4.00	4.00
Structure/Support	4.25	4.25
Low-Voltage Power Supply	1.75	1.75
SUBTOTAL	10.00	10.00
HG-469B TOTAL	30.00	21.75

	Present Configuration	Herringbone
A/D Converter	1.00	1.00
Supporting Structure	.25	.25
Added Connectors, etc.	.25	.25
SUBTOTAL	1.50	1.50
Estimated Grand Total Weight	31.50 lbs.	23.25 lbs.

3.5.3 Power Requirements

The total estimated (from actual breadboard measurements) power required for the HG-469B Beta System is 26 watts without the A/D Converter. This power will remain virtually constant regardless of the input voltage. (within the voltage specification limits). The following tabulation gives a power breakdown:

TABLE 3-2

Detector	
Reference Light Assembly	0.28 watts
Disc Motor	2.56
Photomultipliers and Power Supply	2.00
Preamplifiers	0.12
	4.96 watts
Electronics Package	
Filtering/Limiting, Reference	0.70 watts
Filtering/Limiting, Image	1.80
Light Level Indication	0.14
Driver/Memory	0.80

Disc Servo Amplifier		1.00
Compensation Amplifier		2.20
Integrator		0.20
Output		1.10
Power Amplifier		2.50
		10.44 watts
Low Voltage Power Supply		10.66 watts
	TOTAL	26.00 watts
A/D Converter		0.90
Power Supply Efficiency		0.90
	GRAND TOTAL	27.80 watts

Figure 3-5 illustrates the power distribution.

3.5.4 Hardware Description.

3.5.4.1 Detector. The detector size is constrained by the optical beam splitting system necessary to generate a separate channel for X and Y outputs. The breadboard optical system is shown in Figure 3-6, to the right is a wood model of the optics less supporting structure. Figure 3-7 shows the chopper disc, servo motor, photomultiplier assembly, reference sources and photodiode assembly of the breadboard (less photomultiplier tubes).

3.5.4.2 Electronics Package. Figure 1-2 is an external view of the Prototype Engineering Evaluation Model. The electronics package mounts to the cold plate on the equipment rack and contains:

1. Two identical (X and Y channel) input-output boards.

~~SECRET/D~~

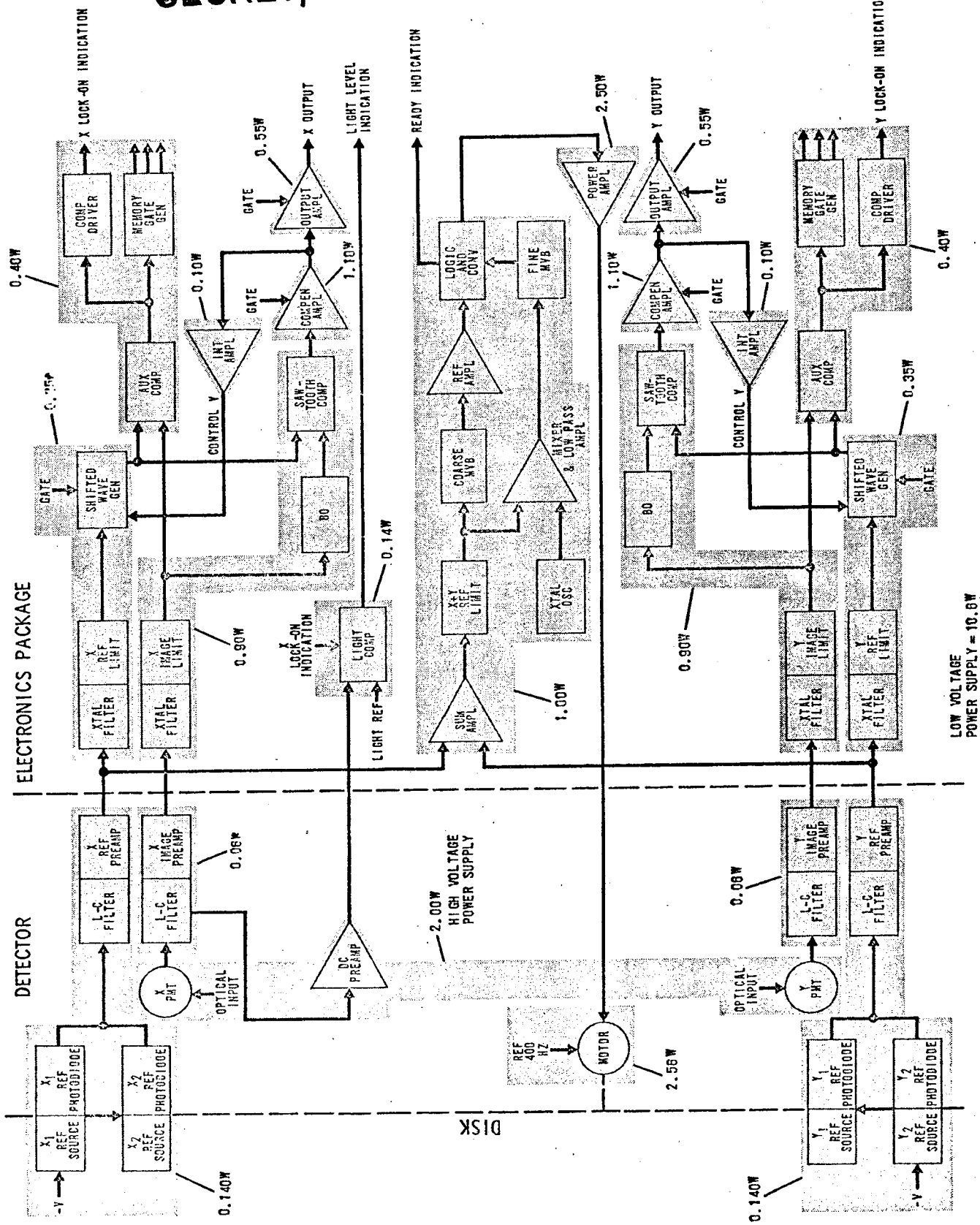

Figure 3-5. Power Breakdown

~~SECRET/D~~

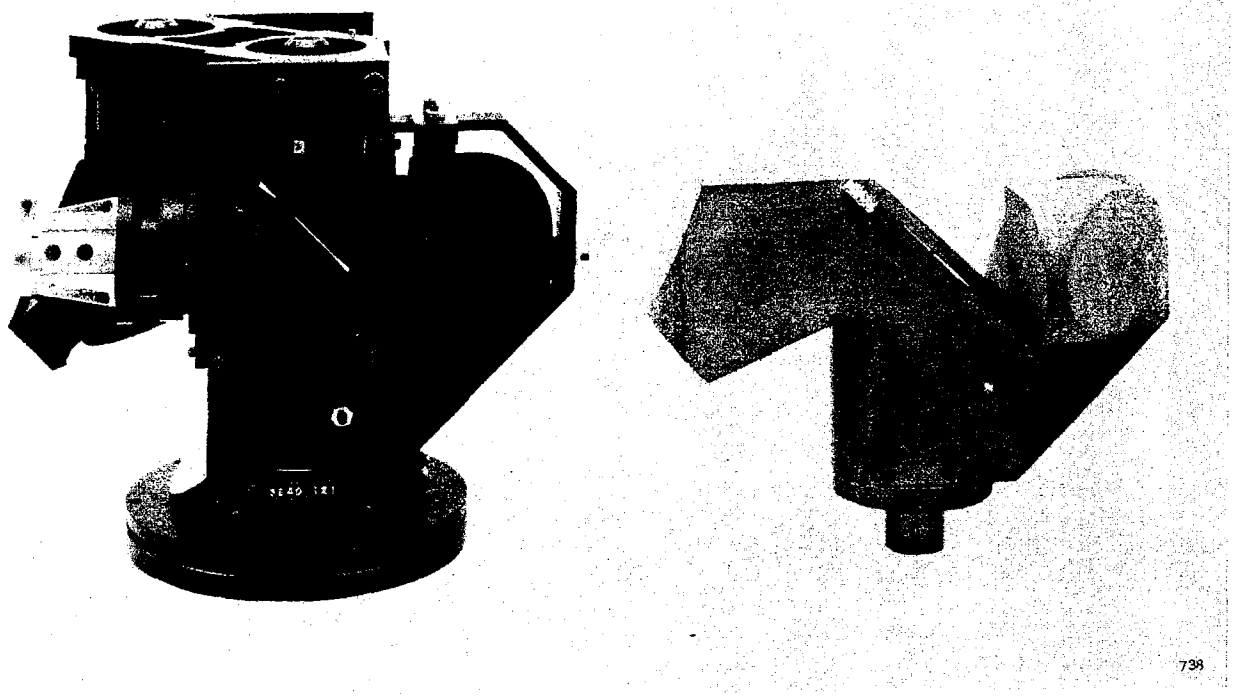

Figure 3-6. Optical Assembly

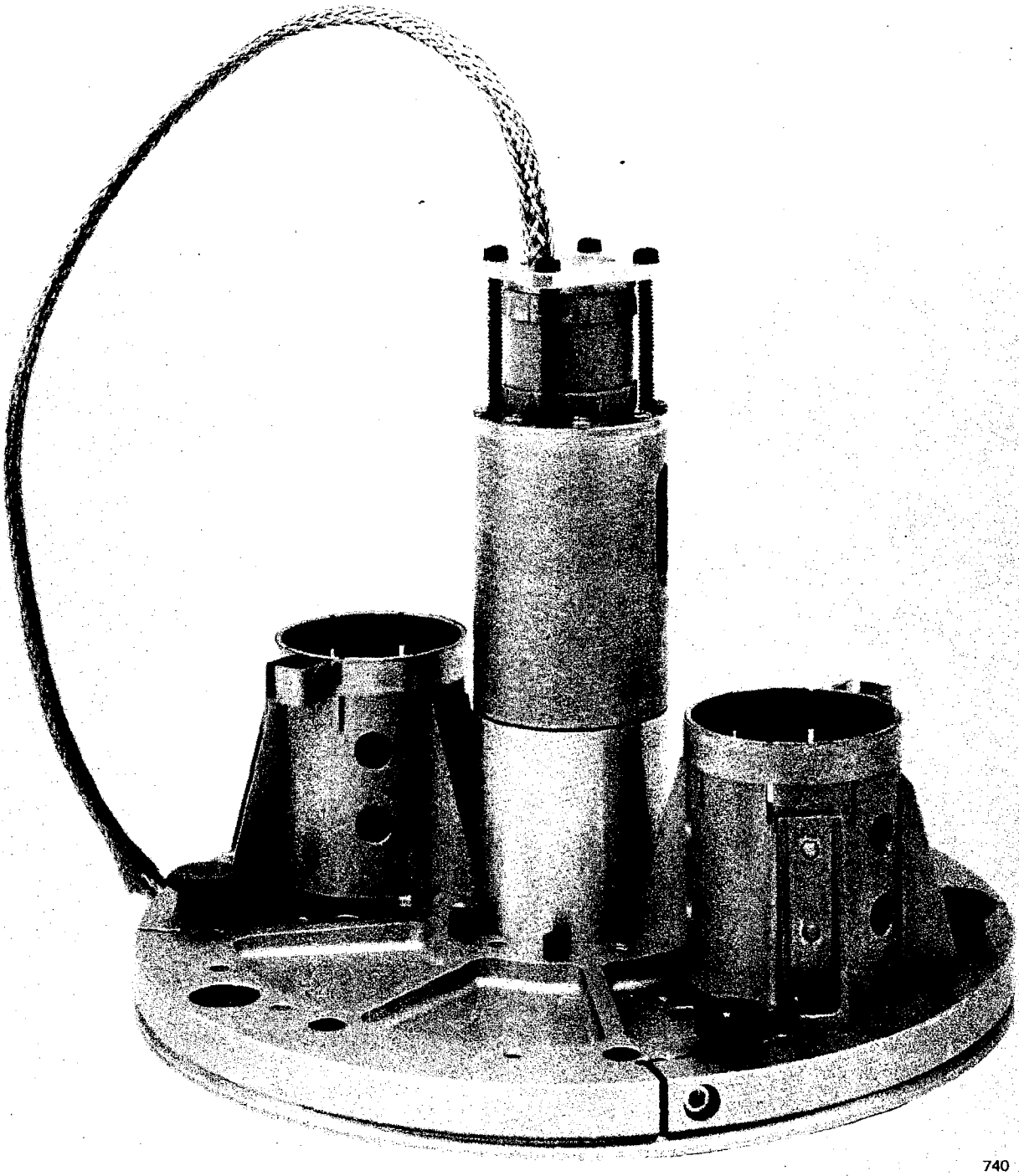

Figure 3-7. Disc, Motor, and Photomultiplier Assembly.

~~SECRET/D~~

2. Two identical (X and Y channels) correlation loop circuitry.

3. One board containing the disc servo amplifier and low light comparator circuitry.

4. One board containing the interboard and input/output connections.

5. Low voltage power supply.

6. The CFE A/D Converter.

7. Five connectors for the detector (1), power (1), input/output (3).

3.6 SPECIFICATION COMPLIANCE

The Hycon Beta System will meet the requirements of EC-701A, Rev. 6 except for the following: (numbers refer to paragraphs of EC-701A, Rev. 6.)

1. 3.1.1.1.1. Insert this sentence after the fourth sentence: "A notch filter network at 30 Hz is permitted." See Figure 3-8.

2. 3.1.2.4 Insert this sentence after the third sentence: "The IVS head shall not be required to meet the 4 inch pivot drop requirement of DR 1100B, Table I (Nov. 1967)."

3. 3.2.1.2.1.1f No change except that: 1) Maximum average power consumed should be 28 watts including the A/D Converter. (Hycon Beta will not increase power consumption with increase of input voltage.) 2) Maximum turn-on transient energy content shall not exceed 100 millijoules over and above the maximum operating condition.

4. 3.2.1.2.2.1 Specification EC 1602, A/D Converter, was not supplied with the RFP. Based on preliminary size, weight, and power data, Hycon can accommodate this item within the Beta electronics package.

5. 3.2.1.2.3.2 Agreed, except that height should be 7 inches. If the 6 inch height is mandatory, other accommodations could be negotiated.

PHASE AND AMPLITUDE PLOT OF β TRANSFER FUNCTION

$$\frac{e_o}{V_{image}}(s) = 10\,\frac{\left[s^2+(2\pi\times 30)^2\right]}{\left[\frac{s}{2\pi\times 7.2}+1\right]\left[\frac{s}{2\pi\times 90}+1\right]\left[s^2+0.4(2\pi\times 30)s+(2\pi\times 30)^2\right]}$$

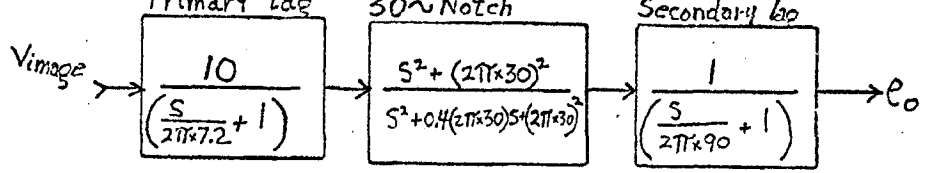

0db
-10db
-20db
-30db
-40db
-360db
0°
-40°
-80°
-120°
-160°
-200°
-240
PHASE LAG
-72db
0.1
1.0
10
50
100
500
1000
FREQUENCY- HERTZ

M. HILLMAN
25 JAN. 68

Figure 3-8

6. 3.2.1.2.3.3 Change to: "The total weight of the IVS System exclusive of cabling and sensor head adaptor shall not exceed 30 pounds." (One of the options meeting the requested weight specifications is summarized in Section 3.5.2 and Appendix A2 of the Proposal. The others will be in an addendum to be submitted at a later date.)
7. 3.2.1.2.5.2 The mounting configuration of the sensor head for testing to 4.4.3.2.A of DR 1100B remains to be defined.
8. 4.1.3.4.2 Add to end of last sentence: ". . . except that the vibration curve is the lower curve of Figure 8, EC-701A, Rev. 6."
9. 4.1.3.4.3.B Change to: "Paragraph 4.4.3.5 of DR 1100B applies except use higher curve of Figure 8, EC-701A, Rev. 6."
10. 4.1.3.4.3.G DR 1100B, 4.4.3.15f says these tests do not have to be run if the leakage requirements of 4.4.3.11 of DR 1100B are met. (It is assumed that the yet-to-be-determined leakage requirements (4.1.3.4.3.N below) will still allow an exception to this test.)
11. 4.1.3.4.3.H Same as 4.1.3.4.3.G.
12. 4.1.3.4.3.M Change "Zone 3" to "Zone 2".
13. 4.1.3.4.3.N Expect to meet, however, test conditions are yet to be determined. To establish preliminary requirements and to meet the intent of para. 4.4.3.15f of DR 1100B, Hycon will assume the leakage test is that of DR 1100B.

3.7 THE PROBLEM, RISKS, AND SOLUTIONS

3.7.1 The Problem

The Beta System requirements call for an image velocity sensor that measures orthogonal velocity components with high accuracy. Ultimate system use calls for a reliable, compact, and lightweight device. In addition to velocity information, the sensor must generate an image lock-on signal, a readiness signal, a low-light signal, a saturation signal and various diagnostic signals.

The Hycon HG-469B Beta System meets all the requirements. It is a null-type device which detects and indicates image motion plus-or-minus from zero. The sensor is applicable to a closed loop servo system for maintaining true image motion compensation.

3.7.2 The Risks

Much of the potential risk will be avoided in that this is not a new design but an extension of an original design. Hycon has been producing the proprietary HG-453 Heterodyne Image Motion Sensor which resulted from an applied research and development program directed towards image velocity detection and true image stabilization. The program resulted in a new principle of image velocity measurement based on heterodyne and correlation concepts. The HG-453 uses scene scanning at enhanced rates to overcome the dynamic limitations of previous fixed grid sensors. These limitations it overcomes are, limited bandwidth and the inability to distinguish between positive and negative velocity components.

The HG-469B Beta System consists of essentially two V/R Sensors inside a single package. One half detects and indicates the forward

motion components, the other half detects and indicates the cross-track motion. It is of critical importance that both halves of the sensor view the same scene at the same time and this requires a suitable beam splitting optical system.

3.7.2.1 Eccentricity of the Sensor Disc. An apparent risk might be the degree of concentricity required for the sensor disc since an eccentricity would result in a second order error in the detected image motion rates. However, this problem has been minimized by use of: 1) a servo motor utilizing large, precision, external bearings for improved alignment and long life; 2) a highly accurate, deposited metal on glass disc pattern; 3) a pair of reference lights on each side of the detector and at the same radius as the detector to balance out any lead and lag error caused by eccentricity. In addition, the disc is mounted on the shaft by a microscope positioning technique such that the residual eccentricity of the disc is less than 1/10,000 of an inch.

3.7.2.2 Photomultiplier Tube. Because this item is a cold cathode vacuum device, the reliability is better than a filament device, however it is not equal to a semiconductor device. Since input light levels dictate use of this part, critical study and careful design must be depended on to reduce risks. Several vendors have supplied photomultiplier tubes for other programs with environmental conditions similar to that required for the Beta environment. In addition, packaging methods will be used to minimize vibration and high temperature problems associated with this type of device. The corona and other high voltage problems normally encountered will be eliminated by careful design of the package.

3.7.2.3 Optics. The risks in the optical system design lie mainly in the environmental areas. Extremely careful design is being accomplished to allow the optics to perform within specification after being subjected to temperature and vibration extremes. This design is also complicated by the need to minimize weight. Prototype efforts to date have shown that all objectives on this item are achievable.

3.7.2.4 Hermetic Seal. Use of a hermetic seal on the Beta is the subject of a trade-off study in progress. Positive factors are minimization of: atmosphere compatibility problems, humidity problems, high voltage and corona problems, piece-part selection problems. Negative factors are: structure and interface design complexity to allow reliable sealing of the units, including a field lens seal in the sensor head. Prototype packaging has shown that careful design will minimize risks and extensive testing will be used to enhance reliability.

3.7.2.5 Interface. A potential high risk relates to the interface of the sensor with the prime system. The mockup, breadboard, and prototype deliverable items reduce this risk. A common understanding of all facets of the relationship of the sensor to the prime system, including mechanical, optical, electrical, and thermal environment parameters, is necessary. The liaison program should continually update the interface information.

3.7.2.6 Schedule. The long-lead time required for procurement of high reliability components and preliminary qualification and testing of special parts and assemblies may not be compatible with the present schedule without added early endeavor and agreement on interface and parts. Hycon will attempt in all respects to design the Beta to minimize risks associated with this problem.

3.8 A/D CONVERTER

This is specified to be a CFE item with the following preliminary characteristics:

a. Size: 4 x 3 x 1.5 inches

b. Weight: 1 pound

c. Input Power: ±12 VDC ±5% 0.15 watt, + 4 VDC ±5% 0.7 watt

d. Reference Voltage: +5 VDC ±1%, 10 ma.

e. Output Capacity: 24 bits serial consisting of 10 bits each channel plus 4 bits sign.

This item will be installed into the electronics package and interfaced with the existing circuitry. The required power will be supplied from the existing low voltage power supply which will be upgraded 1.8 watts to allow for 0.9 watts to the A/D Converter and 0.9 watts for power supply efficiency and safety factor.

Since only the +12 VDC of the input voltages presently exist, circuitry will be added to the present Beta to generate the required voltages. This will take the form of zener regulators for the ±5% power and an integrated circuit regulator for the ±1% reference voltage. Electronics package weight will increase 1.5 pounds, 1 pound for the A/D Converter and .5 pound for the added structure and hardware.

3.9 TESTING

3.9.1 Self-Test Capability

3.9.1.1 Purpose. The purpose of the self-test capability is to provide a confidence test of Beta System operation, both in ground test and during a mission. A confidence test gives evidence that the system is in working condition, but it is not intended to serve as a calibration test certifying to quantitative aspects of operation. Accordingly, the test method need not be capable of quantitative measurement to the specified

Beta System precision. Since proper functioning of the Beta System involves the photodetectors and spinning grid as well as the subsequent electronic circuitry, the self-test method should introduce the stimuli optically so that all system elements participate in the test. While it might be possible to image a moving test pattern through the Beta System optical train, the mechanization would involve mechanical drives and added optical elements which add to weight and size. For these reasons, we propose a test method which creates an illusion of pattern motion due to the modulation of intensity of four discrete point light sources which can be imaged by the existing Beta optical system.

3.9.1.2 Method. A given fixed point source of light, when imaged upon the spinning grid of the Beta System, produces an electrical component in the output of the photomultiplier which is sinusoidal in waveform (after filtering), has exactly the reference frequency, and has a phase which corresponds to its (image) position on the grid relative to the position of the fixed reference image (the reference lamp). If the grid is thought of as being stationary with one of its lines placed exactly upon the reference position, which may be called the zero-degree phase condition, then as the test point source is moved relative to the (stationary) grid, the test point phase will change by 360° with each traverse of a complete grid cycle. This is the principle of velocity measurement employed in the Beta System.

By using four fixed light sources placed in quadrature (0°, 90°, 180°, 270°) with respect to the grid cycles and modulating the intensity of the sources in time quadrature, an illusion of a single point source can be

created moving across the grid at uniform velocity. The effective velocity of the point is the grid period multiplied by the frequency of modulation of the light sources. The direction of the effective motion is determined by the phasing of the modulation signals applied. The situation is entirely similar to the generation of a "rotating electric field" in induction motors by the time quadrature excitation of electrical windings in space quadrature. In our case, four light sources are used, rather than two, because the lights cannot generate negative intensities.

Figure 3-9 illustrates the possible location of a reference source and a test source within the aperture and relative to the grid, and the resulting photosignals are shown at the left of the figure. Figure 3-10 shows the manner in which photosignals of different phase with respect to the reference may be represented by directed vectors or "phases".

Figure 3-11 depicts the generation of a resultant photosignal equivalent to a point moving at constant velocity (constant phase rate or phasor rotation) by the summation (at the photomultiplier) of the light received from four fixed light sources whose intensities are appropriately modulated. Figure 3-12 shows that each modulation is half-wave sinusoidal, obviating negative intensity requirements, and the locations of the images of the fixed sources, A B C and D, are such as to yield the phases (relative to one another) 0°, 90°, 180°, 270°. The sense of the motion (clockwise or counterclockwise) is determined by the sign chosen for the quadrature component of the modulation. Any one or more such fixed sources unmodulated in intensity represents a zero-velocity condition.

~~SECRET/D~~

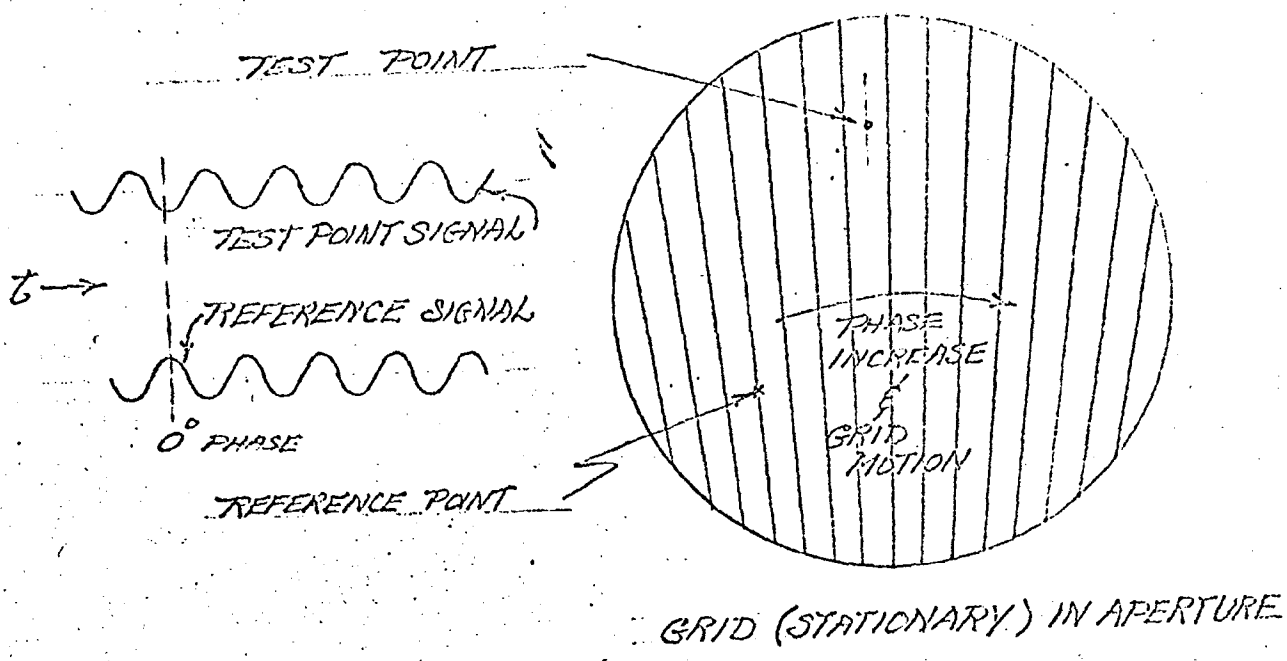

Figure 3-9. Effect of Test Point Position Upon Phase of Generated Photosignal

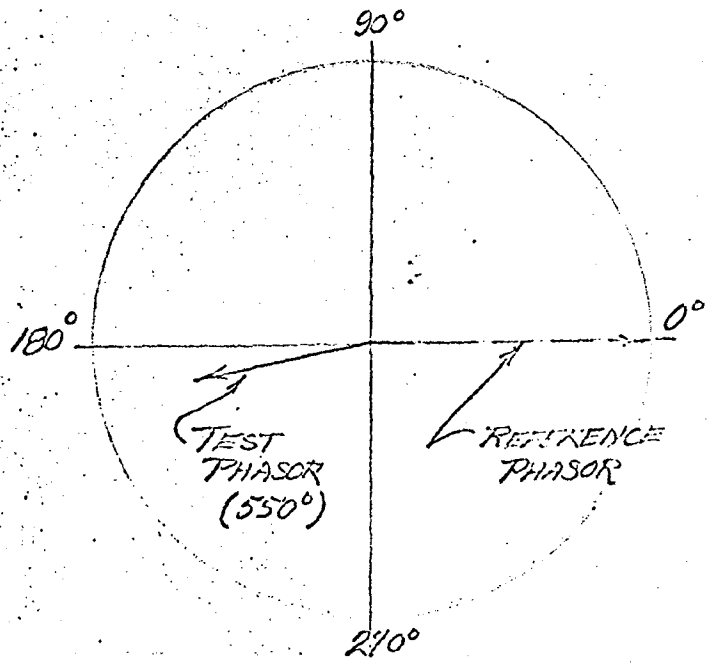

Figure 3-10. Phasor Representation

~~SECRET/D~~

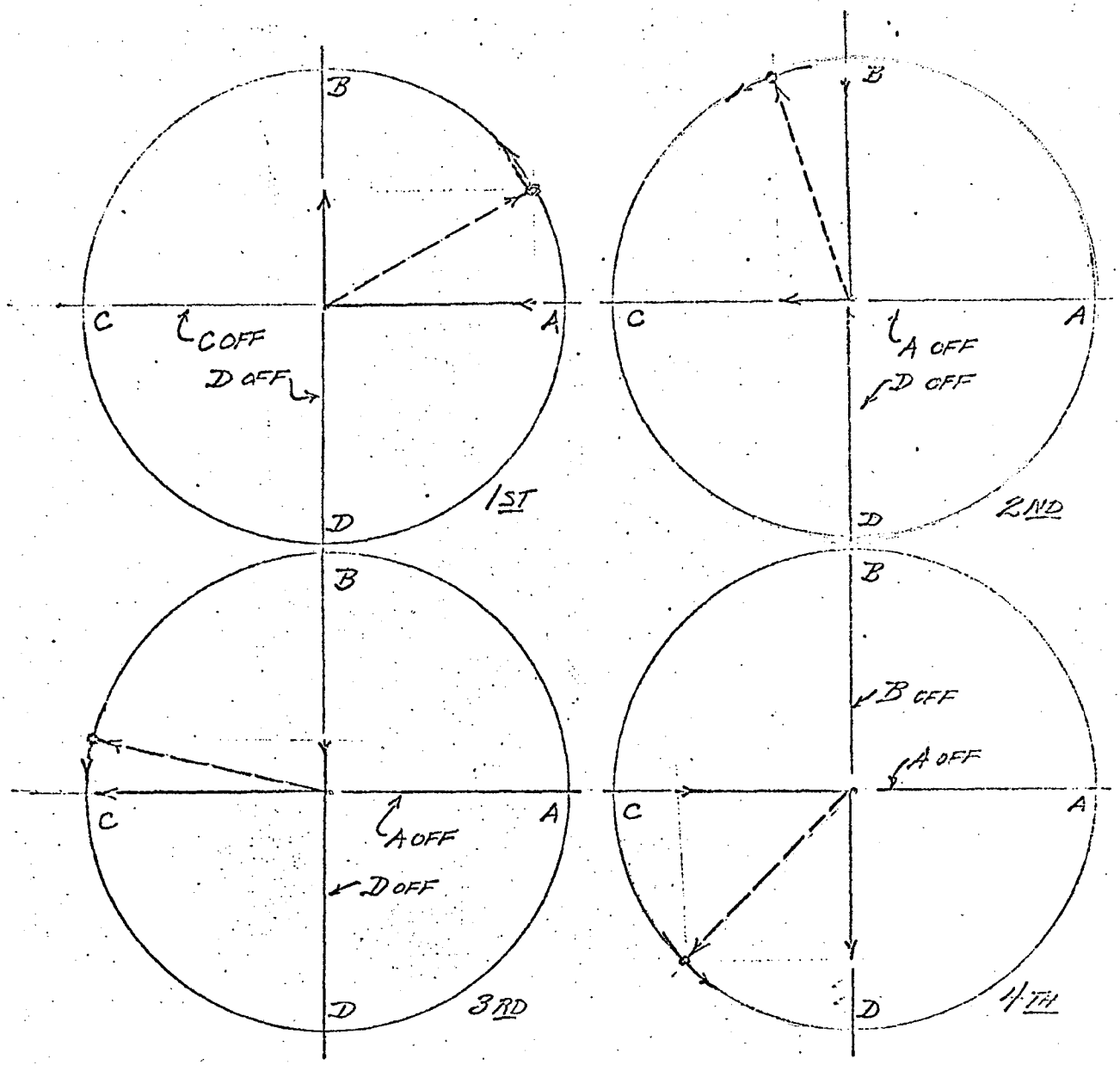

Figure 3-11. Effective Phase Progression (Rotation) of Resultant Photosignal Phasor (Shown Dashed) Due to Superposition of Photosignal Components from Four Fixed Sources, Modulated in Intensity (Positive Only), in Space Quadrature.

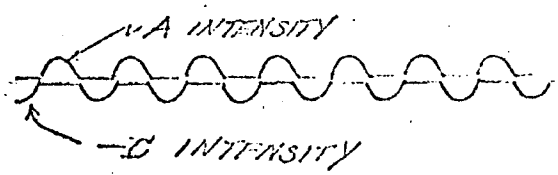

Figure 3-12. Generation of Full Wave By Addition of Positive-only Waves.

3.9.1.3 Physical Configuration. The four test light sources are placed in a plane which is imaged on the spinning disc as illustrated in Figure 3-13. The Beta System uses a beam splitting prism to form two separate (X and Y) channels. The fourth side of the prism (in plan) is currently unused (opaqued) and may be used as the input surface for the test-point array. Since the optical system normal images the input aperture upon the disc, a subsidiary field lens may be required to place the test-point array at a similar focus.

The test light sources are silicon carbide visible light point sources which are positioned in the input plane so as to generate photosignal responses at phases 0°, 90°, 180°, and 270° (for A, B, C, and D, respectively) in both channels. Thus one test array serves to test both channels. A fraction of the light from each test source is diverted to a photosensor, the output of which is used to servo the source intensity to the desired modulation signal. There is one such servo photosensor for each of the four test sources.

The light from the test sources is split by the beam splitter to form two test patterns. When the test sources are not lighted, the Beta System will not experience any effect from the presence of the test array.

3.9.1.4 Intensity Modulation. Since the grid period subtends about 0.1 inch at the input aperture, a modulation frequency of 1 Hz will produce an apparent velocity of 0.1 inch per second. The modulating signals are derived from an oscillator composed of three operational amplifiers, the first two being used as integrators and the third as an inverter.

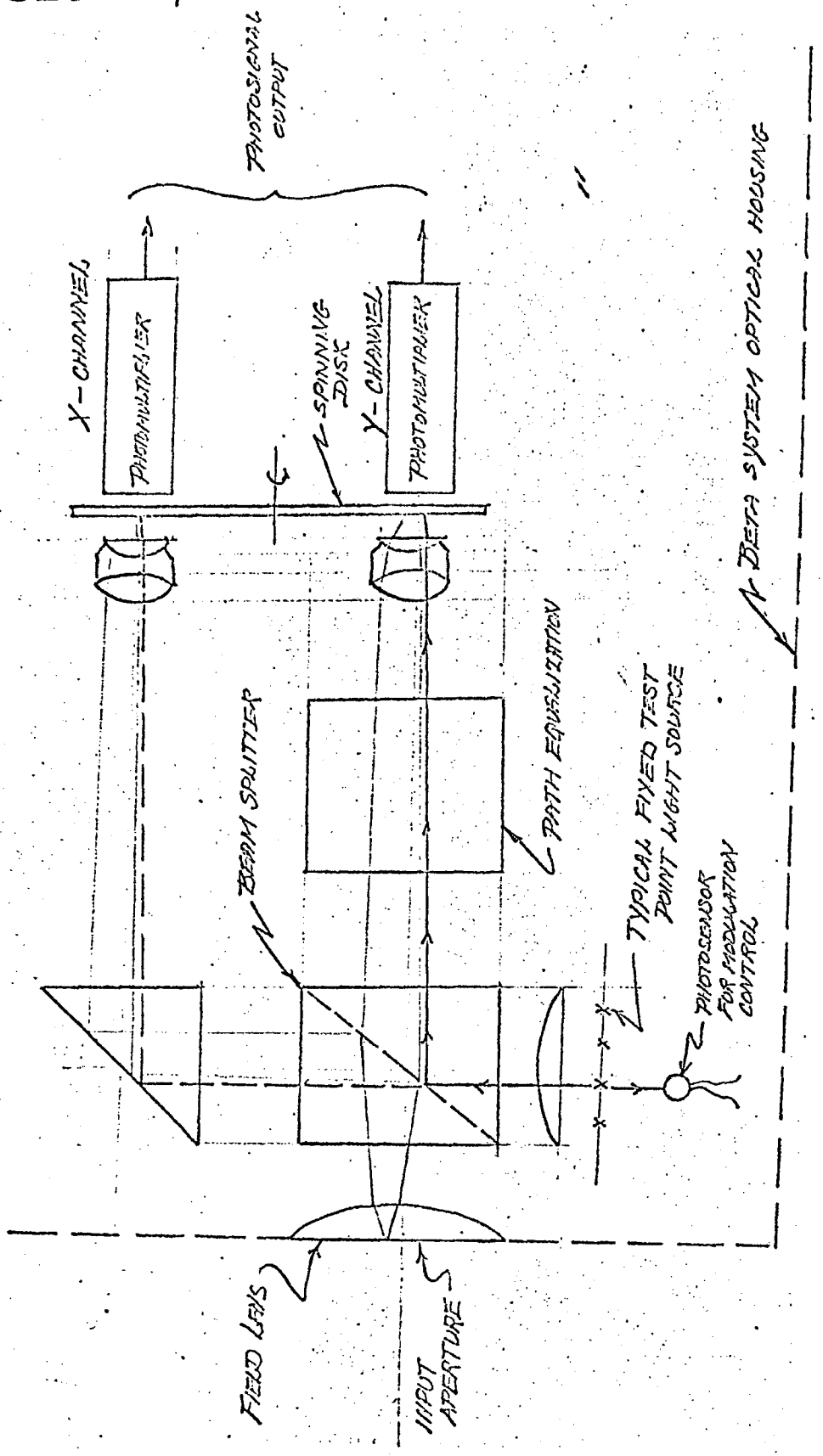

Figure 3-13. Method of Introducing Modulated Light Sources for Self-Test.

The configuration is commonplace in analog computing. (See Figure 3-14.) If the output of the first amplifier is taken to be the cosine wave (all waveforms are sinusoidal and of equal amplitude and frequency), the second amplifier yields the negative sine and the third the positive sine. The radian frequency is 1/RC.

By using cosine and negative sine as the quadrature components for modulation, a forward moving test source is simulated. When the negative sine is replaced by the positive sine, the effective motion of the point is reversed. A null-velocity test source is obtained by lighting any one of the four sources at constant intensity.

It cannot be depended upon that the modulating signals will be converted linearly to intensity variation for most visible light sources. For this reason, two additional operational amplifiers are used as servo amplifiers to compare the modulating signals with the photosignals generated by each source. Photodiodes are employed which have a highly linear relation between photocurrent and incident light intensity. The light source current is switched by diodes to the proper member of each pair (A-C, B-D) by the sign of the control signal. The emitted light produces a proportional photocurrent through the photosensor. The operational amplifier servo loop gain acts to maintain the photocurrent equal to the input current through the input resistor from the modulation control signal. The servo action causes the source intensity to be an accurate replica of the controlling sinusoidal signal.

The switches, which are here shown schematically, will be FET solid state switches driven by switching circuitry used to produce the required self-test cycle.

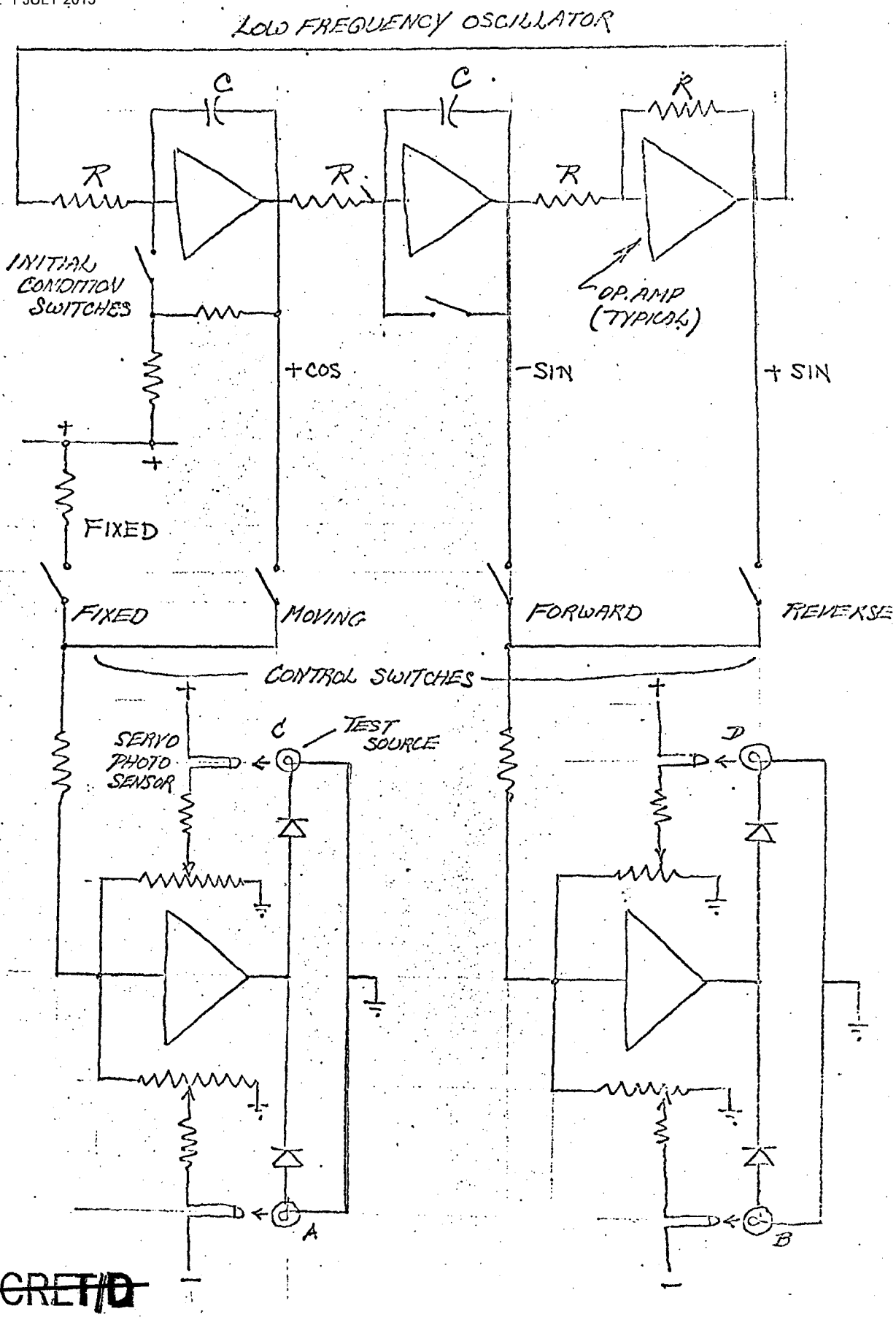

Figure 3-14. Intensity Modulation Servos and Low Frequency Oscillator with Quadrature Outputs.

3.9.1.5 Cycle Control. The self-test cycle is initiated by a single input command pulse. Upon receiving the command, the test circuitry turns on the power to the operational amplifiers, and after a delay to allow the establishment of initial conditions, steps through a cycle of NULL, FORWARD, NULL, REVERSE, NULL and turns itself OFF. The circuit blocks which control the cycle are shown in Figure 3-15.

The self-test command pulse is received by the flip-flop (1) which is set by the pulse. The setting of the flip-flop causes the binaries (8-11) to be reset, and turns on the AND gate (7) by connection (17). With the flip-flop set, the power is applied to the principle portion of the self-test equipment, that part enclosed by the dashed line (16). (The binary resets may be moved to the "delay" stage to avoid troubles due to power turn-on lags, a practical detail.)

A delay (3) is introduced to allow the oscillator to settle at its desired initial conditions as well as to permit power supply transients to settle out. At the end of the delay, the initial condition switches (4) are opened and the low frequency oscillator (5) commences cycling. At a given point in each cycle (preferably a zero crossing), the detector and pulse former (6) emits a pulse which passes through the AND gate (7) to step the binary counter sequence (8-11). The two states of each binary are available for use by the control logic (12). The control logic activates and deactivates the four control switches (13) which determine the NULL, FORWARD and REVERSE velocity modes of the test source array driven by the light source servos (14).

~~SECRET/D~~

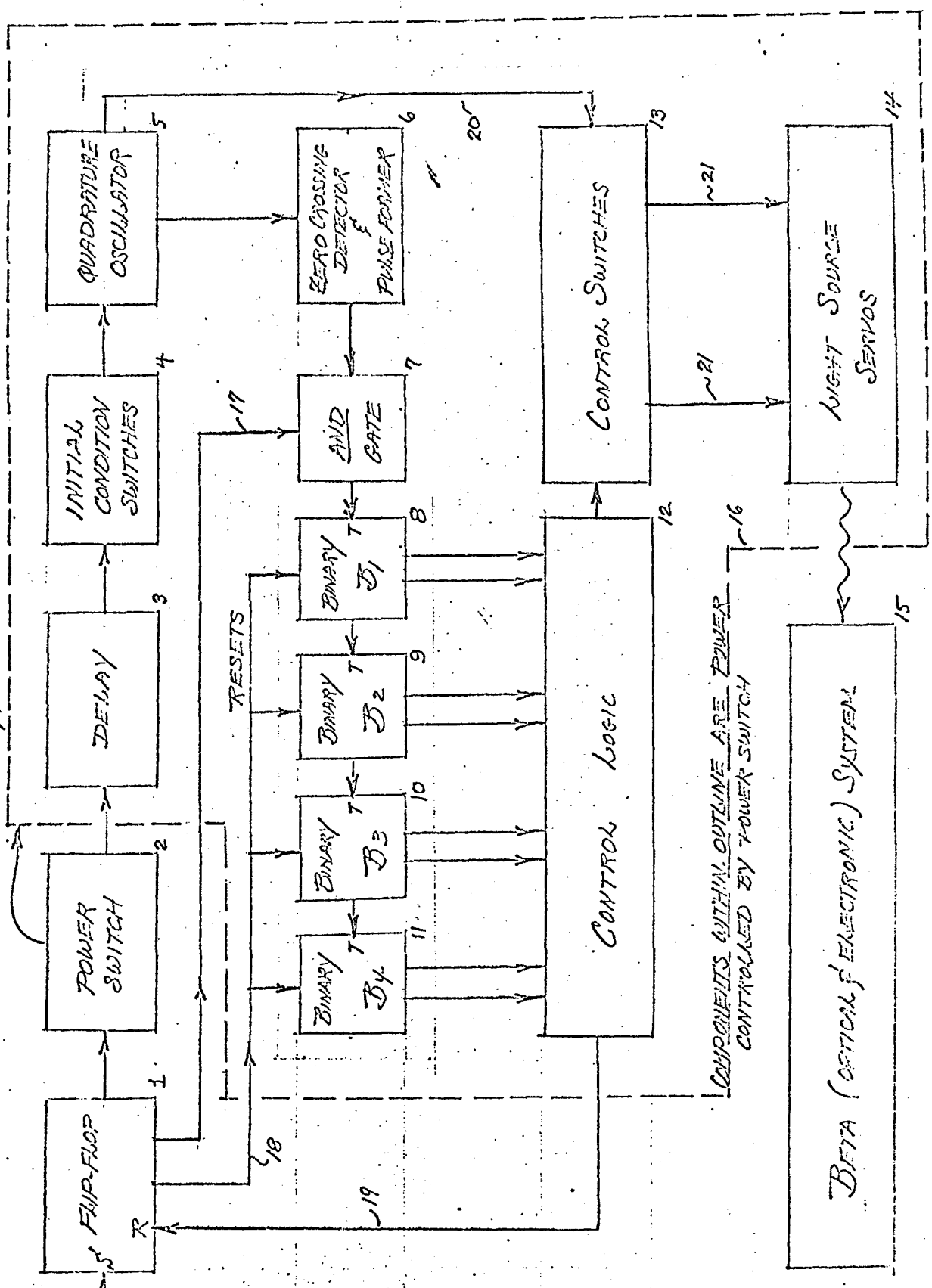

Figure 3-15. Block Diagram of Cycle Control Circuitry for Beta System Self-Test Capability

~~SECRET/D~~

The test sequence is determined (for example) as follows:

1. The binaries start in the state 0000 due to reset by the flip-flop (1). At the end of the first oscillator cycle (1 sec), the counter steps to 0001; at the end of two cycles, it steps to 0010; and so on. During this first 2 sec. period a NULL velocity is required.

2. During the next two-second interval, the counter will indicate 0010 and 0011, and a FORWARD velocity is called for (approximately 0.1 inch per second).

3. The next two-second interval produces NULL velocity again, the counter states being 0100 and 0101.

4. The fourth interval causes REVERSE velocity, the counter states being 0110 and 0111.

5. The final interval returns to NULL velocity, with states 1000 and 1001.

6. At the end of the fifth interval, the counter steps to state 1010, and the self-test system turns itself OFF by resetting flip-flop (1) which controls the power switch.

A time picture of the self-test cycle (as described; other cycles can be produced by simple logical changes) is as follows:

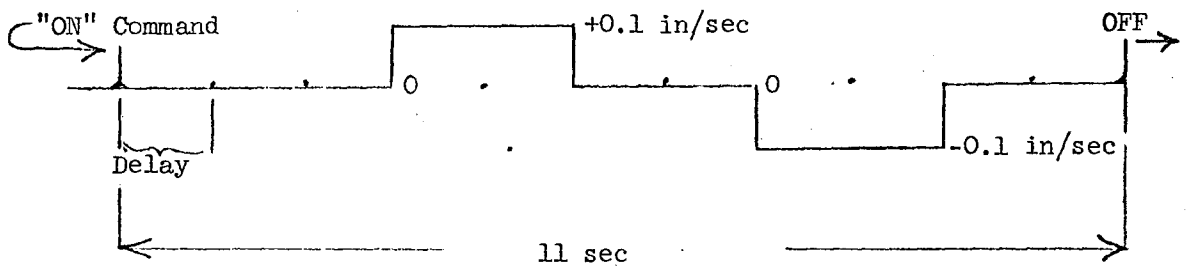

~~SECRET/D~~

~~SECRET/D~~

The logic shows that whenever B_2 (9) is in state "0", a NULL velocity is called for. When B_2 is in state "1", the velocity is either FORWARD, when B_3 (10) is "0", or REVERSE, when B_3 is "1". The OFF condition is signalled when the state 1010 is reached. The execution of such logic is very simple and straightforward.

3.9.1.6 Weight, Size, and Power of Self-Test.

1. Weight. The added weight to the detector head is estimated to be ten ounces.
2. Size. The lamp assembly will be approximately 4" x 1" x $\frac{1}{2}$". The added control electronics will be a printed circuit board 5" x 3" x $\frac{1}{2}$". The detector housing size should not change.
3. Power. An added three (3) watts of power, including power supply efficiency, will be required, during the self test period only.

~~SECRET/D~~

3.9.2 Diagnostic Signals

The purpose of these output signals is to provide information on Beta status to the telemetry. They will all be dc signals normalized to the voltage range of 0 to +5 VDC. Study of these functions will enable problem isolation to a relatively small quantity of circuitry or a single function. The list of preliminary functions to be monitored is as follows:

a. X channel velocity output

b. X sense

c. Y channel velocity output

d. Y sense

e. Servo control voltage

f. X channel correlation voltage

g. Y channel correlation voltage

h. HV power supply control voltage

i. X reference signal

j. Y reference signal

k. ±15 VDC power

l. +12 and -6 VDC power

m. +24 vdc voltage input

n. +24 vdc current input

o. Detector internal temperature

p. Electronics package internal temperature

3.9.3 Test Hardware

3.9.3.1 Special Test Setup. The special test setup for field test of of the Beta System is the same equipment to be used for acceptance test.

Thus, data from the acceptance tests will correlate directly with field test data for the same system. Figure 3-16 is an artist's concept of the Special Test Setup.

The test setup consists of an input section which provides simulated image motion to the detector and an output section which monitors and records system outputs and diagnostic signals.

Basically, the input section consists of a cathode ray tube (CRT) image motion simulator and the optical elements to project the moving image into the detector. The CRT image motion simulator is comprised of a standard oscilloscope, a standard low frequency oscillator and necessary controls and interconnections. A standard dc power supply provides Beta System power.

The output section consists of a digital display of A/D converter outputs, an array of critical signal GO, NO-GO indications, a digital voltmeter for monitoring output and diagnostic signal dc levels, an oscillograph for monitoring and recording dynamic signals, and the necessary test points, interconnecting cables, and input/output switching. This is the minimum equipment required for every test of the Beta System. (For diagnosis, an oscilloscope and electronic counter will be required at the factory.) The test setup is housed in two standard modular enclosures that bolt together and mount on casters to form a test console. One enclosure is a rack which drawer mounts:

a. Output test points and A/D output display.

b. Input controls.

c. A storage drawer for cables, manuals, and procedural support data.

d. Commerical test equipment.

e. Cooling blower and filter.

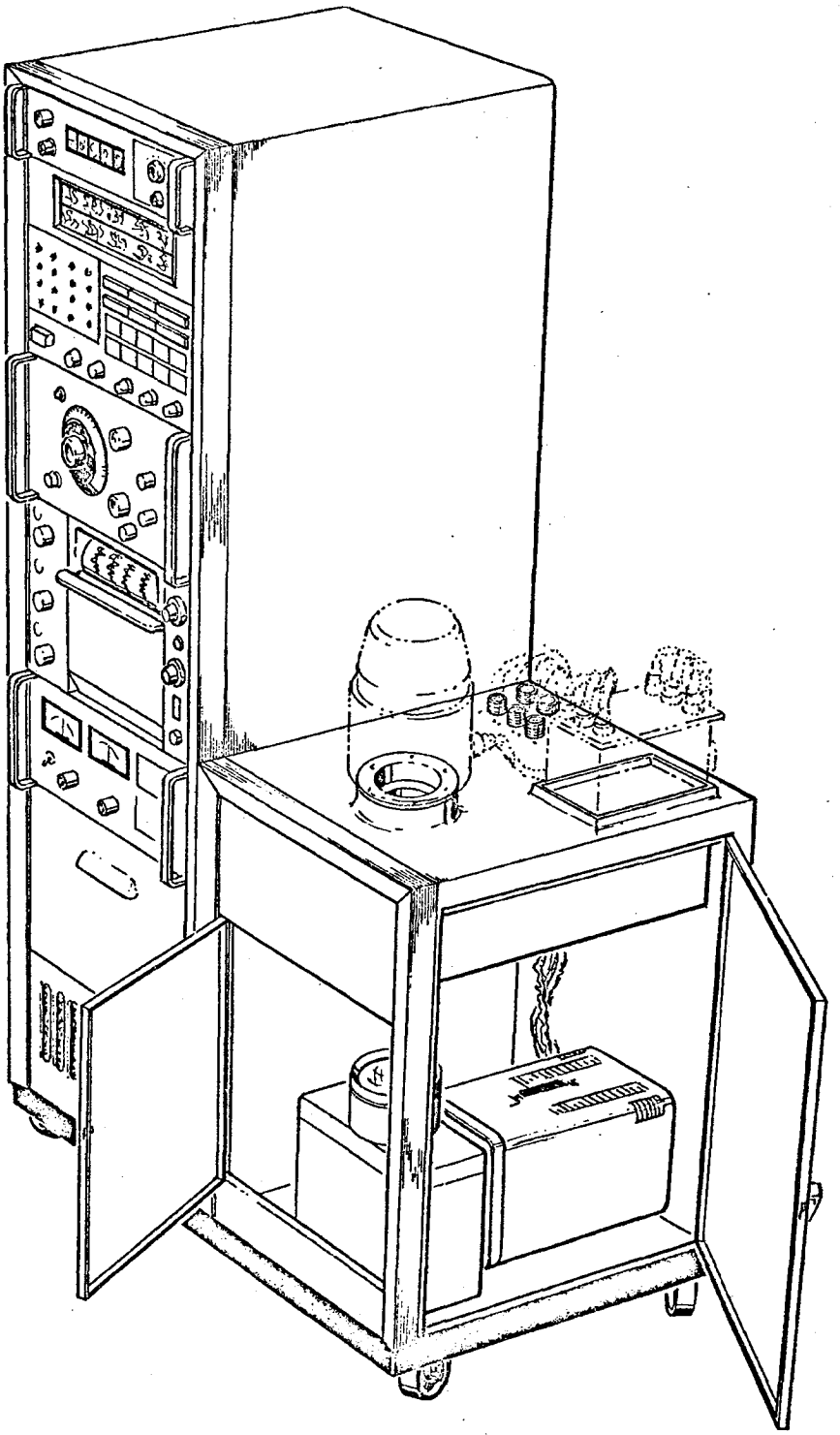

Figure 3-16. Beta Special Test Setup

~~SECRET/D~~

The other enclosure contains the input optics (a lens and mirror) oscilloscope, and the working surface where the system is mounted and connected for test.

The Beta electronics package rests on a heat sink on the working surface of the input section and cables connect inputs and outputs at conveniently located connectors. The detector views downward into the optics of the image motion simulator and connects by a cable to the electronics package. The test is conducted by applying various types and rates of image motion (the oscilloscope trace controlled by the low frequency oscillator) and by rotating the detector to predetermined angles to simulate various direction of motion. For each input, the critical GO-NO-GO indications and dc outputs would be monitored and compared with the digital readout. For selected inputs, a recording of diagnostic signal dynamic characteristics would be made and compared to a master recording for the same test conditions. The power supply will allow various voltage levels and conditions to be supplied to the Beta System.

3.9.3.2 Special Test Set Requirement. The production schedule and intended usage indicates the need for three Special Test Setups, one for acceptance testing, one for qualification testing, and one for remote site operational verification. Certain general purpose test equipment will be required and are not items included in the special test set cost. These items should be relay rack mounted, and are:

1. Digital Voltmeter - Hewlett Packard 3440A with 3441A selector
2. Oscillograph - Brush Mod. 16-2308-00-3490
3. Power Supply - Hewlett Packard 6265A

~~SECRET/D~~

4. Oscillator - Hewlett Packard 203A

or equivalents.

3.9.4 Optical Bench Tester.

Figure 3-17 illustrates the first tester used. This tester lacked the ability to recognize certain dynamic test problems, including scalloping (a function of the haze factor and minimized by proper aperture shading) and pseudo velocities introduced by scene elements entering and leaving the aperture with changes in obliquity. As a result, using the Customer's Beta Tester as a guide, an optical Bench Tester has been devised and breadboarded. This tester has the appearance of Figure 3-18. The purpose of optical portion of simulation is to present the Beta System under test with a ray bundle having a half angle of four degrees. The optics consist of three f/2.5, 12 inch Aero Ektar lenses and an aperture stop. The first lens in the optical system produces an image at the focal point of the second lens. The second lens collimates the image rays. The collimated bundle is passed through the aperture stop. The location and diameter of the aperture is such as to restrict the final ray bundle to four degrees. The aperture also serves another function: the introduction of "haze" light into the system. A small lamp is situated in the center of the aperture. The lamp is at the focal point of the last lens in the system. The haze light is presented to the Beta System as a collimated bundle. The last lens directs the four degree bundle to the Beta System and forms an image on the Beta field lens.

Stereo track is simulated by mounting the target scene on a rate table. Oblique angles during stereo track are obtained by tilting the scene on the rate table prior to rotation.

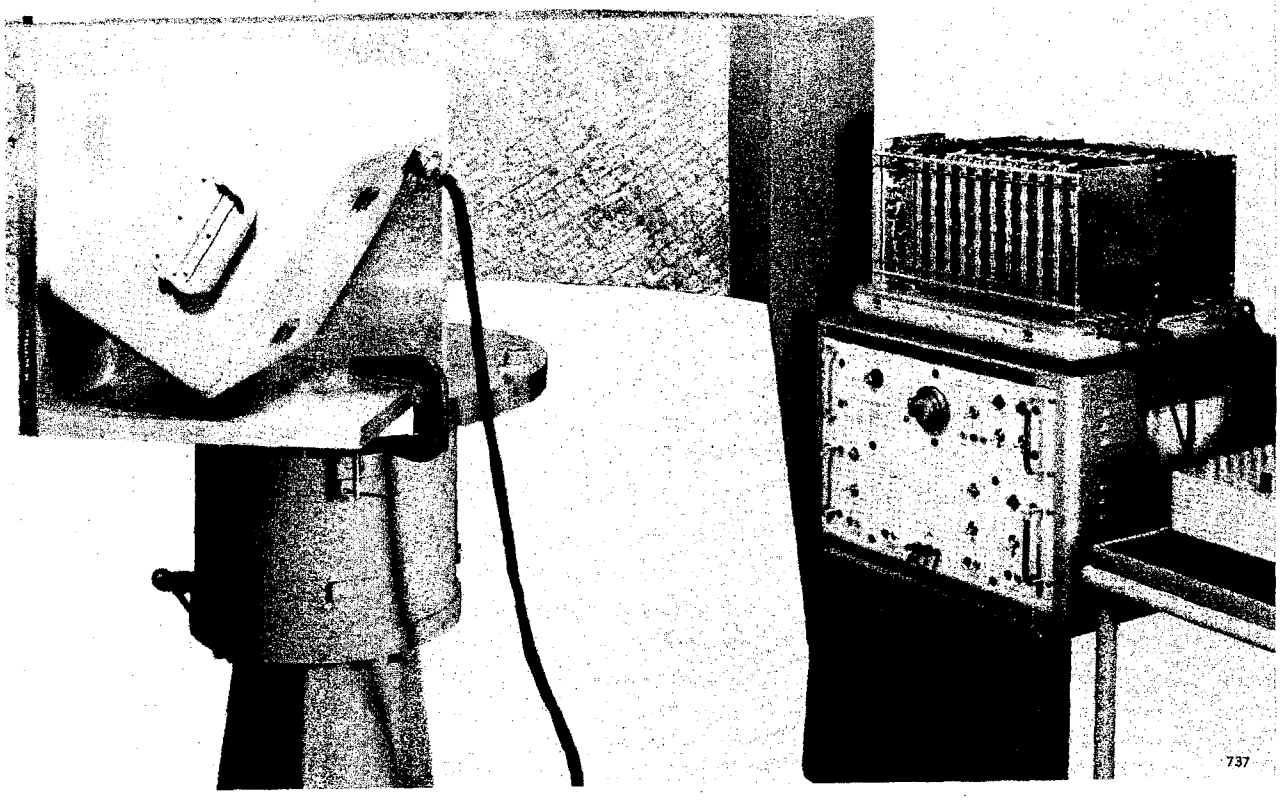

Figure 3-17. Initial Beta Testing

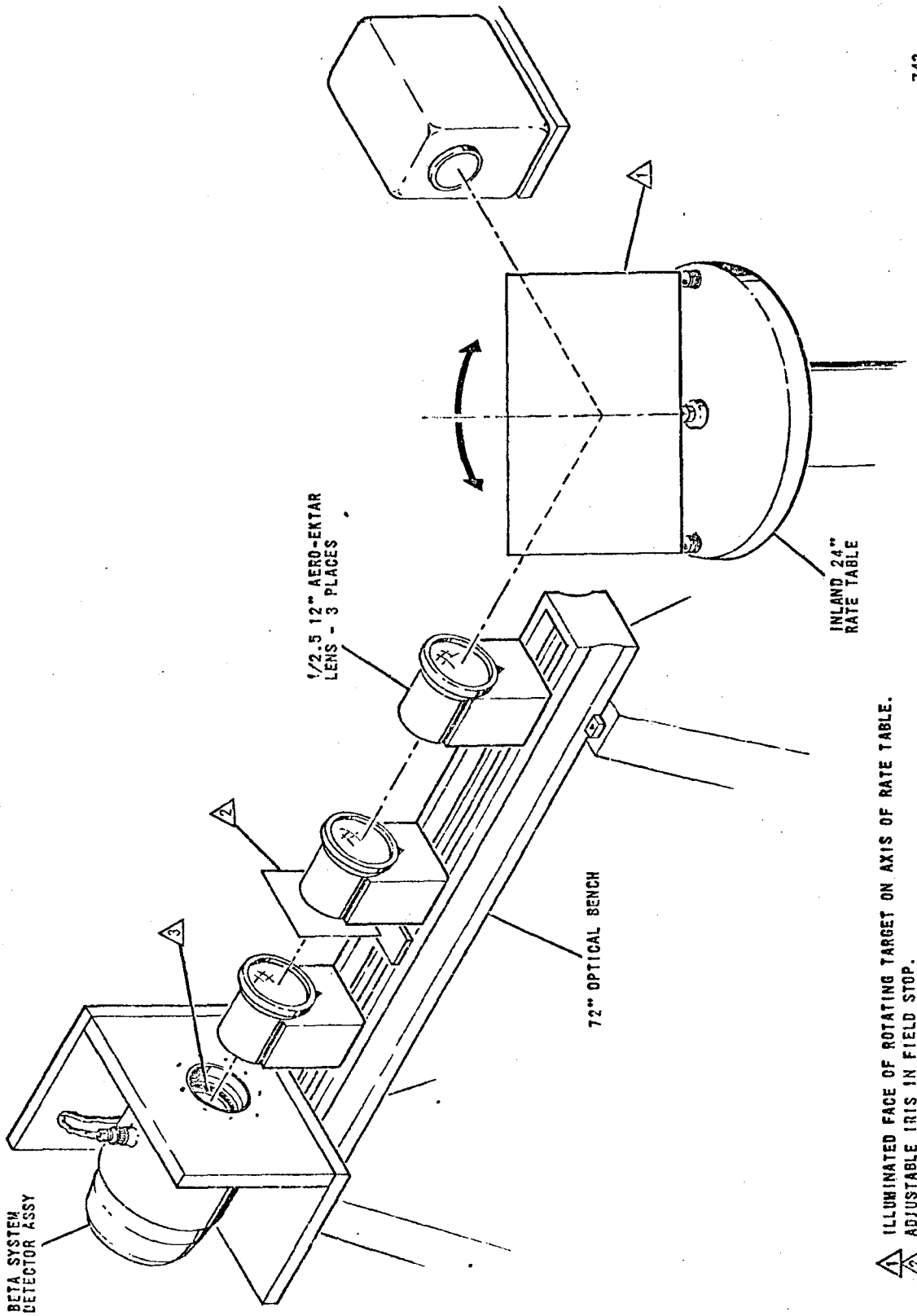

Figure 3-18. Optical Bench Tester

~~SECRET/D~~

Section 4

MAINTAINABILITY AND RELIABILITY

4.1 MAINTAINABILITY

The primary design criteria dictate extremely reliable gas-filled, sealed units that must be returned to the factory for repair. This system is packaged for: (1) rapid trouble isolation using test points carefully selected to indicate functional loop and subassembly status, (2) ready replacement of plug-in circuit cards and other modular subassemblies, (3) least possible calibration time by adjustment of a few basic circuit values. In addition, testing time is minimized by carefully analyzing parameters to identify those that must be checked to prove operability at acceptance and prior to each use.

4.1.1 Test Points

As listed in Paragraph 3.9.2, diagnostic monitoring signals are brought out at a connector. These signals allow trouble isolation to the functional circuit. In nearly all cases, analyzing the signals will isolate the trouble to a circuit card or subassembly while the units remain sealed. The detector assembly can be fully diagnosed by means of these external signals. Inside the electronics package, testing at circuit board connectors allows complete diagnosis of any trouble.

4.1.2 Modular Construction

Each printed circuit card performs one major function. Thus replacing a card to correct one malfunction will not invalidate calibration of other functions. The optics assembly and the motor disc assembly are

mounted in a manner that will allow replacement in minimum time and without damage to structure or assemblies.

4.1.3 Calibration and Testing

By selecting about five basic circuit values the system is permanently calibrated. Subsequent testing is reduced to its simplest form by use of a test set that provides optical input and monitors diagnostic signals as well as system outputs (including A to D Converter outputs). Certain parameters are proved by design qualification and will not change with use or differ among units. Careful selection of parameters that must be tested will simplify the tests and reduce test setup time while providing high assurance of system readiness without ambiguity.

4.1.4 Maintainability Program

Maintainability is designed into the system. However, it must be proved and maintained by a comprehensive program. Refer to Volume I under Section 5, Plans, for a discussion of the program including Evaluation, and Reporting with specification basis and example forms.

4.2 RELIABILITY

4.2.1 Introduction

Reliability Engineering is a line function reporting to the Chief Engineer. The group is responsible to ensure that all contract requirements in this discipline will be met by establishing a comprehensive reliability program and parts selection program early in the design phases and by extending the programs over the contract period. The following paragraphs describe the Hycon reliability program.

4.2.2 Reliability Program

The reliability program will be implemented corresponding to the development and production phases of the contract. In the development phases, the reliability group will assume active participation in design reviews including performance of reliability figure of merit analysis and parts selection. The program will begin with an analysis of the engineering model configuration and extend this analysis and parts selection program to the production configuration. Every effort will be made to identify and correct any possible sources of unreliability and eliminate any unreliable parts and components in preparation for the preproduction and production models. The production models will undergo formal qualification testing. The production phase will consist principly of adequately monitoring the performance of the production units to assure that the required reliability has been met.

The following paragraphs describe the preliminary reliability program implementation in a description of the reliability tasks, and formal documentation. The program as described herein will conform to R-1001F,

Reliability Assurance Requirements for Subcontractors. A more definitive program will be prepared, submitted for approval, and maintained per DRL MSM-R-107.

4.2.2.1 Design Reviews. The reliability engineers to the project will actively participate in all design reviews and will prepare design review check lists, reliability stress analyses, and reliability predictions for aides in equipment evaluation. The check lists will be prepared as comprehensive guides for an impartial evaluation of the technical data and will permit determination of possible design weaknesses or reliability inadequacies. They will also provide assurance that applicable human factors have been considered and appropriately resolved. The following paragraphs define the design review panel and design review scheduling.

The design review panel will be composed of engineering managers, reliability engineers, and cognizant design engineers. The design review panels will consider interfaces, parts application, materials, circuits, processes, thermal design, mechanical design, and configuration. The equipment design will be carefully checked against the design review check list to assure that the decision reflects conformance with the basic specification as regards performance, reliability, and maintainability. When appropriate, recommendations will be made to change or approve the design.

Three design reviews will be scheduled during the design program to provide a periodic evaluation of each phase. Additional reviews will be scheduled as necessary whenever special problems are encountered.

a. Preliminary Design Review. A PDR will consider the detailed circuit analysis and layout and will be scheduled as soon as the principle design areas are formulated. This review will include a check of component interfaces, system block diagrams, preliminary schematics, a preliminary parts list, and consideration of the effects of malfunctions, failures or performance degradation of each part.

b. Critical Design Review (CDR). The critical design review will emphasize design excellence and establish conformance to recommendations arising from the preliminary design review, and will consider any additional data that has become available since the preliminary design review. This review will be scheduled when prototype designs are available in a packaged configuration.

c. First Article Configuration Inspection (FACI). The final design review will be scheduled at the end of the design phase after completion of the first model, of the prime hardware. Its purpose will be to review drawings, specifications, problem areas, manufacturing processes or procedures, overall production performance and maintenance improvement areas.

4.2.2.2 Reliability Analysis. Reliability is an engineering design parameter. The procedures used to predict product reliability parallel those used to arrive at other production characteristics relating to parts or materials, and to the stresses anticipated in their application. A complete reliability analysis provides all calculations necessary for a reasonable prediction of equipment reliability and includes the use and application of parts, materials, and processes; a reliability figure of merit analysis; a failure modes and effects analysis; and a hazard modes

and effects analysis, if applicable. These analyses will be prepared in the breadboard phase and revised as required as the design and development of the equipment progresses. The results of these analyses will be submitted per MSM-R-112-1 as scheduled by the DRL.

4.2.2.3 Parts, Materials, and Processes. The selection of parts, materials, and processes will be controlled through the Reliability group for analysis and assurance that each part, material, or process selected will meet the requirements of the equipment specification. In the electronic circuits, microelectronics will be used wherever feasible. In those instances where it is not feasible, discrete components parts may be used. Those elements and/or parts shall be selected in accordance with Contractor Specification DR 1110, Selected Parts List. In the event it becomes necessary to use parts which are not in DR 1110, data will be furnished in accordance with the requirement of DR 1110 for possible inclusion as a preferred part. Where discrete parts are required, Hycon will obtain approval from the Contractor prior to their use. This includes approval of the packaging technique to be employed. All other parts, materials, and processes shall be selected in the following order of precedence:

Contractor Specification Numbers DR1100, DR 1112, DR 1113, DR 1115

Applicable portion of MIL-E-25366 and MIL-E-5400

Prior Use

Commercially available standard MIL, AN, and MS electronic and electrical parts.

All selected parts not on the Contractor preferred list (DR 1110) shall be submitted to the Contractor for approval per the requirement of MSM-S-126-1, Request for Approval, Parts, Materials, or Processes.

4.2.2.4 Reliability Figure of Merit Analysis. A reliability figure of merit analysis shall be developed following the procedures of TRA-873-74, dated 1 September 1961. The figure of merit analysis will include the development of a reliability block diagram and a mathematical model.

Information for the models will be developed by analyzing all the functional parts and listing these parts with their corresponding operational stress levels. For each part application, a failure rate shall be stated using failure rates from MIL-HDBK-217 for electrical and electronic parts, and SP 63-470, Vol. 1-FARADA for all other parts. If other rates are used, they will be justified by data derived from tests of prior proven experience in equivalent applications. With the data derived above, the MTBF for the equipment will be computed and submitted as part of DRL MSM-R-112-1, Reliability and Safety Analysis Report.

4.2.2.5 Failure Modes and Effects Analysis. A failure modes and effects analysis will be conducted on the system and documented as part of DRL MSM-R-112-1, Reliability and Safety Analysis Report. The failure modes and effects analysis will identify all failure modes of each critical part, material, and process and list probability of occurrence, most likely condition of failure, and effect on the performance of the hardware.

4.2.2.6 Hazard Modes and Effects Analysis. A hazard modes and effects analysis will be conducted to result in a systematic examination of all the apparent ways that an equipment malfunction, material degradation,

improper environment, or operational misuse may generate a hazard to the Beta System, associated or adjacent equipment, or to the user. This report will include a logic block diagram, showing hardware functions, their interrelations and the external interfaces. Each block shall be analyzed to ensure a safe application of the end-item. The hazard modes and effects analysis will be supplied as part of DRL MSM-R-112-1, Reliability and Safety Analysis Report.

4.2.2.7 Reliability Data. All failure and failure analysis reports resulting from development subsystem testing, acceptance, and qualification testing will be accumulated and summarized as a tool for corrective action initiation and follow-up. In addition, on each deliverable component the operating time will be recorded in summary reports and component logbooks as defined by DRL MSM-P-101.

The following paragraphs describe the failure report and analysis system. The failure summary reports and the corrective action information flow functions.

a. Failure and Failure Analysis Reports. During development testing of subsystem, acceptance test of the system, and qualification test programs, the failure report (Figure 4-8) and the failure analysis report (Figure 4-9) will be maintained. These reports will be submitted in accordance with DRL MSM-R-102-1.

b. Failure Summaries. Failure summaries will be prepared at monthly intervals during the life of a program and will be prepared for each system and subsystem. Since all failures that occur are not necessarily attributable to the failure of a specific system or subsystem, the sifting of pertinent

~~SECRET/D~~

FAILURE REPORT

1 NEXT ASSEMBLY S/N	2 MODEL	3 DATE	4 REPORT
5 NAME	6 CONTRACT	10 ESTIMATED OPERATING TIME	CYCLES / HOURS
7 FAILED ITEM NAME	8 PART NUMBER / 9 SYMBOL	THIS TEST:	
		ACCUMULATED	

11 FAILED DURING: (CHECK)
☐ ACCEPTANCE TEST ☐ INSPECTION
☐ QUALIFICATION TEST ☐ FLIGHT
OTHER:

12 CAUSE OF FAILURE: (CHECK)
☐ ASSEMBLY ☐ PART ☐ MATERIAL
☐ WORKMANSHIP ☐ DESIGN ☐ TEST EQUIPMENT
OTHER:

13 SYMPTOMS AND CAUSE OF FAILURE	14 PRODUCTION STAMP	15 INSPECTION STAMP	15 INSPECTION DATE	16 CUSTOMER STAMP	16 CUSTOMER DATE
17 EFFECT OF FAILURE					
18 ACTION AND REMARKS					
19 RECOMMENDATIONS					
20 REF. TWX OR TELECON:					

21 DISPOSITION: (CHECK)
☐ REWORK ☐ REPLACE ☐ SCRAP
☐ MRB ☐ OTHER: ☐ ENGINEERING ANALYSIS

22 ENVIRONMENTAL CONDITIONS
TEMP. _____ HUMIDITY _____
ALTITUDE _____
OTHER:

23 TIME OF FAILURE	24 TEST LOCATION	25 TEST CONDUCTOR

HMC 1686 -1 REV. 3/64

Figure 4-8.

~~SECRET/D~~

FAILURE ANALYSIS REPORT			1. REPORT NUMBER
2. FAILED PART NAME	3. SYSTEM NAME	4. CONTRACT NO.	5. FAILURE REPORT DATE
6. SYMBOL	7. MODEL NUMBER	8. CUST. DATA REQ. NO.	9. PREVIOUS FAILURE REPORTS
10. FAILED PART NUMBER	11. SYSTEM PART NUMBER	12. OPERATING USAGE	
			1. CYCLES / 2. HOURS
13. FAILED PART SER. NO.	14. SYSTEM SER. NO.	THIS TEST	
		TOTAL ACCUM.	

15. CAUSE OF FAILURE (CHECK)

1 ☐ ASSEMBLY
2 ☐ PART
3 ☐ MATERIAL
4 ☐ TEST EQUIPMENT
5 ☐ WORKMANSHIP
6 ☐ DESIGN
7 ☐ OTHER _____

16. STRESS CAUSING DAMAGE (CHECK)

1 ☐ ELECTRICAL
2 ☐ MECHANICAL
3 ☐ PRESSURE
4 ☐ TEMPERATURE
5 ☐ HUMIDITY
6 ☐ OVERLOAD
7 ☐ OTHER _____

17. DESCRIPTION OF FAILURE (ATTACH REPRODUCIBLE PHOTOS OR DRAWINGS WHEN POSSIBLE)

18. RECOMMENDED CORRECTIVE ACTION (INCLUDE DETAILS IN SEQUENCE OF OPERATION)

19. SIGNED	20. DATE	21. CARR ECN NO.	22. PAGE_____ OF _____

HMC 1715 REV. 5/65

Figure 4-9.

failure data is necessary. The failure summaries, however, will list the failures that occur by system or subsystem. They will identify each failure and failure report number, and describe the disposition.

4.2.3 Preliminary Reliability Analysis

The preliminary analysis of the failure rates that can be expected for the Beta System indicates that the reliability goal of 10,000 hours MTBF is achievable with a concentrated reliability effort and a comprehensive part selection program which will include minimizing operating levels and screening of all individual parts.

This conclusion is based on a preliminary analysis (see Table 4-3) accomplished by evaluating the prototype unit. The results indicate a reliability of greater than 21,000 hours (MTBF) with the following assumptions:

1) All parts are thoroughly screened and properly stressed to realize minimum failure rates for each individual part.
2) Application factor of 1.0 has been considered in all calculations.
3) Mechanical parts and electrical connectors were considered to have negligible failure rates.

In actual practices some degradation of the calculated failure rates can be expected, however, these must be controlled to maintain the minimum reliability goal of 10,000 hours MTBF. Under a controlled reliability program, the 10,000 (MTBF) is an achievable goal which will be met by continuous application of reliability principles in the design and development stages.

~~SECRET/D~~

TABLE 4-3

PRELIMINARY FAILURE RATE ANALYSIS
(Failures per Million Hours)

PART	FAILURE RATE		QUANTITY	SUBTOTAL
	Value	Source *		
Detector Unit				
Resistor, MIL-R-55182	.0011	A	43	.0473
Resistor, MIL-R-26	.0060	A	2	.0120
Resistor, MIL-R-39008	.002	A	14	.0280
Capacitor, MIL-C-39014	.005	A	2	.0100
Capacitor, MIL-C-5	.0003	A	4	.0012
Capacitor, MIL-C-39001	.005	A	4	.0200
Capacitor, MIL-C-38102	.005	A	9	.0450
Diode, TX	.100	A	1	.1000
Diode, Zener	.600	A	2	1.2000
Diode, Power Rect.	.280	A	8	2.2400
Photodiode	.300	C	4	1.2000
Light Source	.300	C	4	1.2000
Transistor	.100	A	2	.2000
Micromodules	.050	A	5	.2500
Photomultiplier	.625	C	2	1.2500
Servo Motor w/Large Bearings	.500	D	1	.5000
Coil, MIL-T-21038	.300	A	4	1.2000
Power, Supply, Hi-Volts	2.400	A (Parts Count)	1	2.4000
		TOTAL, DETECTOR UNIT		11.7535

* A = MIL-HDBK-217
C = Manufacturer
D = Estimated

TABLE 4-3 (cont.)

PRELIMINARY FAILURE RATE ANALYSIS
(Failures per Million Hours)

PART	FAILURE RATE		QUANTITY	SUBTOTAL
	Value	Source *		
"X" and "Y" Channels				
Resistor, MIL-R-55182	.0011	A	358	.394
Resistor, MIL-R-26	.0100	A	8	.080
Resistor, MIL-R-39008	.0020	A	18	.036
Capacitor, MIL-C-39014	.0050	A	106	.530
Capacitor, MIL-C-39003	.002	A	10	.020
Capacitor, Polystyrene	.002	A	10	.020
Capacitor, Ceramic	.002	A	56	.112
Diode, TX	.100	A	82	8.200
Diode, Zener	.600	A	10	6.000
Transistors, TX	.100	A	48	4.800
Micromodules	.05	A	44	2.200
Filters, Hybrid Active	.16	A	8	1.280
Transformer, MIL-T-21038	.3	A	2	.600
		"X" and "Y" CHANNEL TOTAL		24.272

* A = MIL-HDBK-217A

TABLE 4-3 (cont.)

PRELIMINARY FAILURE RATE ANALYSIS
(Failures per Million Hours)

PART	FAILURE RATE		QUANTITY	SUBTOTAL
	Value	Source *		
Motor, Speed Control/ Pwr. Supplies				
Resistors, MIL-R-55182	.0011	A	60	.066
Capacitors, Polystyrene	.002	A	10	.020
Capacitors, MIL-C-39014	.005	A	24	.120
Capacitors, MIL-C-39003	.002	A	5	.010
Diodes, TX	.100	A	9	.900
Diodes, Zener	.6	A	3	1.800
Transistors	.1	A	6	.600
Micromodules	.05	A	11	.550
Low Voltage Power Supply	6.4	A (Parts Count)	1	6.400
		ASSEMBLY FAILURE RATE		10.466

TOTAL SYSTEM FAILURE RATE

Detector	11.754
"X" and "Y" Channel	24.272
Motor Control and Power Supplies	10.466
BETA SYSTEM FAILURE RATE	46.492 failures/ 10^6 hours or
	21,509 hrs. MTBF

* A = MIL-HDBK-217A

~~SECRET/D~~

APPENDIX 1

BETA SIGNAL SLOPE LIMITER.

The first portion of this report was submitted as an action item resulting from the Technical Direction Meeting of 9 - 10 May 1968. The second portion is an addendum resulting from Contractor direction at the Technical Direction Meeting of 27 June 1968.

The concepts discussed are not a part of the Engineering Prototype Evaluation Model (EPEM) now under fabrication.

~~SECRET/D~~

BETA SIGNAL
SLOPE LIMITER

REPORT ON
TD ACTION ITEM
1B
(TD MEETING 9-10 MAY 1968)

It is desirable to limit the maximum rate of change of Beta output voltage. Since the magnitude of Beta output voltage corresponds to velocity, the rate of change (slope) of this voltage indicates acceleration.

Before considering the detailed means by which acceleration limiting can be implemented, a brief look at the scale factors is desirable. The Beta velocity scale factor is 10 volts per inch per second, or

$$0.1 \text{ volts} = 0.01 \text{ inches/sec.}$$

Assuming we choose to limit indicated acceleration to 0.001 inches/second^2, the corresponding output voltage slope must not exceed 0.1 volts/second.

Figure 1 shows a suitable method for limiting Beta output to any predetermined maximum acceleration. The section of Figure 1 contained within the dotted rectangle performs this function. The remaining structures depicted in the upper third of Figure 1 are existing circuitry in the Beta unit. Operational amplifier AR-5 is used to provide single pole low pass filtering and memory functions, in addition to voltage gain. The voltage gain of AR-5 is established by the ratio of R_f/R_i, the pole location is established by the R_fC_f product, and the memory function is provided by the "gate" field-effect transistor. The proposed modification achieves its slope limiting action by providing strong negative feedback around AR-5 whenever the derivative of AR-5's output voltage exceeds a threshold value established by circuit parameters. As can be seen by inspection of the proposed modification, these parameters include the differentiator network RC product, the gain of AR-10 (as determined by the R_2/R_1 ratio), and the threshold voltage of the series diodes.

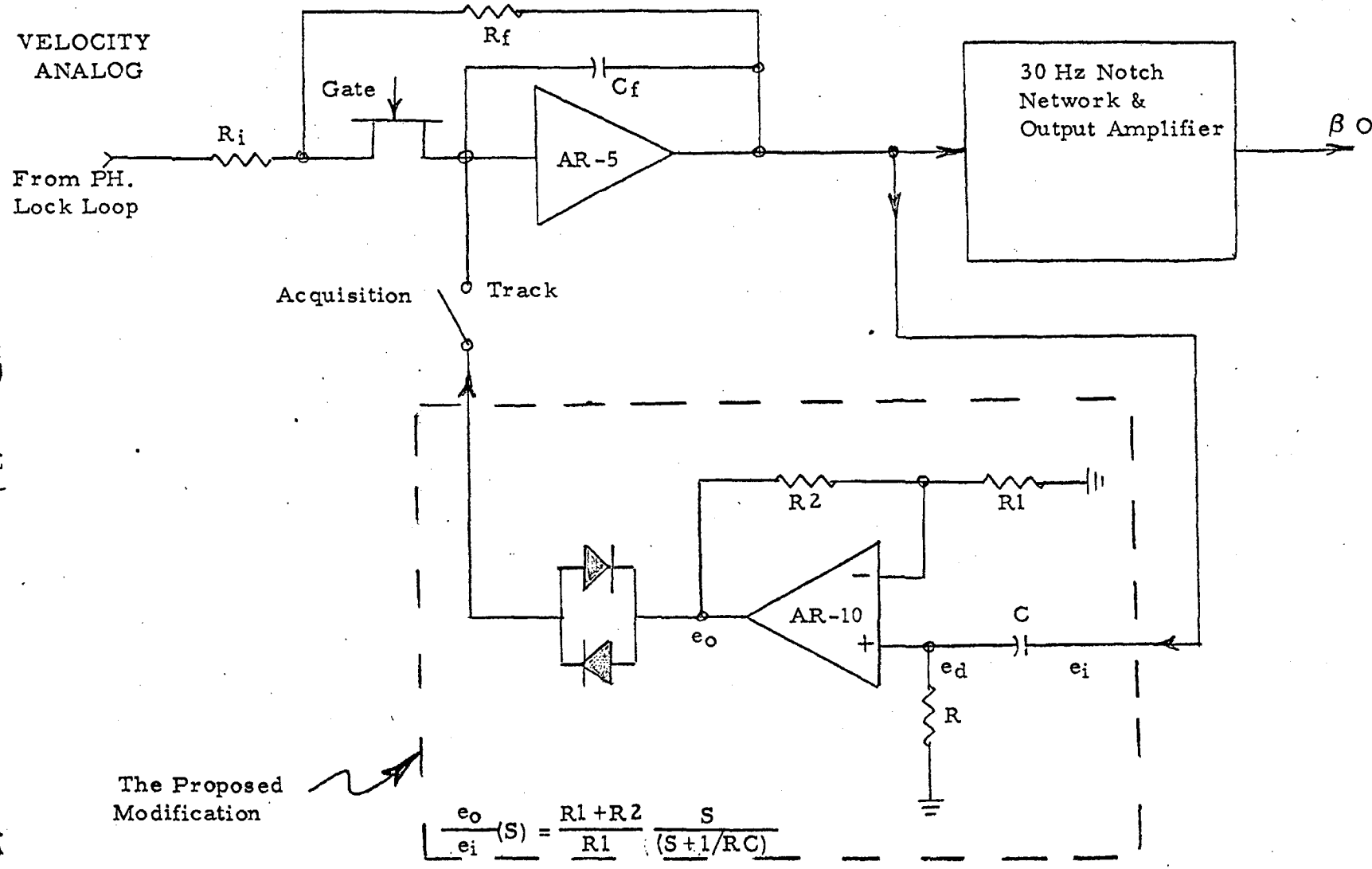

FIG. 1 ACCELERATION LIMITER

~~SECRET/D~~

The transfer function of the differentiator network is:

$$\frac{e_d}{e_i}(S) = \frac{S}{(S + 1/RC)}$$

To evaluate the e_d resulting from a ramp input voltage e_i having a slope of 0.1 volts per second we write the following Laplace transformed relationship:

$$e_d(S) = \frac{.1}{S^2} \frac{S}{(S + 1/RC)} = \frac{.1}{S(S + 1/RC)}$$

In order to obtain e_d as a function of time we perform an inverse transformation as follows:

$$e_d(t) = \mathcal{L}^{-1} \frac{.1}{S(S + 1/RC)}$$

Employing partial-fraction expansion:

$$\frac{1}{S(S + \gamma)} = \frac{K_o}{S} + \frac{K_1}{(S + \gamma)}$$

$$K_o = \left.\frac{S}{S(S + \gamma)}\right|_{S=o} = \frac{1}{\gamma}$$

$$K_1 = \left.\frac{1(S + \gamma)}{S(S + \gamma)}\right|_{S=-\gamma} = \frac{1}{-\gamma}$$

Hence:

$$e_d(t) = \mathcal{L}^{-1}\left[\frac{.1\,RC}{S}\right] + \mathcal{L}^{-1}\left[\frac{-.1\,RC}{(S + 1/RC)}\right]$$

$$e_d(t) = .1\,RC - .1\,RC\,\mathcal{E}^{-t/RC} = .1\,RC\,(1 - \mathcal{E}^{-t/RC})$$

~~SECRET/D~~

The above result shows that a Beta output voltage slope corresponding to an acceleration of 0.01 in sec^2 generates a step voltage output of 0.1 RC volts at the input to AR-10. Since silicon diodes D_1 and D_2 have a threshold voltage of 0.6 volts, the gain of amplifier AR-10 should be adjusted so that the step voltage input magnitude of 0.1 RC volts will result in an output of 0.6 volts.

The circuit as described in Figure 1 will achieve the desired slope limiting for the Beta sensor signal. In the existing breadboard No. 2 this circuit has shown its value by limiting the signal output "lumps" to a slope less than 0.1 volts/second. The use of the "Acquisition-Track" switch allows the effect to be studied by placing the circuit in and out of use.

~~SECRET/D~~

BETA SIGNAL SLOPE LIMITER WITH RAPID RETURN TO ZERO

(ADDENDUM TO THE BETA SIGNAL SLOPE LIMITER PAPER OF 22 MAY 1968)

A previous paper[1] has described a circuit modification which is effective in limiting the maximum rate of change of Beta output voltage. This circuit has the property of providing equal maximum slopes for voltages both departing from zero and returning to zero. A further refinement consists in modifying the limiter circuit so that the slope of voltages departing in either direction from zero (positive or negative going) is restrained to some predetermined moderate value, while the slope of recovery toward zero, either positive or negative, is allowed to be much greater.

Figure 1 presents a configuration which incorporates this refinement. The portion of Figure 1 shown above the dashed line is the basic Beta output section. The portion of Figure 1 below the dashed line shows the additional circuitry required for the slope limiting function.

Operation of the slope limiter circuit can be most easily understood from the viewpoint of current limiting. The current that is being limited is the current flowing through C_D. This current, i_c, flows through R_D to produce voltage e_D.

Voltage e_D is amplified by AR-10 whose gain is accurately established by the negative feedback network composed of R_1 and R_2. When the field effect transistor switch (FET 3) is open the gain of AR-10 is:

$$A = \frac{R_1 + R_2}{R_1}$$

1. BETA SIGNAL SLOPE LIMITER. Report on TD Action Item 1B (Technical Direction Meeting 9-10 May 1968) dated 22 May 1968.

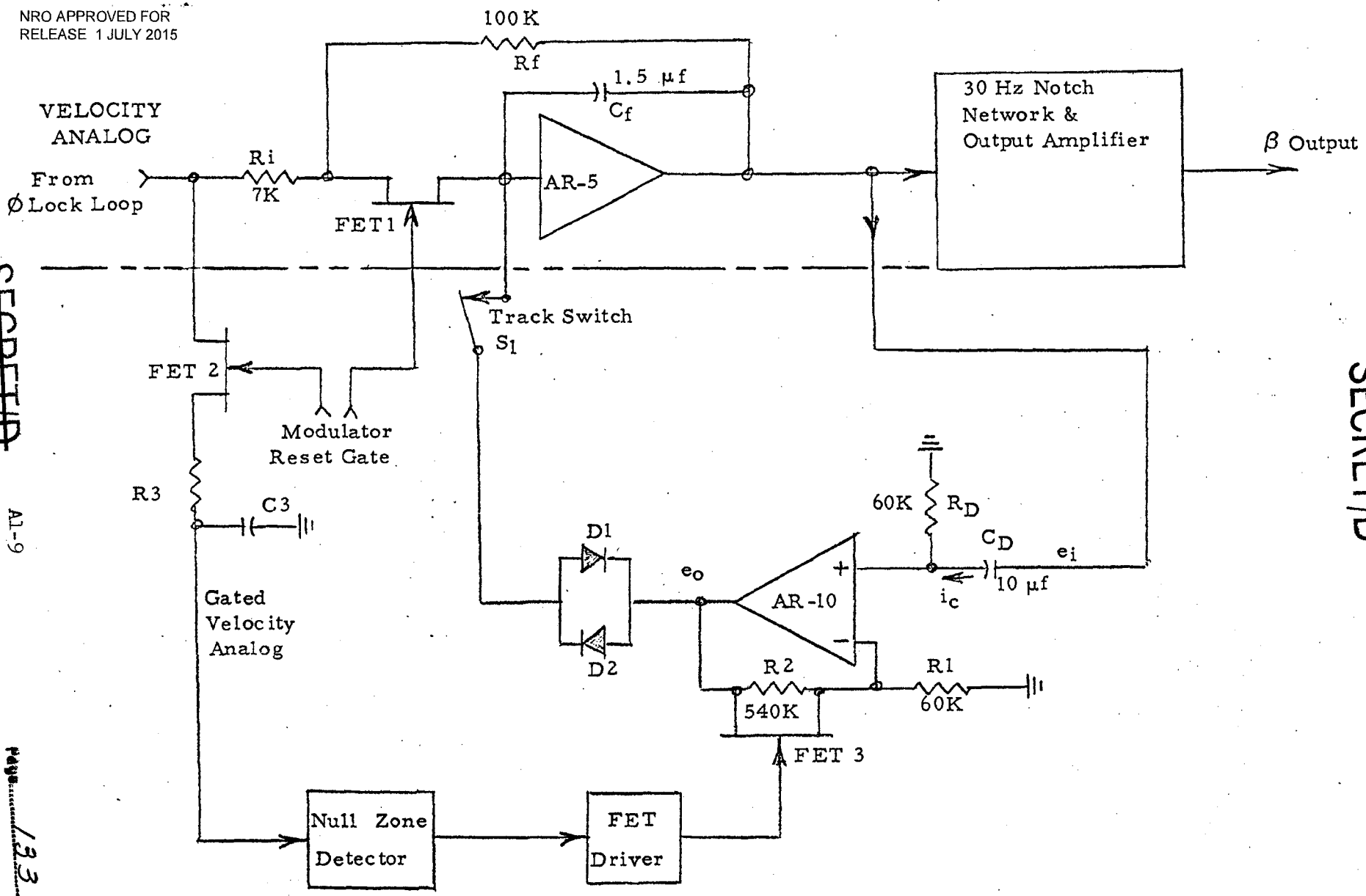

FIG. 1 SLOPE LIMITER WITH RAPID RETURN TO ZERO

For the values shown in Figure 1 the gain is 10. When FET 3 is closed the gain of AR-10 is unity. The current limiting level is established by the forward threshold of the silicon diodes D_1 and D_2, the gain of AR-10, and the value of R_D. For silicon diodes the threshold voltage is approximately 600 millivolts which results in e_D having a value of 60 millivolts under limiting conditions. Since e_D is produced by i_c flowing through the current sampling resistor R_D, we can write:

$$i_c \text{ max.} = \frac{e_{D \text{ max.}}}{R_D} = \frac{60 \times 10^{-3}}{60 \times 10^{3}} = 1 \mu a$$

This maximum current of one microampere flowing through C_D produces a voltage drop across C_D which is:

$$e_{C_D} = \frac{1}{C_D} \int i_c dt$$

Substituting values we get:

$$e_{C_D} = \frac{1}{10 \times 10^{-6}} \times 1 \times 10^{-6} t = 0.1t$$

The voltage e_i is the sum of the voltages appearing across C_D and R_D, Hence:

$$e_i = e_D + e_{C_D} = 0.060 + 0.1t$$

The above result shows that under limiting conditions (for signals of either polarity departing from zero and FET 3 open) the voltage e_i and the β output voltage will be a ramp with a slope of 0.1 volts per second superimposed on a baseline value of 60 millivolts. This corresponds to an indicated maximum output acceleration of 0.01 inches per second squared.

In order to provide the "rapid recovery toward zero" characteristic the raw velocity analog voltage produced by the phase lock loop is appropriately sampled via FET 2 and has filter network R_3C_3. The resultant gated velocity analog is sensed by the null zone detector, which is a bipolar amplitude comparator. Whenever the velocity analog is within a predetermined plus or minus region about zero, the null zone detector output causes the FET driver to activate FET 3 which in turn shorts out R_2. Shorting R_2 produces unity gain of AR-10. This forces e_D to assume a value of 600 millivolts during the recovery to zero, as opposed to the 60 millivolts existing under limiting conditions for signals departing from zero. During the recovery toward zero the capacitor current is increased tenfold relative to its value during departure from zero, hence the β output voltage recovery toward zero will be rapid.

The described circuit provides a means for differential limiting as a function of departure from, or recovery toward zero. It should be noted that the track switch S_1 provides a means for disabling the limiter action during acquisition periods when large signal dynamics prevail.

APPENDIX 2

Special Report on the HERRINGBONE IMAGE RATE SENSOR SYSTEM.

The following report is of special interest since this concept coupled with a much simpler optical subsystem (one-path) results in a system that has equivalent performance, yet will meet the weight specifications of EC-701A, Rev. 6. This weight is compared with the two-path version in Section 3.5.2 of this proposal.

In preparation is a Hycon paper defining a dual-path Herringbone Image Rate Sensor System. Such a system promises to minimize "drop-outs" as an alternate to the approach taken with slope limiting.

SPECIAL REPORT ON THE HERRINGBONE IMAGE RATE SENSOR SYSTEM

Prepared Under AFE No. 9026-01

INTRODUCTION

The herringbone two orthogonal axes image motion sensor is a system which detects two separate velocity channels using a single channel optical input and single photo sensor. This is accomplished by superimposing two orthogonal grid patterns of different spatial frequencies, each of which make a 45 degree angle to a radial line through the center of the disc. When the disc is turned at a fixed angular rate, each pattern yields a different carrier frequency.

The image is focused on the grid pattern, allowing the motion of the image to modulate the carrier frequency of the disc (Doppler effect). The output of the photodetector is the sum of the two image motion channels. These two channels are separated using standard filtering techniques and finally fed to the Beta electronics as is done with the present Beta sensor. Here the image channels are demodulated with respect to the carrier frequencies and each resultant image wave is converted to a dc voltage proportional to image rate for that axis.

The inherent advantages of such a system over the existing Beta System are:

a) Elimination of the beamsplitter portion of the optics (cost, weight and space saving).

b) Elimination of one photo sensor and associated electronics (cost, weight and space saving).

c) Increased reliability of the sensor head due to fewer parts.

DISC DESIGN

The basic disc design is shown in Figure 1. The aperture is shown with a line passing through its center. Each line passing through the

~~SECRET/D~~

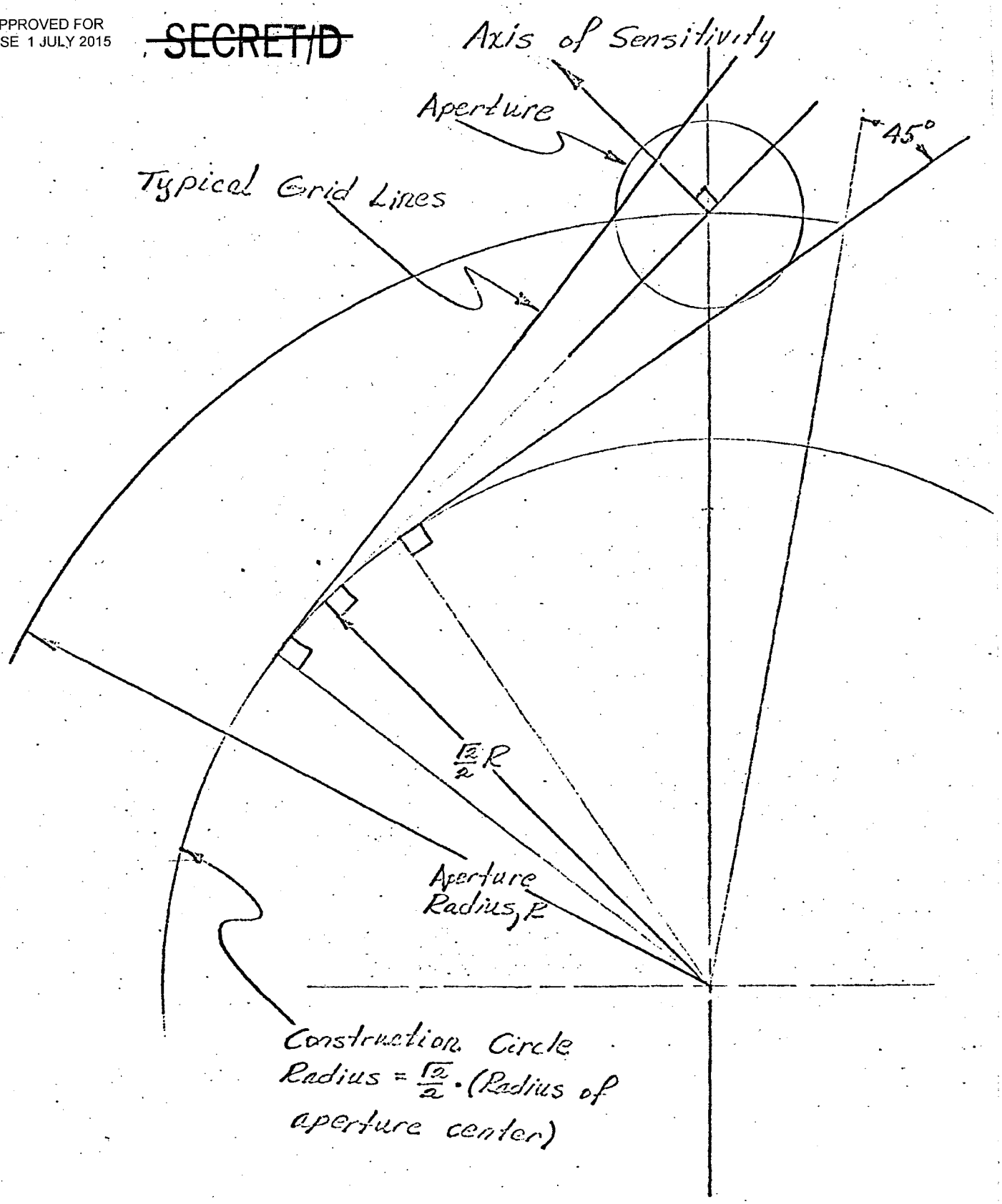

Figure 1. Construction of Herringbone Grid Lines

~~SECRET/D~~

center of the aperture is tangent to a circle of radius $\frac{\sqrt{2}}{2}$ times the radius to the center of the aperture. A by-product of this constraint is that each line will make a 45 degree angle with a radial line when both lines intersect at the disc radius of the aperture center. On one channel there are 750 dark and 750 clear spaces. This yields a clear space width of approximately 0.005 inches, similar to the Beta System.

$$\text{Width of clear space} = \frac{\pi \text{ (Disc dia. at aperture center)}}{2 \text{ (Number of clear spaces)}} \cdot \frac{\sqrt{2}}{2}$$

The spatial frequency of the remaining channel is selected such that is is not a harmonic of the first, but yet still can be separated from the sum of the two. During the feasibility testing of the herringbone breadboard, the ratio 15/19 was used. The signals were separated with crosstalk measured at less than 0.1%. Since it has been found that scene energy is concentrated at the lower spatial frequencies, a lower grid wave number is used for the second channel. The second channel has 15/19 (750) or approximately 590 cycles per revolution.

SIGNAL PROCESSING

Signal processing was performed on the herringbone breadboard as follows. The signal from the photodetector was amplified with a double peaked response, one peak at each carrier frequency. The higher the Q of the peaks, the better will be the rejection of harmonics in the vicinity of the carrier frequencies. By putting a notch filter at the higher carrier frequency, the lower image channel can be separated from the sum. Similarly, by putting a notch at the lower frequency, the

higher image channel can be selected. Achievable attenuations of active notch filters are in the range of 500 to 1000.

RESULTS OF THE HERRINGBONE BREADBOARD

The herringbone theory was reduced to practice using two radial discs mounted with their aperture grid lines at right angles at the detector field of view. The discs were geared together by the ratio 15/19. A photo source and a light sensitive diode were used to sense the reference frequency of each disc. In this manner each image rate could be measured with respect to its own reference frequency. As mentioned above, the output of the single photodetector was amplified by a double tuned amplifier. The channels were separated using two active notch filters.

The results of the test were conclusive in that it is possible and feasible to build two patterns on one disc which are orthogonal and capable of modulating a focused scene at a given carrier frequency. The quality of the output image signals suffered slightly because:

a) The discs were geared, giving rise to short term disc speed variations.

b) The input scene brightness to the photodetector was low because of the long focal length lens used on the breadboard.

These problems notwithstanding, the breadboard sensed and separated the two image rates in good stead; no design or feasibility problems were encountered.